Utilizing Microfibrous Entrapped Catalyst Mixtures as a Means to Overcome Transport and Equilibrium Limitations of Dimethyl Ether Synthesis via a Methanol Intermediate

by

William Robert Yantz, Jr.

A dissertation submitted to the Graduate Faculty of
Auburn University
in partial fulfillment of the
requirements for the Degree of
Doctor of Philosophy

Auburn, Alabama
December 16th, 2017

Keywords: Microfibrous Entrapment, Methanol, Dimethyl Ether, Heat Transfer, Process Intensification

Approved by

Bruce J. Tatarchuk, Chair, Charles E. Gavin III Professor of Chemical Engineering
Yoon Y. Lee, Professor Emeritus of Chemical Engineering
James Radich, Assistant Professor of Chemical Engineering
Daniel Harris, Associate Professor of Mechanical Engineering

Abstract

Due to the highly exothermic nature of single-step dimethyl ether synthesis, a highly conductive catalyst support known as microfibrous entrapped catalyst (MFEC) was utilized in order to mitigate the heat generation within the single reactor, as well as improving product quality for both a 15mm ID and 29mm ID reactor. When compared to the MFEC reactor, a packed bed had a 1.36 – 1.91 increase in centerline temperature than the MFEC reactor. Further, the MFEC consistently produced a higher content of the goal product, dimethyl ether, while also completely eliminating the side production of methane that was observed in the 29mm ID packed bed reactor. COMSOL was used to examine the surface temperature of catalysts in the MFEC reactor, and it was observed that the MFEC reactor consistently had lower catalyst surface temperature when compared to a packed bed.

Acknowledgments

To my friends and family, I simply could not have finished my career at Auburn without your constant support. As far back as I can remember, my parents have encouraged all my academic endeavors. Mom and Dad, if it were not for you, I would not be where I am today. Thank-you both for tireless encouragement and support, I love you both.

To my wife J.D., who has been with me from start to finish in my Auburn career, words simply fail to express how much you have helped me. For the countless hours you have helped me with every aspect of my time here, I cannot thank you enough. I love you immensely J.D., and I would not have finished without you in my life.

Table of Contents

List of Tables

List of Figures

List of Abbreviations

MFEC	Microfibrous Entrapped Catalysts
MeOH	Methanol
DME	Dimethyl ether
MFC	Mass flow controller
K	Equilibrium constant
G	Gibbs free energy
H	Enthalpy
R	Universal gas constant
T	Temperature
Re	Reynolds number
GC	Gas Chromatograph

Chapter 1: Introduction and Motivation

1.1 Initial Motivation

Highly exothermic and highly endothermic reactions present many problems in both academic and industrial reaction engineering. This dissertation will focus on the problems and their potential solutions to highly exothermic reactions only. The sudden release and/or buildup of heat within a reactor can have any number of outcomes: catalytic performance reduction, product degradation, loss of selectivity, thermal runaway, or harm to persons and/or property.

In a typical chemical engineering curriculum, students are taught the fundamentals of a packed bed reactor and a batch/continuously stirred tank reactor. Depending on the catalyst and reactants, heat transfer can be a significant problem. In order to alleviate these problems, students are taught to scale down the reactor, dilute the reactants and/or bed with inert materials, and vary the flow rates of the reactants. While all of these techniques to mitigate the heat generation in a reactor may work, they are merely solutions that only cover up the symptoms of a highly exothermic reaction, rather than removing the problem in the design of the reactor itself. In order to more effectively combat these problems, several different types of reactors have been developed to improve heat transfer within the reactor.

One of the most effective ways to remove heat from a reactor is to increase the heat transfer at the wall by changing the fluid that is contacting the wall and/or increasing the area of heat transfer. By changing the reactor design to include a large heat sink, the reactors are able to run highly exothermic reactions without temperature excursions (Fogler, 2009). Three examples of this kind of reactor are shown in Figure 1.

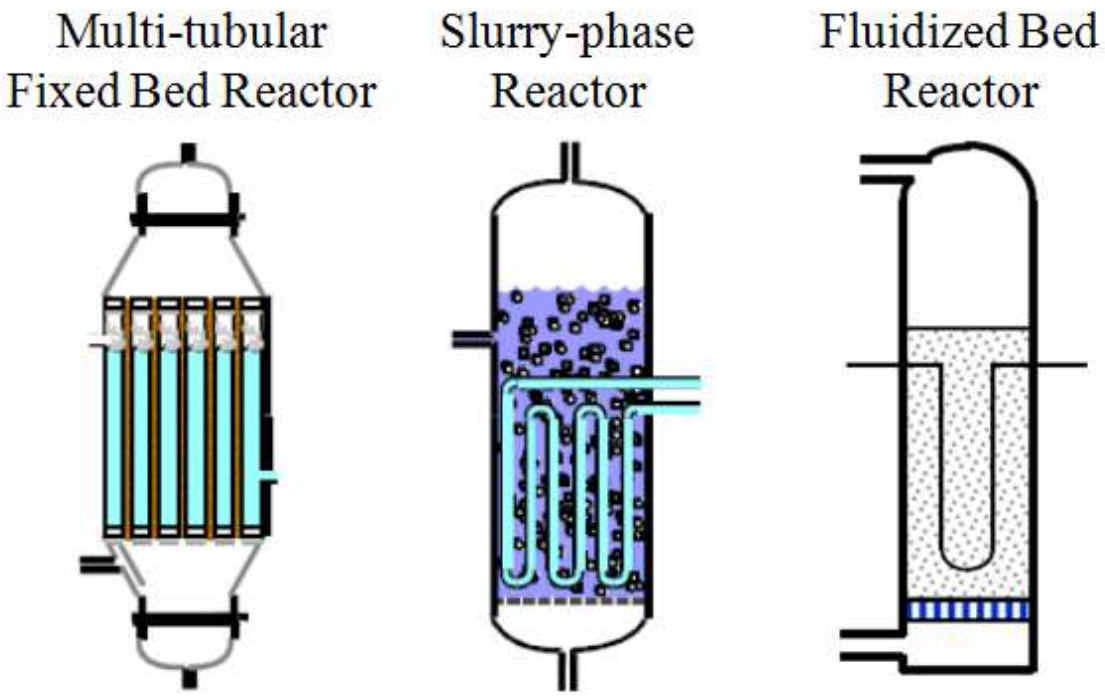

Figure 1. Three examples of reactors used for highly exothermic reactions (Jager, 2003).

The multi-tubular fixed bed reactor is able to dampen temperature spikes by increasing its surface in contact with a cooling fluid. This is accomplished by reducing the diameter of each individual tube filled with catalyst. The slurry-phase and fluidized bed reactors are also able to increase their heat transfer capabilities by including a large heat sink with higher heat transfer within the reactor design; liquid for the slurry-phase and a rapidly churned solid for the fluidized bed.

In addition to the above mentioned reactors, reactors utilizing a supercritical media, metal monolith catalyst structures, metallic foams, and micro-channel reactors have all been used in highly exothermic reactions. One common flaw between all of the aforementioned reactor designs is their difficulty and/or expense in scaling the reactor to the design criteria. Another

alternative reactor design takes scalability into account while still providing a high amount of heat transfer.

Consisting of a micron-sized network of fibers with entrapped catalyst particles, MFEC is able to improve heat and mass transfer properties when compared to a traditional packed bed. The media was developed by Dr. Tatarchuk's research group at Auburn University in the 1980s. For highly exothermic reactions, metallic fibers would form the sheet of MFEC, but polymer and ceramic fibers have been utilized for other applications as well.

The MFEC media is prepared through a wet-lay process. The fibers of choice are mixed with cellulose in water then subsequently wet-laid. Depending on the final application, catalyst particles, absorbents, or dispersants may be added during the wet-lay process. The sheet is then dried, oxidized to remove the cellulose, and finally sintered in a furnace. Figure 2 is an example of what a copper MFEC sheet looks like that has been made of copper fibers.

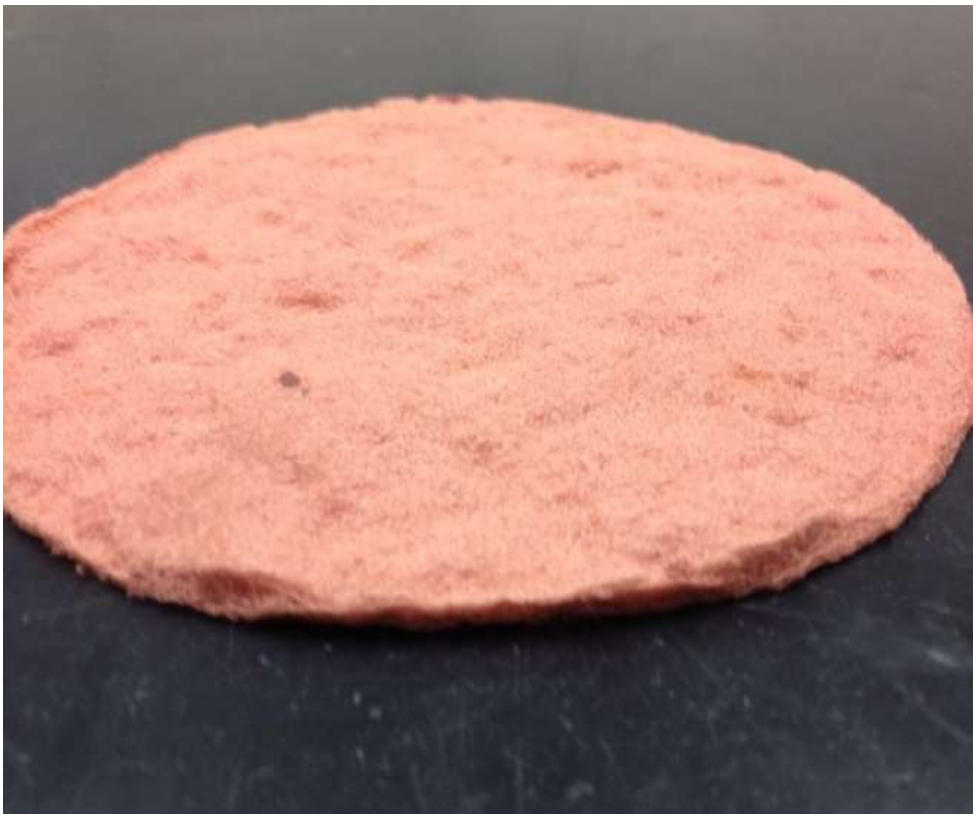

Figure 2. Example of a copper MFEC sheet after sintering, prior to catalyst entrapment.

Upon completion of the MFEC media, the catalyst or absorbent of choice can be entrapped within the media. This is accomplished by using small catalyst particles (50-250 μm in diameter) that can be gently shook into the void spaces between the fibers. The media is subsequently compressed to ensure the particles remain trapped within the matrix of fibers, as shown in Figure 3.

Figure 3. SEM of copper MFEC with 149-177µm particles entrapped in 12µm copper fibers.

It should be noted that while the MFEC appears to be dense, it is actually mostly void space. A typical void amount for MFEC is 90% void, but can reach as high as 98%. This in turn allows for minimal pressure drop across the MFEC bed.

As mentioned before, the MFEC has enhanced heat transfer characteristics compared to that of a packed bed. This makes good sense since the MFEC can be composed of metallic fibers, which would inherently have a higher thermal conductivity. Studies have been done to quantify the effective thermal conductivity of the MFEC for various metallic fibers (Sheng, Yang, Cahela, & Tatarchuk, Novel catalyst structures with enhanced heat transfer characteristics, 2011), and the results are shown in Table 1. Interestingly, as the flow rate through the media is increased, the effective thermal conductivity increases as well due to a combination of the

convective and conductive heat transfer pathways. As can be seen, the copper MFEC has an effective thermal conductivity of roughly 56 times that of a traditional packed bed in stagnant conditions, and roughly 215 times under flowing conditions. This large increase in thermal conductivity suggests that MFEC will be efficient at removing heat from highly exothermic reactions.

Table 1. Effective thermal conductivities of various MFEC media

Packing Material	**Voidage**	**Thermal Conductivity (W/mK), Re = 0**	**Thermal Conductivity (W/mK), Re = 4**
Alumina Packed Bed	0.36	0.16	0.21
SS MFEC	0.76	1.09	2.2
Ni MFEC	0.77	3.77	12.1
Cu MFEC	0.85	9.05	45.2

1.2 Previous Research with Microfibrous Entrapped Catalysts

Previous work by Sheng et al. (Sheng, et al., High conductivity catalyst structures for applications in exothermic reactions, 2012) studied Fischer-Tropsch synthesis (FTS), which is governed by Eqn. (1), with a ΔH_R = -165 kJ/mol (Kölbel & Ralek, 1980).

$$nCO_{(g)} + (2n+1)H_{2(g)} \leftrightarrow C_nH_{2n+2(g)} + nH_2O_g \qquad \text{Eqn. (1)}$$

Additionally, the products from FTS can be modeled by the Anderson-Schulz-Flory (ASF) product distribution (Friedel, 1950) as shown by Eqn. (2). The α-value was later determined

experimentally to be strongly temperature dependent as proposed by Song et al. (Song, Ramkrishn, Trinh, & Wright, 2004) in Eqn. (3).

$$x_n = (1-\alpha)\alpha^{n-1} \qquad \text{Eqn. (2)}$$

$$\alpha = \left(0.2332\frac{x_{CO}}{x_{CO}+x_{H_2}} + 0.6330\right)[1 - 0.0039(T-533)] \qquad \text{Eqn. (3)}$$

It was due to the highly exothermic nature of FTS, as well as its strong product temperature dependence, that microfibrous entrapped catalysts (MFEC) were used in a reactor in an attempt to control the temperature in a manner that was superior to a packed bed. While running FTS at a wall temperature of 255°C, Figure 4 shows the temperature profiles of a packed bed, while Figure 5 shows the temperature profiles for a MFEC bed. As can be seen, the MFEC bed allows for a nearly uniform temperature profile, and does not form the hot spot that appears in the packed bed run.

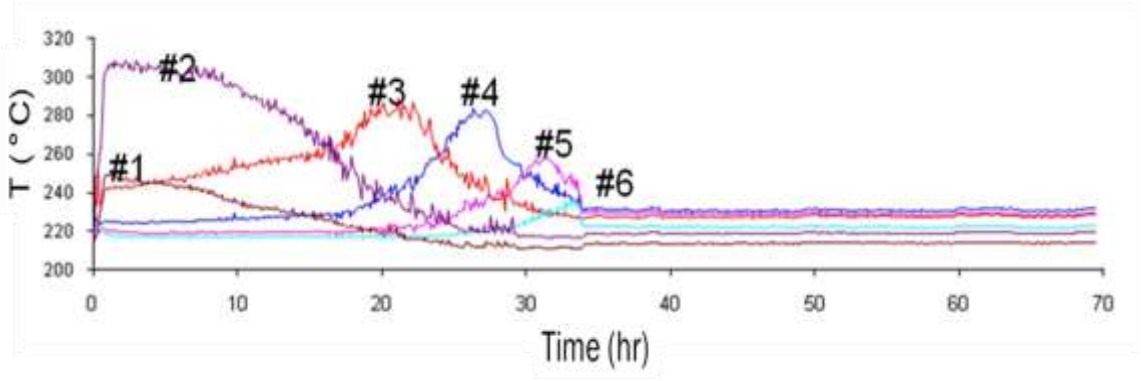

Figure 4. Temperature profiles inside a packed bed of Co/Al_2O_3 catalyst running FTS, ID = 15mm, T = 255°C, P = 20 bar, H_2:CO ratio of 2:1, GHSV = 5000/h

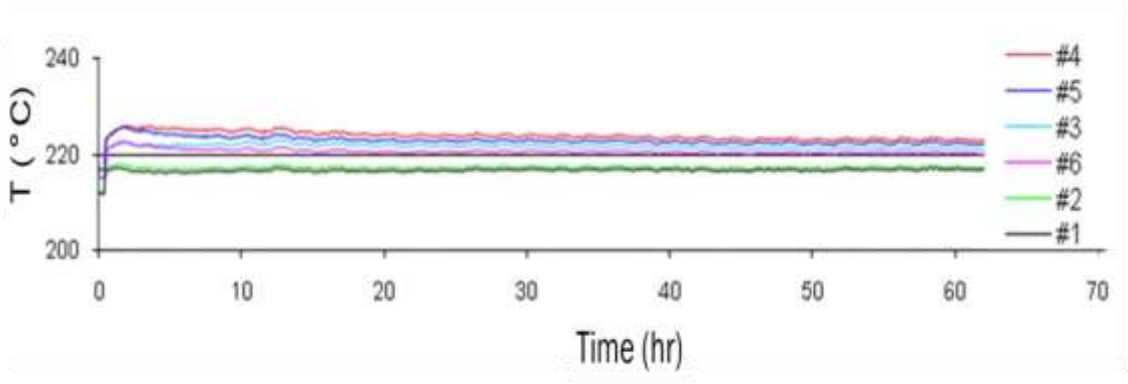

Figure 5. Temperature profiles inside a MFEC Bed of Co/Al_2O_3 catalyst running FTS, ID = 15mm, T = 255°C, P = 20 bar, H_2:CO ratio of 2:1, GHSV = 5000/h

The ability of the MFEC bed to effectively remove temperature deviations along the reactor bed at various wall temperatures is depicted in Figure 6.

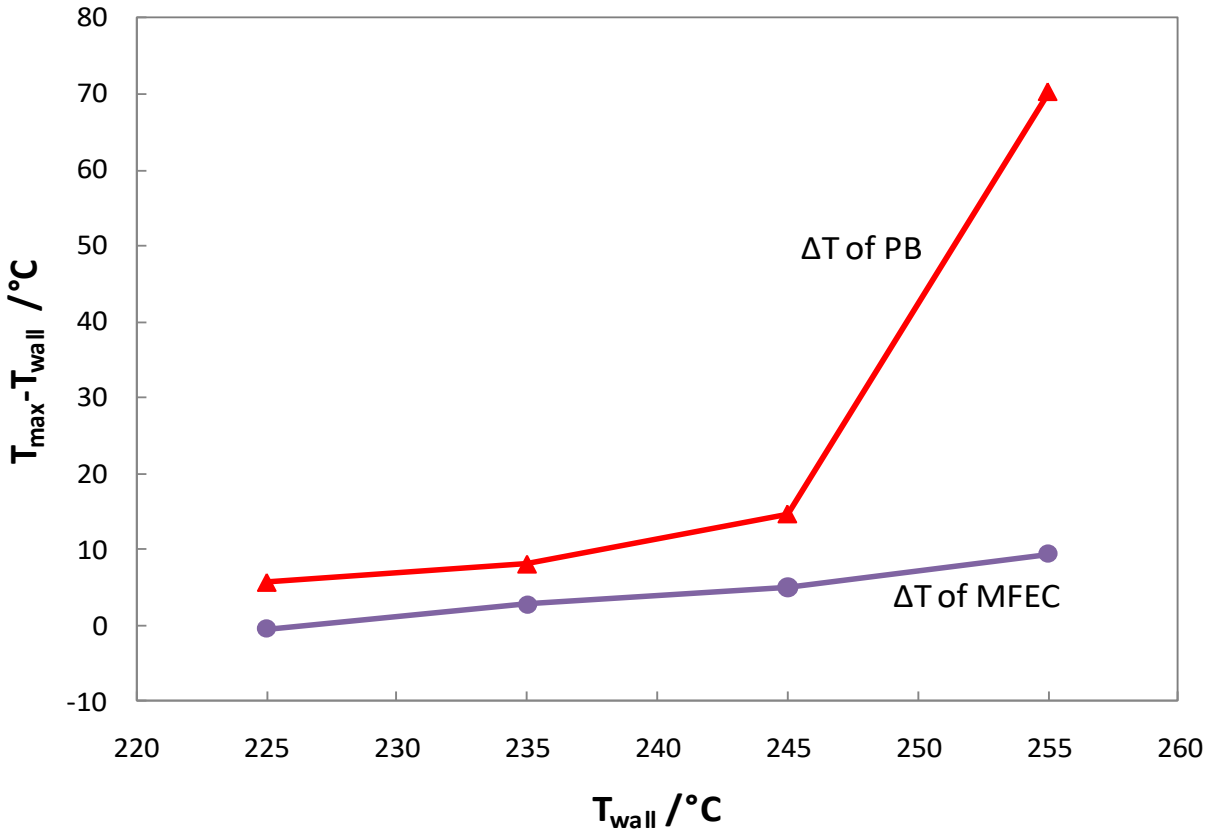

Figure 6. Max temperature deviations along the centerline to the wall for a FTS reaction using Co/Al_2O_3 catalyst, ID = 15mm, P = 20 bar, H_2:CO ratio of 2:1, GHSV = 5000/h

In addition to maintaining nearly uniform temperature profiles when compared to the packed bed, the MFEC was also able to fine tune the products by varying the α-value. While changing the wall temperature and maintaining a uniform temperature profile, product composition can be modified to a more desirable alkane distribution. This is an ability that is lacking in a packed bed design as shown in Figure 7, since it cannot maintain a higher α-value.

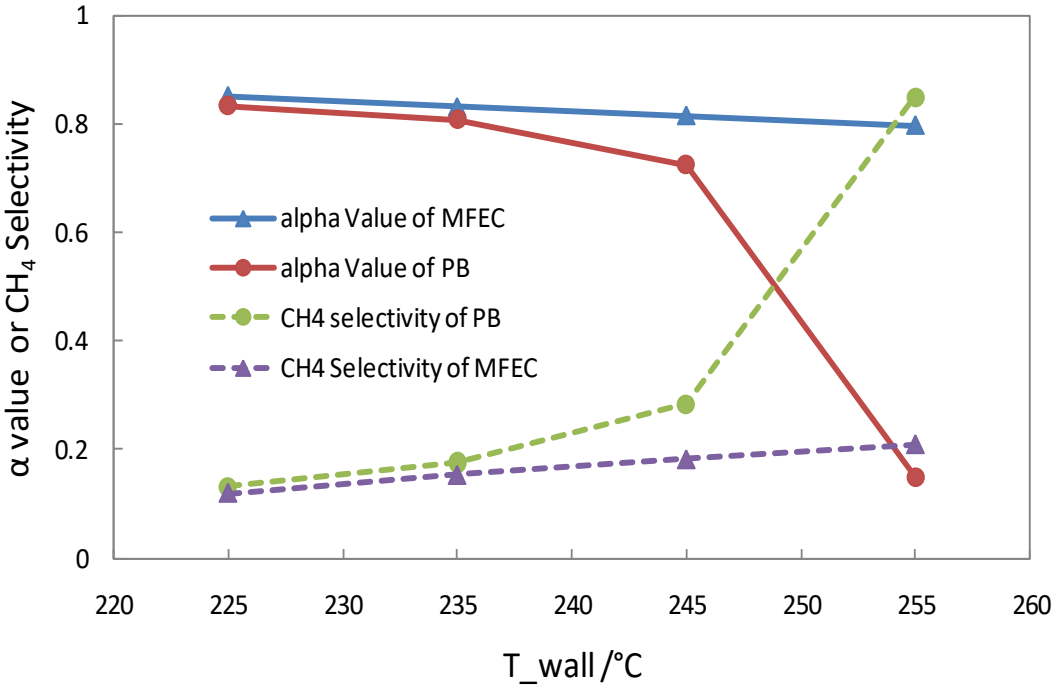

Figure 7. Methane selectivities and α-values for FTS runs with a Co/Al_2O_3 catalyst at various wall temperatures, ID = 15mm, P = 20 bar, H_2:CO ratio of 2:1, GHSV = 5000/h

The reactor was then scaled up to a 41mm ID, and run with the same catalyst. The packed bed reached a maximum temperature deviation of 464°C at a wall temperature of 185°C, whereas the MFEC only had a maximum temperature deviation of 6.4°C at a wall temperature of 245°C. This indicated that the MFEC was able to effectively remove heat from a highly exothermic reaction, and allowed for the scale-up of the reactor size.

The results of these studies led to more questions about the MFEC reactor, and how it could be applied in other ways. Not only did we want to understand what occurred in the reactor at a more fundamental level, but also what industrial applications to which it could be applied. In particular, a focus on process intensification with a goal of producing a single liquid product was maintained.

1.3 Goal of Research

The initial research of the group has shown that MFEC has a potential use in highly exothermic and/or endothermic reactions. Based on this knowledge, it is the purpose of this research to expound upon the interaction of the catalysts and the network of metallic fibers, while also finding new and exciting uses for MFEC. In particular, the goal of this research is to develop a reactor that can be taken to a remote location and convert syngas into a single liquid product (due to being easily transported). The reaction that will be studied in this dissertation is single-step dimethyl ether synthesis.

The focus of this research is on single-step dimethyl ether synthesis due to its potential ability to allow for many levels of process intensification. In no particular order, single-step dimethyl ether synthesis fits this role when combined with a MFEC reactor because it: overcomes heat generation problems, overcomes mass transfer limitations, has less pressure drop than a PB, uses a single reactor to convert syngas to DME, overcomes the equilibrium limitations of methanol synthesis, and it is hypothesized to increase conversion and selectivity.

Chapter 2: Equilibrium Calculations for Methanol and Dimethyl Ether Synthesis

2.1 Literature on Equilibrium Studies

Many papers in literature that research single-step dimethyl ether synthesis refer to the well documented limitation on methanol synthesis. This limitation is an upper limit on the maximum obtainable conversion of carbon monoxide into methanol due to equilibrium constraints. In order to overcome this limitation, it has been suggested and shown that directly converting methanol into dimethyl ether within the same reactor increases the overall conversion of carbon monoxide into dimethyl ether. Unfortunately, these aforementioned literature all seem to reference one slide from a conference proceeding for the equilibrium calculations that back up this phenomena. Even then, the slide in question simply shows equilibrium curves without any insight into how they were obtained. In order to gain more insight into these curves, in-house calculations for equilibrium were performed using iterative processes with MatLab.

2.2 Equilibrium Calculations

In order to calculate the equilibrium conversions of carbon monoxide to various products, a few fundamental equilibrium equations must be utilized. Eqn. (4) is used to solve for the equilibrium constant (K) as a function of temperature and the Gibbs free energy. To solve for the Gibbs free energy, Eqn. (5) is used. Similarly, the enthalpy of the reaction is solved for using Eqn. (6).

$$K = exp\left(\frac{-\Delta G}{RT}\right) \qquad \text{Eqn. (4)}$$

$$\Delta G_{ref} = \left(\sum \gamma_i \Delta G^{\circ}_{f,products}\right) - \left(\sum \gamma_i \Delta G^{\circ}_{f,reactants}\right) \qquad \text{Eqn. (5)}$$

$$\Delta H_{ref} = \left(\sum \gamma_i \Delta H^{\circ}_{f,products}\right) - \left(\sum \gamma_i \Delta H^{\circ}_{f,reactants}\right) \qquad \text{Eqn. (6)}$$

The above reactions are then combined together to solve for the Van't Hoff equation, as shown in Eqn. (7). The result of Eqn. (7) gives the equilibrium constant of the reaction at a set temperature.

$$K_{eq,\ T} = K_{eq,\ T_{ref}} \cdot exp\left(\frac{-\Delta H_{ref}}{R}\left[\frac{1}{T} - \frac{1}{T_{ref}}\right]\right) \qquad \text{Eqn. (7)}$$

Additionally, the equilibrium constant can be solved as a function of the activities of the products and reactants, as shown in Eqn. (8).

$$K_{eq,\ T} = \frac{\Pi \hat{a}_{i,\,products}^{(stoich.\ coeff)}}{\Pi \hat{a}_{i,\,reactants}^{(stoich.\ coeff)}} = \frac{\Pi \left(y_{i,\,products} P\right)^{(stoich.\ coeff)}}{\Pi \left(y_{i,\,reactants} P\right)^{(stoich.\ coeff)}} \qquad \text{Eqn. (8)}$$

To solve the equilibrium conversion of carbon monoxide, the iterative steps shown in Table 2 were implemented using MatLab. The code for each individual reaction is shown in the appendix, in subsections i, ii, iii, iv, v, vi, vii, and viii.

Table 2. Logic chart for equilibrium calculations using MatLab

Step Number	**Task of Step**
1	Solve for ΔG_{Ref} using Eqn. (5)
2	Solve for ΔH_{Ref} using Eqn. (6)
3	Solve for K_{Ref} using Eqn. (4)Eqn. (7)
4	Solve for K_1 using Eqn. (7)
5	Set initial extent of reaction to be equal to zero
6	Solve for K_2 using Eqn. (8)
7	If $\lvert K_1 - K_2 \rvert > 0.0001$, then add 0.00001 to the extent of reaction
8	Repeat steps 6-7 until $\lvert K_1 - K_2 \rvert \leq 0.0001$

In order for MatLab to solve Eqn. (5) and Eqn. (6), reference values for individual compounds were needed. Those values are shown in.

Table 3. Gibbs energy of formation and standard enthalpy of formation for various compounds

Component	**Gibbs Energy of Formation at 298.15 K (J/mol)**	**Standard Enthalpy of Formation at 298.15K (J/mol)**
Carbon Monoxide	-137,169	-110,525
Carbon Dioxide	-394,359	-393,509
Methanol	-161,960	-74,520
Dimethyl Ether	-112,900	-184,100
Hydrogen	0	0
Water	-228,600	-241,800

2.3 Results of Equilibrium Calculations

The simulated results for the equilibrium conversion from carbon monoxide to methanol are shown below in Figure 8. As expected for a reaction that is a net reduction in the number of moles, the reaction is highly dependent on pressure. Further, the reaction has a strong dependence on temperature, with increasing temperatures corresponding to losses in carbon monoxide conversion.

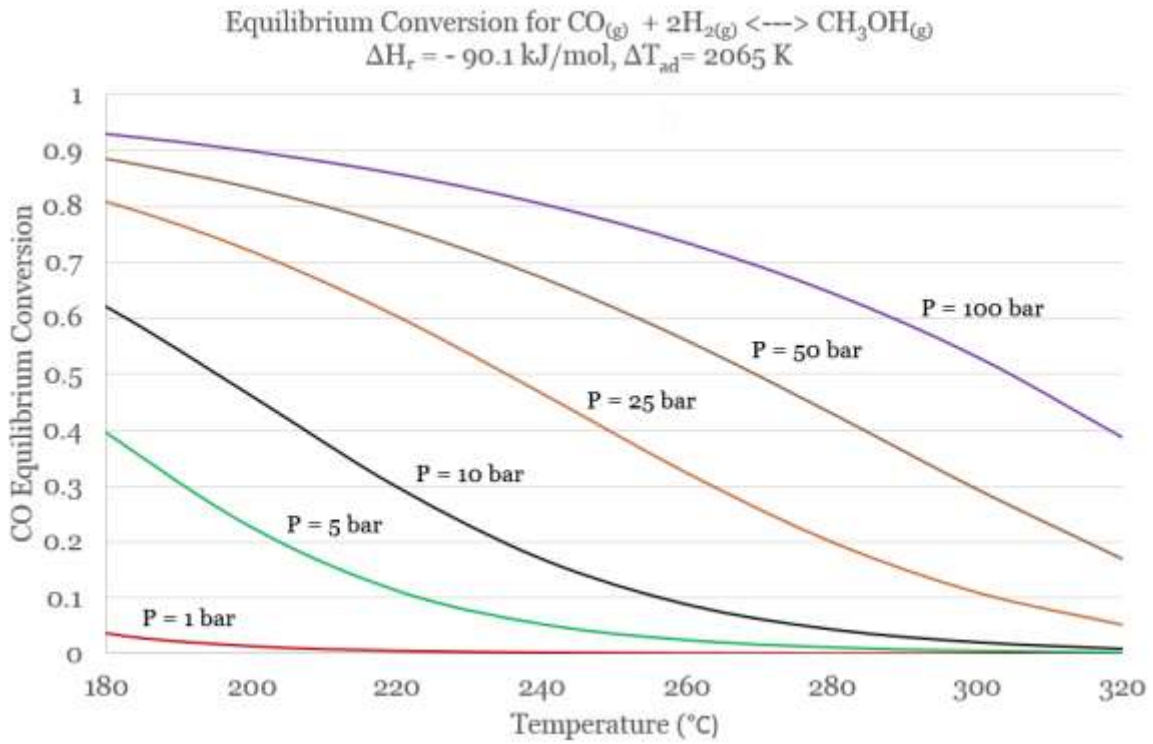

Figure 8. Effect of temperature and pressure on the equilibrium conversion of carbon monoxide to methanol.

The simulated results for the equilibrium conversion of methanol to dimethyl ether are shown below in Figure 9. As expected, the reaction has zero dependence on pressure due to having no change in moles. However, the reaction does still have a slight dependence on temperature, with higher temperatures corresponding to a loss in conversion.

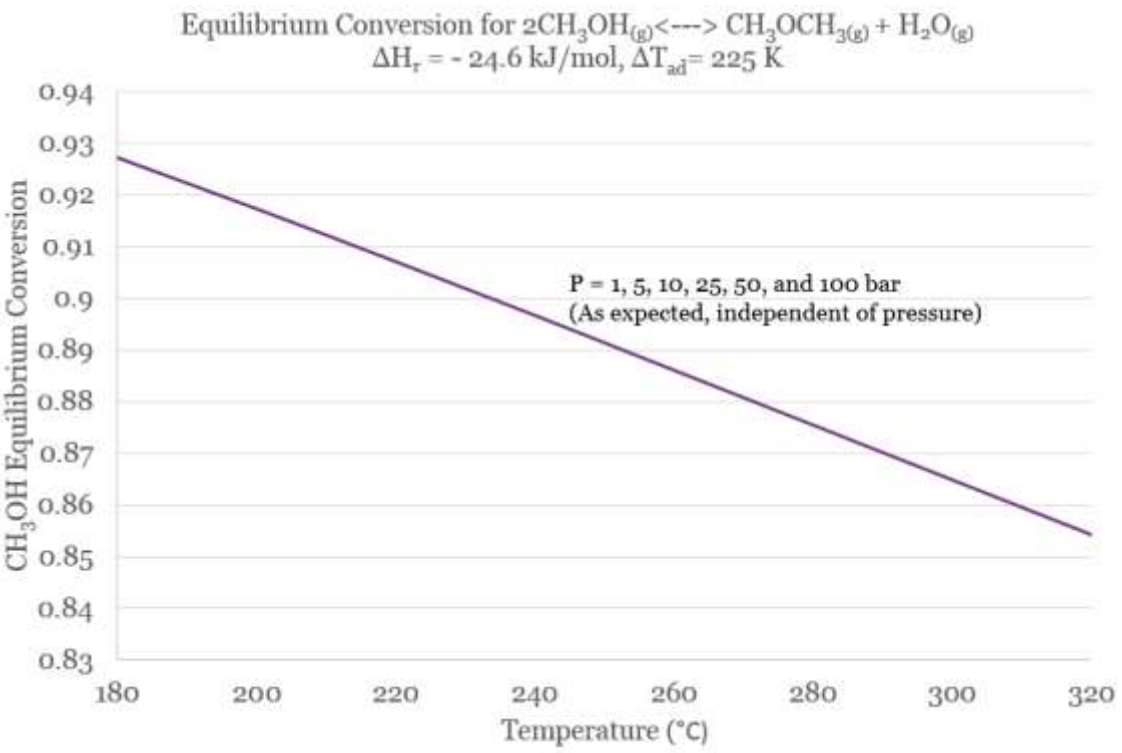

Figure 9. Effect of temperature and pressure on the equilibrium conversion of methanol to dimethyl ether.

The simulated results for the equilibrium conversion of carbon monoxide to carbon dioxide through the water-gas shift reaction are shown below in Figure 10. As expected for a reaction that has no change in the number of moles, the reaction has zero dependence on pressure. However, the reaction does still have a slight dependence on temperature, with higher temperatures corresponding to a loss in conversion.

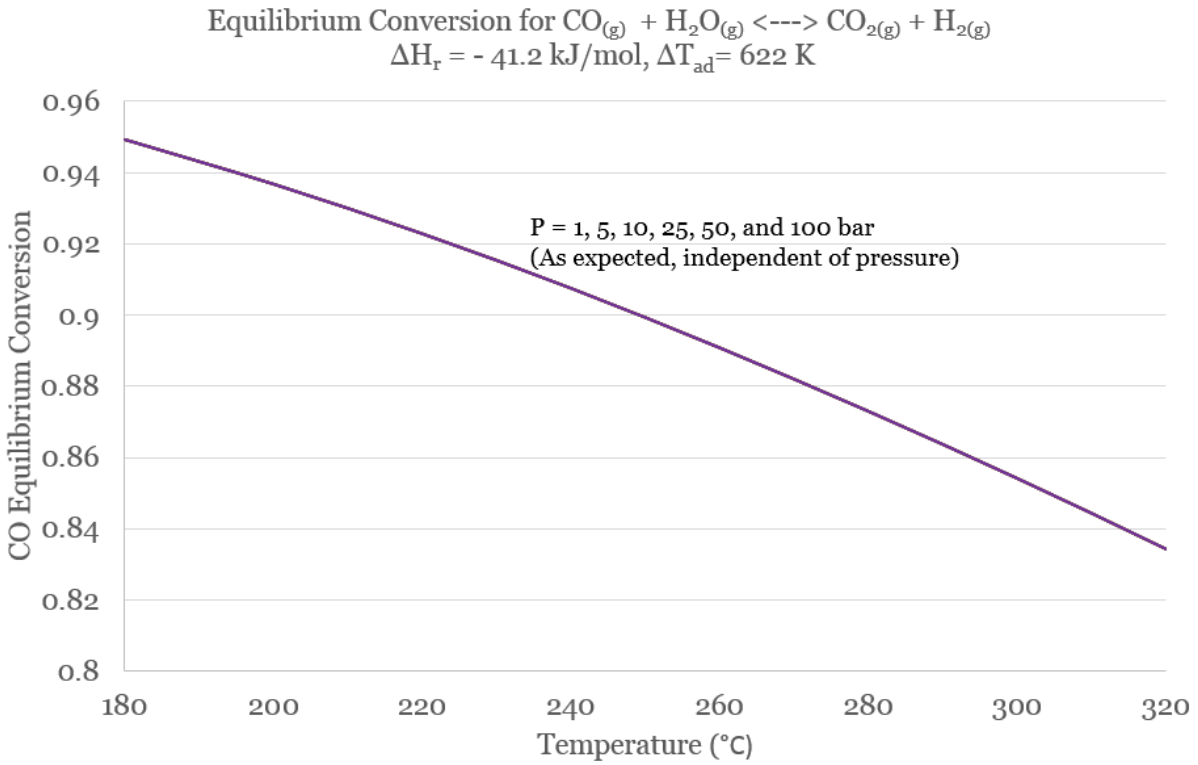

Figure 10. Effect of temperature and pressure on the equilibrium conversion of carbon monoxide to carbon dioxide through the water-gas shift reaction

The simulated results for the equilibrium conversion of carbon monoxide to dimethyl ether in a single step are shown below in Figure 11. Despite having a reduction in the total number of moles, the pressure dependence is not as severe as the methanol synthesis reaction alone. Additionally, the reaction still has a strong dependence on temperature.

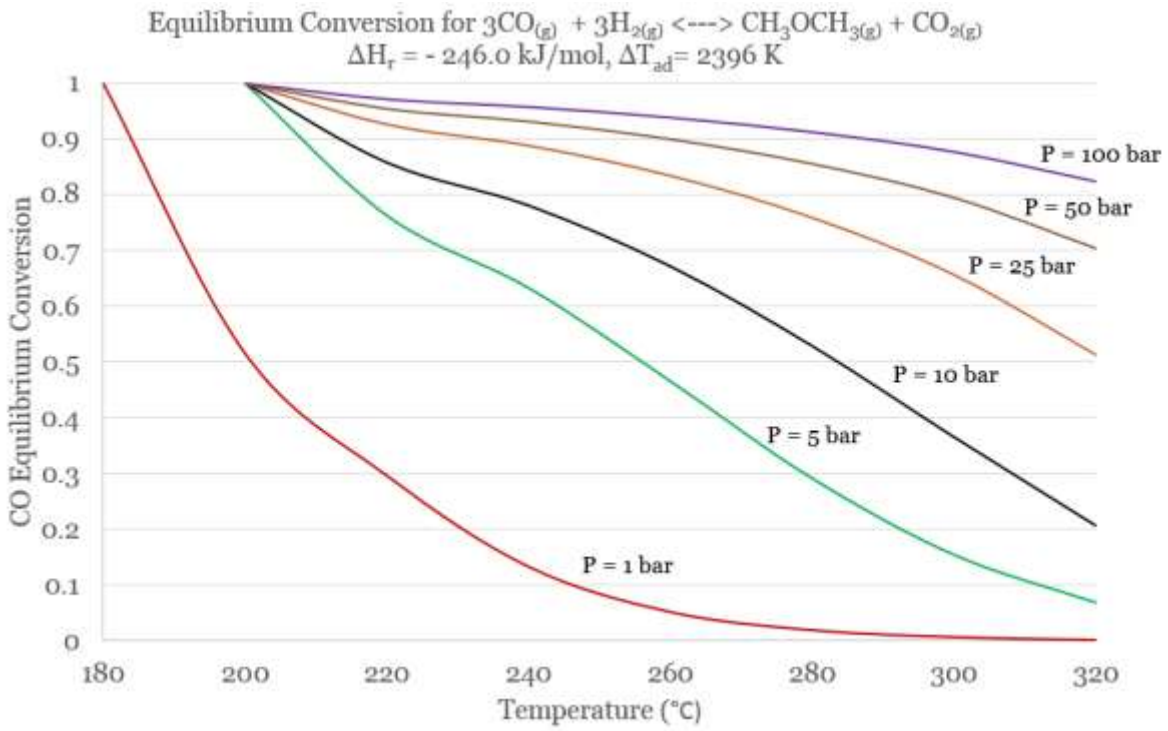

Figure 11. Effect of temperature and pressure on the equilibrium conversion of carbon monoxide to dimethyl ether with methanol being an intermediate product

In order to fully see the impact of combining the methanol synthesis reaction and subsequent conversion of methanol to dimethyl ether in the same reactor, the overall carbon monoxide conversions for each scenario are shown in Figure 12. The two solid lines in the upper portion of the graph correspond to the carbon monoxide conversion for the single-step process. For clarification, the single-step process refers to conversion of carbon monoxide to methanol then to dimethyl ether in the same reactor. As can be seen, even the lower pressure single-step process outperforms the higher pressure two-step process. In order to generate the two-step process lines, the maximum conversions from each individual step were multiplied together to find the overall maximum possible conversion.

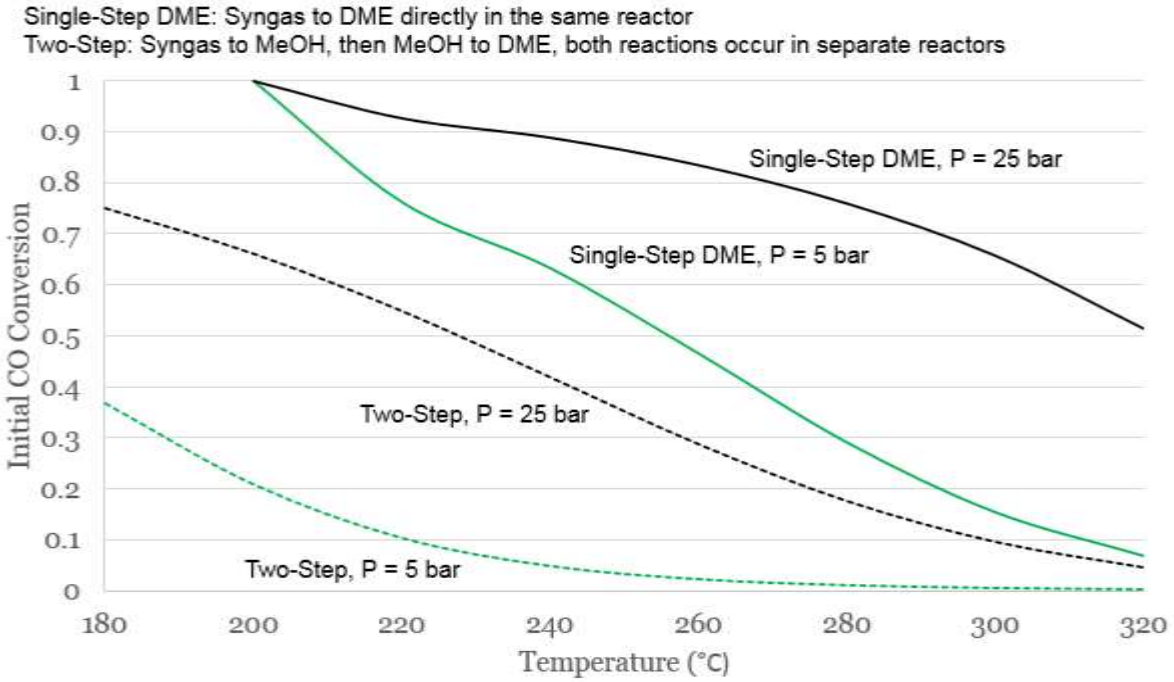

Figure 12. Effect of combining the methanol synthesis and dimethyl ether synthesis reactions in a single reactor compared to that of separate reactors.

Chapter 3: Methanol Synthesis

3.1 Relevant Reactions and Industrial Production

Methanol is formed through the hydrogenation of carbon monoxide over a metal catalyst as shown in Eqn. (9).

$$CO_{(g)} + 2H_{2(g)} \leftrightarrow CH_3OH_{(g)} \quad \text{Eqn. (9)}$$

With a heat of reaction of ΔH_R = -91 kJ/mol (Bos, Borman, Kuczynski, & Westerterp, 1989), methanol synthesis is a reaction that must be run in a system that is able to control the large amount of heat generation. Unfortunately, the formation of methanol must also compete with the water-gas shift reaction as shown in Eqn. (10), and the formation of n-alkanes as shown in Eqn. (11).

$$CO_{(g)} + H_2O_{(g)} \leftrightarrow CO_{2(g)} + H_{2(g)} \quad \text{Eqn. (10)}$$

$$nCO_{(g)} + (2n+1)H_{2(g)} \leftrightarrow C_nH_{2n+2(g)} + nH_2O_{(g)}, 1 \leq n \leq 10 \quad \text{Eqn. (11)}$$

To account for just the formation of methane, Eqn. (11) can be rewritten to equate n = 1, as displayed in Eqn. (12).

$$CO_{(g)} + 3H_{2(g)} \leftrightarrow CH_{4(g)} + H_2O_{(g)} \quad \text{Eqn. (12)}$$

The three main factors in active catalysts for methanol synthesis are to nondissociatively adsorb carbon monoxide, the catalysts must also be a decent hydrogenation catalyst, and the catalysts need to allow for the hydrogenation of both ends of the carbon monoxide molecule

(Klier, 1982). As determined by Broden et al. (Brodén, Rhondin, Brucker, Benbow, & Hurych, 1976), Table 4 shows which elements will nondissociatively adsorb carbon monoxide as a function of temperature. The elements to the left of the line will dissociatively adsorb carbon monoxide, while those to the right will nondissociatively adsorb carbon monoxide.

Table 4. At ambient temperatures, elements to the left of the blue line dissociatively adsorb carbon monoxide while those to the right of the nondissociatively adsorb carbon monoxide. The red line shows the type of carbon monoxide absorption for 200-300°C (Brodén, Rhondin, Brucker, Benbow, & Hurych, 1976).

6B	7B	8B			1B
Cr	Mn	Fe	Co	Ni	Cu
Mo	Tc	Ru	Rh	Pd	Ag
W	Re	Os	Ir	Pt	Au

A study using a 50/50 isotopic mixture of $^{13}C^{16}O$ and $^{12}C^{18}O$ confirmed the theory that the main mechanism for methanol formation is through the nondissociative adsorbtion of carbon monoxide on the surface of the catalyst (Takeuchi & Katzer, 1981). Consequently, the type of carbon monoxide adsorption that occurs is critical in determining whether the final product will be an oxygenate or otherwise. Further, this helps explain the importance of temperature control in the reactor. As the reactor temperature increases, carbon monoxide will dissociatively adsorb on the catalyst surface, resulting in the formation of methane. Literature also confirms a rapid loss in catalytic activity of the catalyst at temperatures above 300°C (Matulewicz, Keijser, Mol, & Kapteijn, 1984).

The industrial production of methanol is one of the most important industrial processes since it currently is one of the top five most shipped chemicals (by volume) annually (Montebelli, Visconti, Groppi, Tronconi, & Kohler, 2014). As one of the simplest oxygenated compounds, methanol can be used as a chemical building block to form many higher valued oxygenates. It can also be utilized as an intermediate to the production of alkanes and alkenes. Additionally, methanol can be used independently as a form of fuels for a wide variety of applications.

Early patents obtained by BASF detailed the production of methanol using a copper oxide based catalyst (United States Patent No. US1791568, 1923) and a chromium based catalyst (United States Patent No. US1569775, 1924). Both patents state that pressure should be at least 50 atm, and the temperature should be in the range of 200°C - 600°C. It was later determined that palladium, platinum, and iridium were also selective towards methanol (Poutsma, Elek, Ibarbia, Risch, & Rabo, 1978). After decades of further research, the catalyst that is now widely accepted as having the best catalytic performance is $Cu/ZnO/Al_2O_3$ (Klier, 1982), (Baltes, Vukojević, & Schüth, 2008), (Li & Inui, 1996), (Spencer, 1999). Despite this general consensus, recent studies have been conducted to look for a better catalyst. Various combinations of active metals and supports have been studied such as copper supported on Zr/Zn (Wang, Zuo, Han, & Wang, 2011), copper supported on Ce_{1-x}/Zr_xO_2 (Yoo, Lee, Kim, Moon, & Lee, 2013), and Au/ZnO (Strunk, et al., 2009) have all been shown to be selective towards methanol synthesis.

Modern industrial methanol synthesis is carried out in two main types of reactors. About 60% of reactors are quench adiabatic, while about 30% are quasi-isothermal (Milani, Khalilpour, Zahedi, & Abbas, 2015). In the quench reactor, a single bed of catalyst is diluted with an inert material and cold reactant/recycled syngas is injected at various locations. Typical reactor

conditions are 50-100 bar and 270°C (Spath & Dayton, 2003). The quasi-isothermal reactor is similar to a shell and tube design in which steam controls the reactor temperature. Typical conditions for this type of reactor ranges from 50-100 bar and 230-265°C (Spath & Dayton, 2003).

3.2 Experimental Setup

A stainless steel reactor was employed to run a MFEC reaction for methanol synthesis. A 15mm ID stainless steel tube with a wall thickness of 2.05 mm was utilized. A schematic of the overall reactor setup can be seen in Figure 13. For the methanol synthesis reaction only hydrogen, helium, and syngas was required. Each of these gases were controlled by mass flow controllers that were adjusted through a PLC (programmable logic controller). The pressure of the reaction was controlled manually through a back pressure regulator that is located physically after the reactor. After passing through the back pressure regulator, the effluent first passed through a hot trap that typically ran at a temperature of 150°C. The effluent then continued through a cooling unit and cold trap that typically ran at a temperature of 4°C. The remaining effluent that is still in the gas phase was then split to be analyzed in an online gas chromatograph before being vented. The GC was calibrated using pure compounds of all present species.

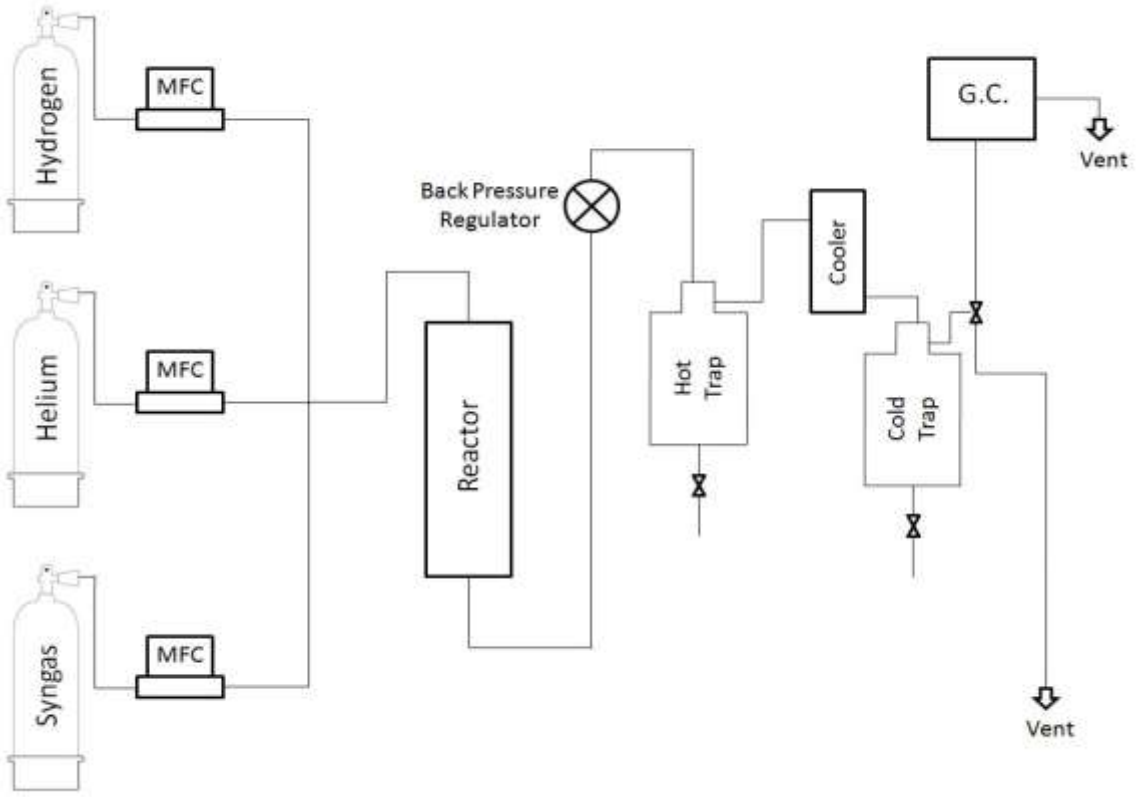

Figure 13. Schematic of the methanol synthesis experimental setup

In addition to controlling the flow rates of the reactants, the PLC also functioned as a temperature controller for the hot trap and reactor. It also recorded the temperature measurements that were obtained from inside the reactor. A thin sheath multipoint thermocouple (Omega, 316SS probe, k-type, 1.59mm OD, 0.15mm wall thickness, 6 measurement points spaced 25.4mm apart) was used to measure the temperature inside the reactor at 6 different points. The thermocouple itself has a low thermal mass and low axial thermal conductivity. The thermocouple was inserted across constant temperature baths at different points with the bathes differing in temperature by over 200 °C, and negligible conduction down the thermocouple was observed. A schematic of a reactor with the multipoint thermocouple in use is shown in Figure 14.

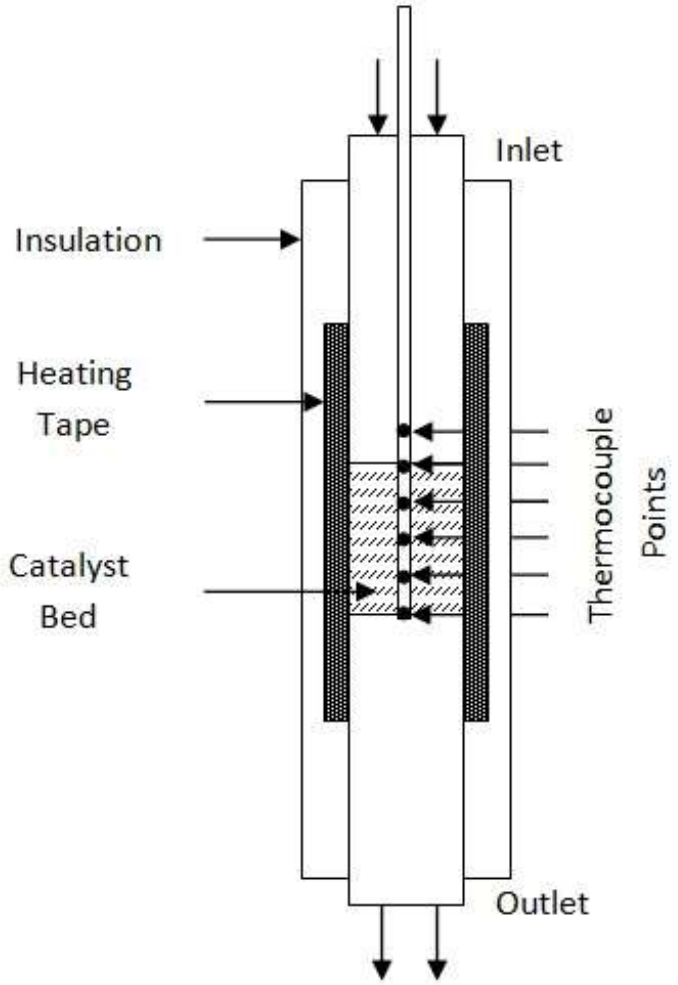

Figure 14. Schematic of a reactor utilizing a multipoint thermocouple

The temperature of the reactor itself was controlled by the PLC through the use of heating tape wrapped around the location of the catalyst bed inside the reactor. A thermocouple was inserted on the outside of the reactor in order to control the reactor wall temperature. The reactor was also wrapped with insulation to try and maintain a uniform reactor surface temperature. The tubing leading into and out of the reactor was also insulted to reduce heat losses to the surroundings.

3.3 Methanol Synthesis Results

Methanol synthesis via the reaction between carbon monoxide and hydrogen was carried out initially in a 15mm ID reactor. As can be seen from Figure 8, the effect of temperature on methanol synthesis directly relates to carbon monoxide conversion. Not only can an increase in temperature produce a drop in theoretical conversion of carbon monoxide, an increase in temperature also has the potential to form methane. If methane is present in the product stream, it can be an indirect way to know that a hot spot has developed within a reactor. The 15mm ID reactor was run at varying inlet temperatures (245°C, 275°C, 290°C) with a MFEC bed, and those profiles are shown in Figure 15, Figure 16, and Figure 17, respectively

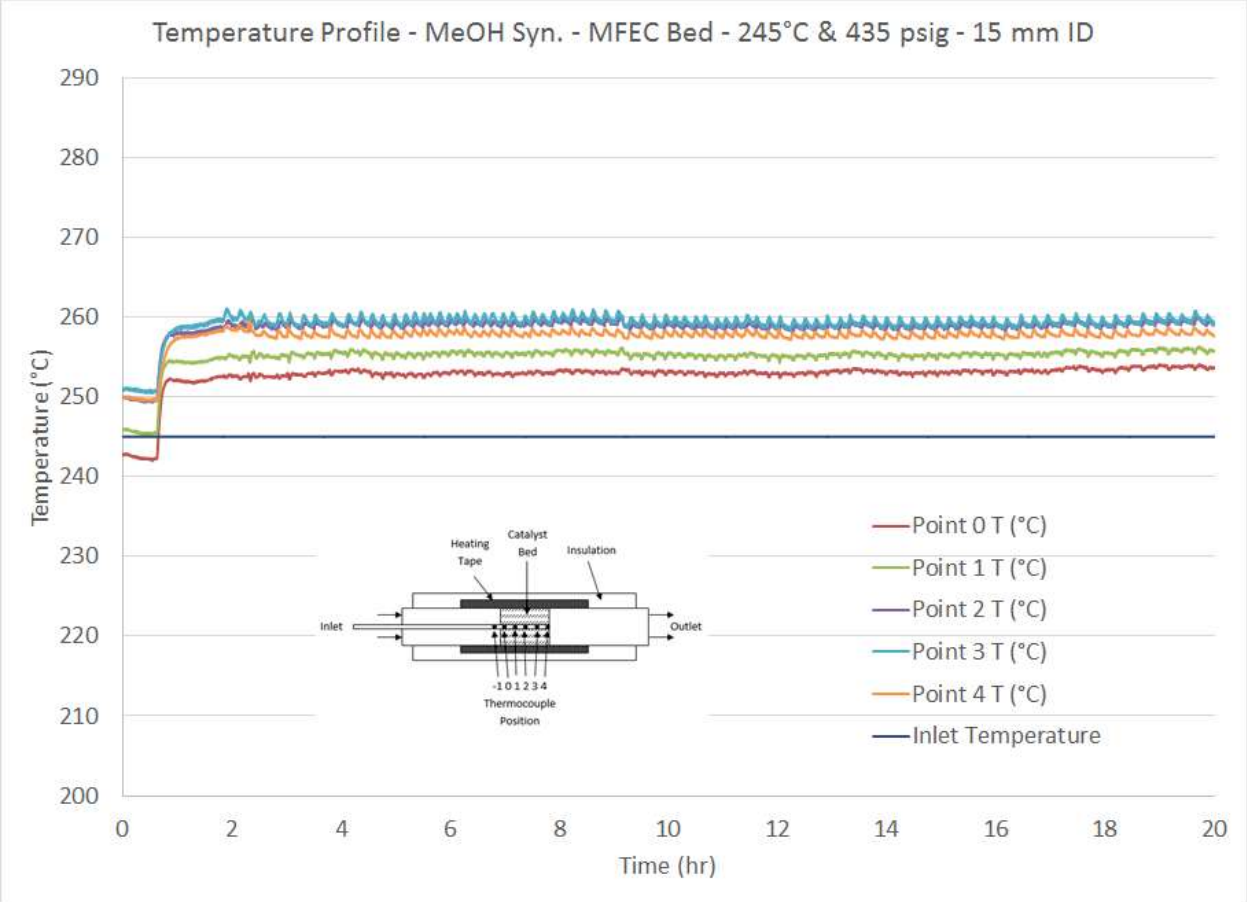

Figure 15. Temperature profile as a function of time for methanol synthesis with MFEC reactor conditions of ID=15mm, P=435psig, T_{Inlet}=26°C, H_2:CO ratio of 3:1, and GHSV=1880 h^{-1}. Catalyst (60-80 mesh, or 180-250 μm) is HiFuelR120

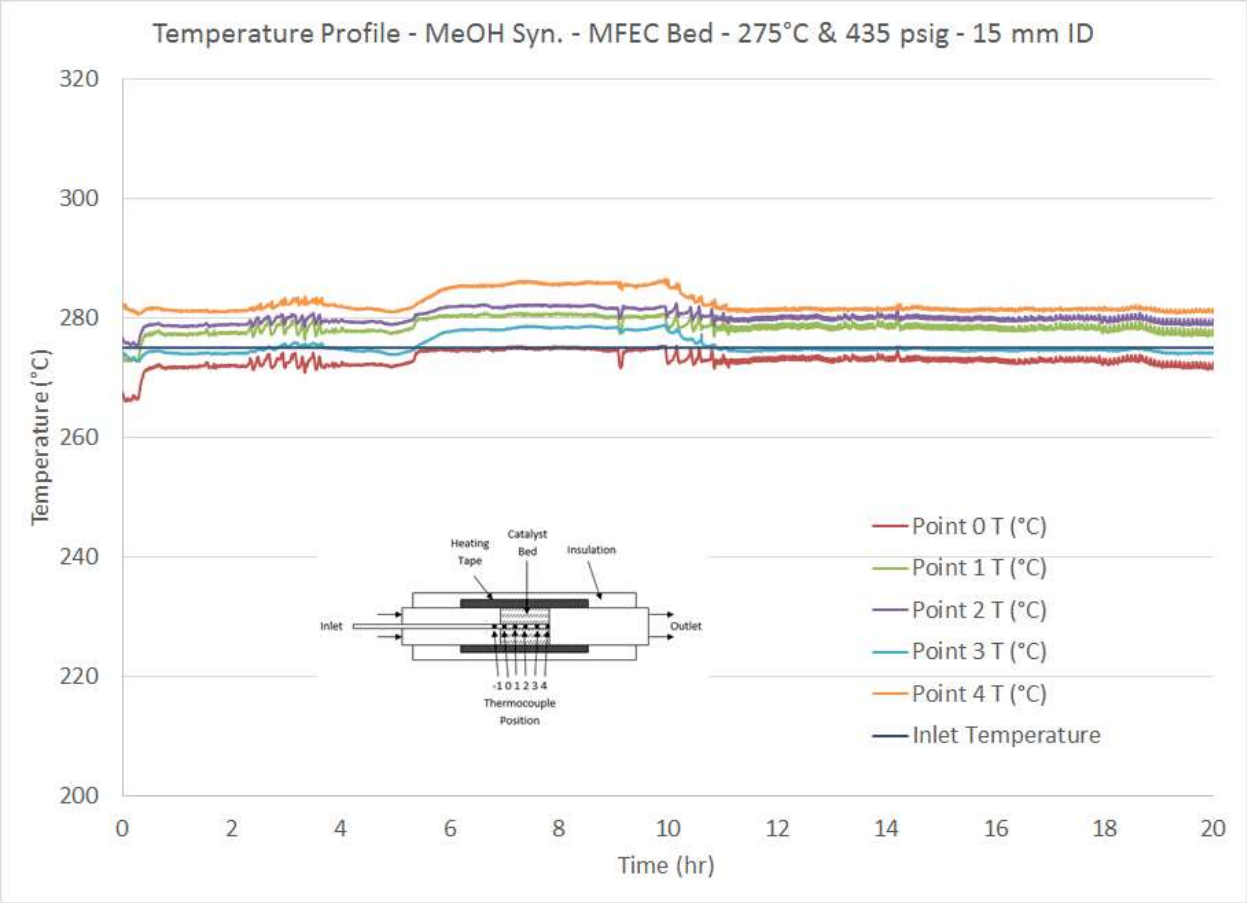

Figure 16. Temperature profile as a function of time for methanol synthesis with MFEC reactor conditions of ID=15mm, P=435psig, T_{Inlet}=275°C, H_2:CO ratio of 3:1, and GHSV=1880 h^{-1}. Catalyst (60-80 mesh, or 180-250 μm) is HiFuelR120

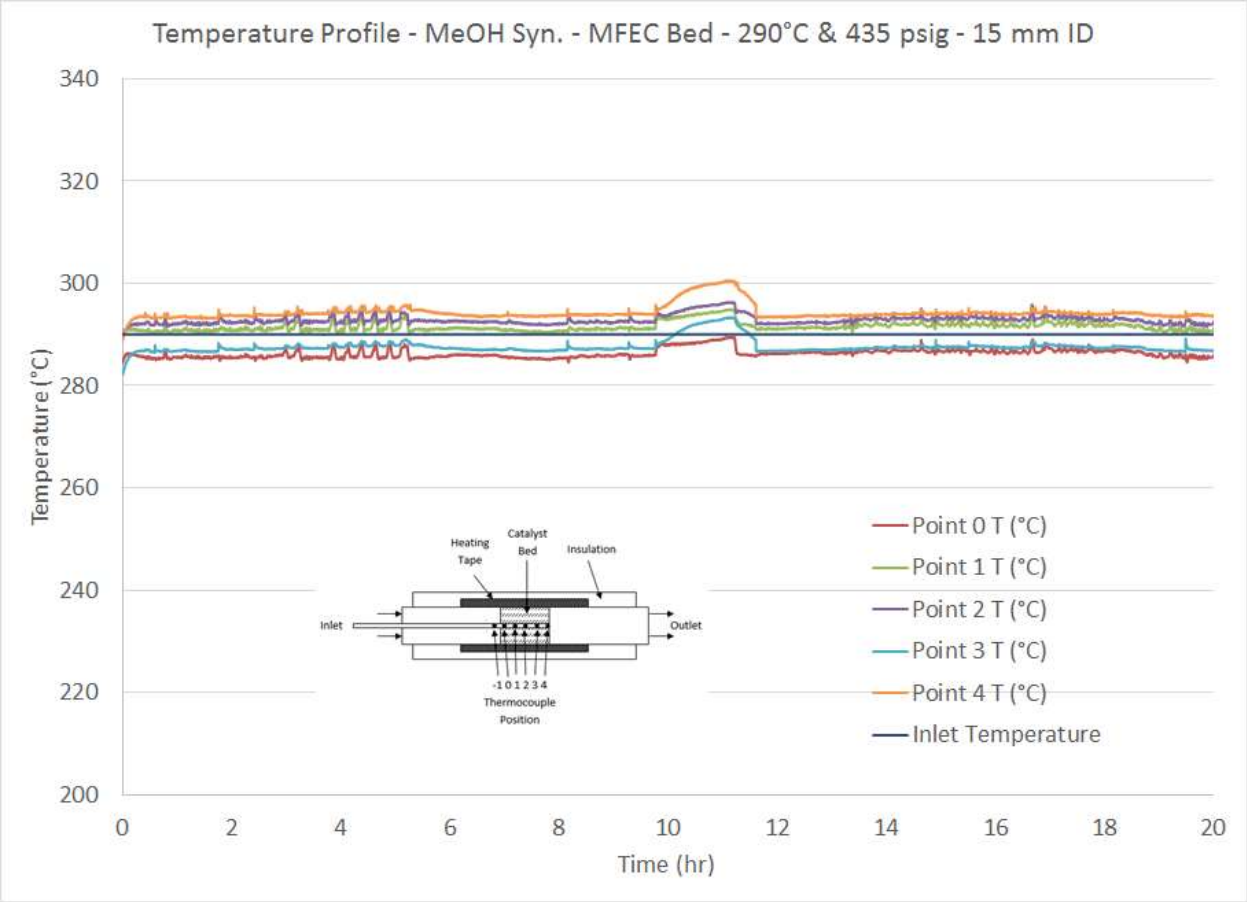

Figure 17. Temperature profile as a function of time for methanol synthesis with MFEC reactor conditions of ID=15mm, P=435psig, T_{Inlet}=290°C, H_2:CO ratio of 3:1, and GHSV=1880 h^{-1}. Catalyst (60-80 mesh, or 180-250 μm) is HiFuelR120

Since methanol synthesis does have a ΔH_R = -91 kJ/mol, each of the previous reactions do have an increase in the temperature of the centerline of the reactor. However, the deviation from the inlet temperature is not dramatic. In order to see what effect this temperature increase has on conversion, Figure 18 shows the carbon monoxide conversion for each of the inlet temperatures. Not surprisingly, the conversion is fairly low, as was expected due to equilibrium constraints. Since the purpose of this dissertation is to focus on the process intensification of a gas-to-liquid process, no further studies on methanol synthesis were done.

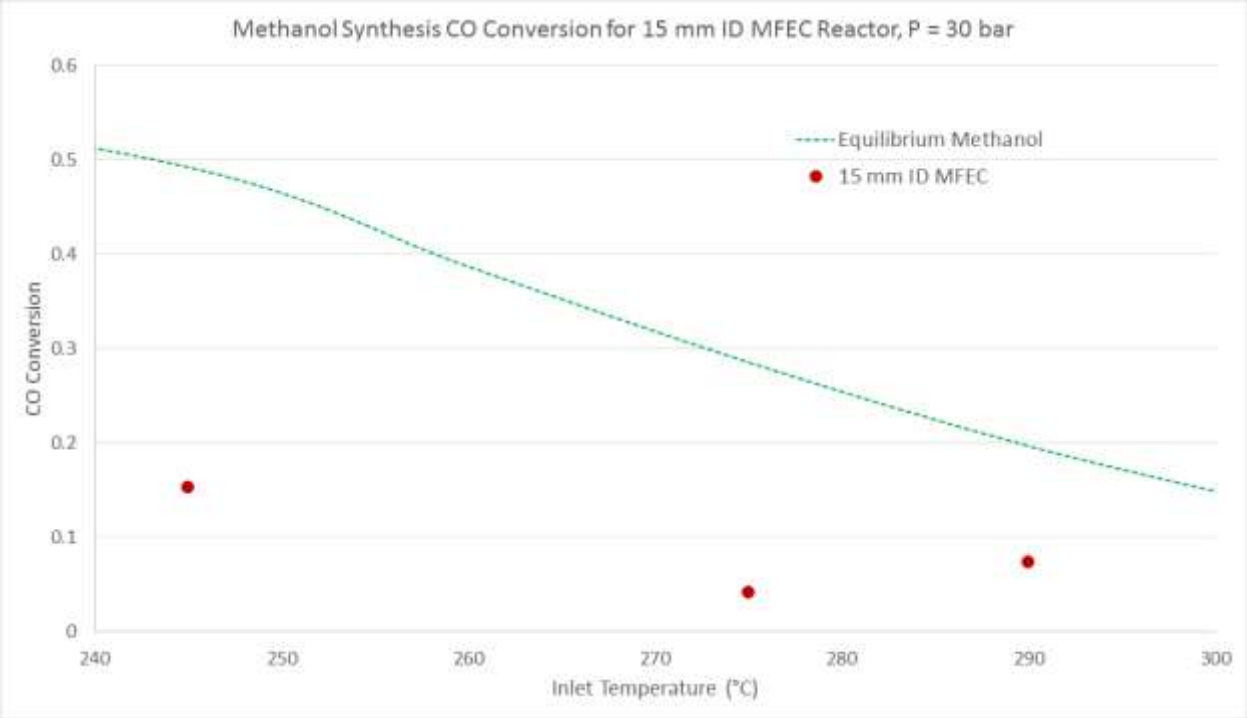

Figure 18. Overall carbon monoxide conversion for methanol ether synthesis at varying temperatures for the MFEC 15mm ID reactor with a H_2:CO ratio of 3:1, and GHSV=1880 h^{-1}. Catalyst (60-80 mesh, or 180-250 μm) is HiFuelR120.

Chapter 4: Dimethyl Ether Synthesis

4.1 Background Information and Industrial Production

Dimethyl ether is a product that was traditionally used as a propellant, but has more recently gained popularity as a potential fuel (Prasad, Bae, Kang, Lee, & Jun, 2008). Due to a low particulate emission and competitive cetane number, DME has been suggested for use in combustion-ignition engines (Arcoumanis, Bae, Crookes, & Kinoshita, 2008), (Omata, Watanabe, Umegaki, Ishiguro, & Yamada, 2002). Additionally, based on its similarity to LPG in properties, DME can potentially be used in most all LPG applications with little change to existing infrastructure (Semelsberger, Borup, & Greene, 2006). In addition to its individual uses, DME is also used as an intermediate in industrial processes such as the production of dimethyl sulfate, methyl acetate, and light olefins (Lei, Zou, Dai, Li, & Chen, 2011).

Dimethyl ether was traditionally produced via a two-step process. Initially, syngas was converted into methanol at a high pressure, and was later dehydrated through Eqn. (13) in a separate reactor to form dimethyl ether (Semelsberger, Borup, & Greene, 2006). It should be noted that the dehydration process is only slightly exothermic with a ΔH_R = -23 kJ/mol (Jamshidi, Barbosa, Nascimento, & Rodbari, 2013). This process was expensive due to the high pressure demands of methanol synthesis, and so an alternative single-step process was developed that combined both steps to directly convert syngas to DME in the same reactor (Bae, Potdar, Kang, & Jun, 2008).

$$2CH_3OH_{(g)} \leftrightarrow CH_3OCH_{3(g)} + H_2O_{(g)} \qquad \text{Eqn. (13)}$$

In the single-step process, Eqn. (9), Eqn. (10), and Eqn. (13) are linearly combined to give Eqn. (14). When these reactions all combine to form single-step dimethyl ether synthesis,

the net reaction is highly exothermic with a ΔH_R = -246 kJ/mol (Ogawa, Inoue, Shikada, & Ohno, 2003). Due to this high amount of heat generation, a reactor that is able to effectively remove heat from the bed is required.

$$3CO_{(g)} + 3H_{2(g)} \leftrightarrow CH_3OCH_{3_{(g)}} + CO_{2(g)} \qquad \text{Eqn. (14)}$$

As previously mentioned, methanol synthesis is favored at higher pressures. As the pressure is increased, the equilibrium conversion is increased. This increase in pressure directly increases the cost of methanol production. In a two-step DME synthesis process, this cost is directly translated to the production cost of DME. By combining the reactions into a single-step process, the equilibrium conversion is greatly increased at lower pressures as indicated by Ogawa et al. (Ogawa, Inoue, Shikada, & Ohno, 2003) in Figure 19. Typical catalysts used in the production of single-step DME consist of a physically mixed metallic methanol catalyst ($Cu/Zn/Al_2O_3$) and a dehydration catalyst (γ-Al_2O_3 or HZSM-5) (Sun, Lu, Qiu, Liu, & Xu, 2003).

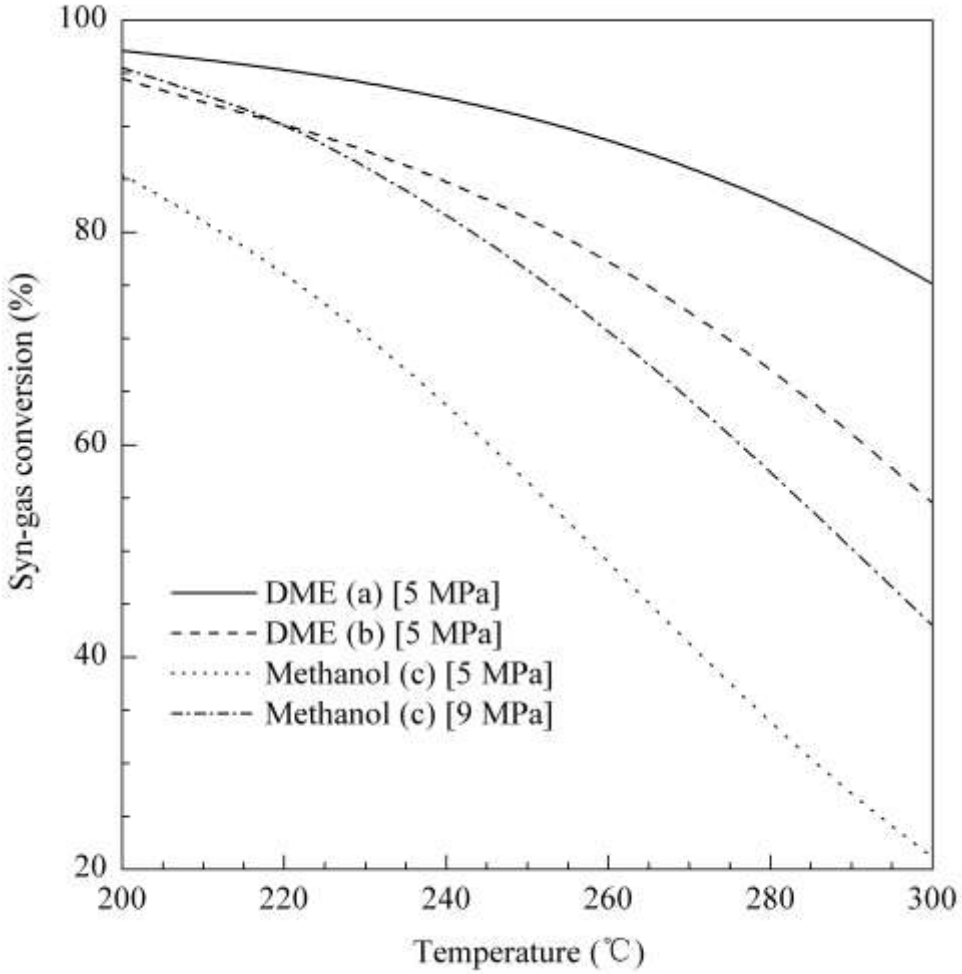

Figure 19. Single-step dimethyl ether synthesis and methanol synthesis equilibrium syngas conversion as a function of temperature (Ogawa, Inoue, Shikada, & Ohno, 2003). Reaction (a) produces DME in the presence of the water-gas shift (WGS) reaction whereas (b) is without the WGS reaction. Reaction (c) is simply the methanol synthesis reaction.

Dimethyl ether is industrially produced in both the two-step and single-step routes. The Lurgi MegaDME® process is coupled with the Lurgi MegaMethanol® process as a downstream dehydration of methanol. Since the dehydration of methanol is only slightly exothermic, the reactor is simply an adiabatic fixed-bed reactor typically consisting of γ-Al_2O_3 (Pontzen, Liebner, Gronemann, Rothaemel, & Ahlers, 2011). The Lurgi MegaDME® process is typically

run around 250°C-360°C with a per pass conversion of 70% - 85% (Pontzen, Liebner, Gronemann, Rothaemel, & Ahlers, 2011), and a capacity of 5000 t/day (Koempel, Liebner, & Wagner, 2005). The single-step process has been established as viable through the use of a bubble column slurry reactor by JFE Holdings, Inc. (Ogawa, Inoue, Shikada, & Ohno, 2003).

4.2 Bifunctional Catalyst Loading: Layered vs. Homogenous Mixing

Since the single-step dimethyl ether synthesis route involves the use of two catalysts, a quick study was done to see the importance of catalyst proximity on overall carbon monoxide conversion. Due to the nature of MFEC, discrete layers can be created of each individual catalyst that may increase the overall conversion by continually converting carbon monoxide in each new layer of catalysts. A visual depiction of this concept can be seen in Figure 20. In order to test the feasibility of this theory, a simple kinetic model can be used.

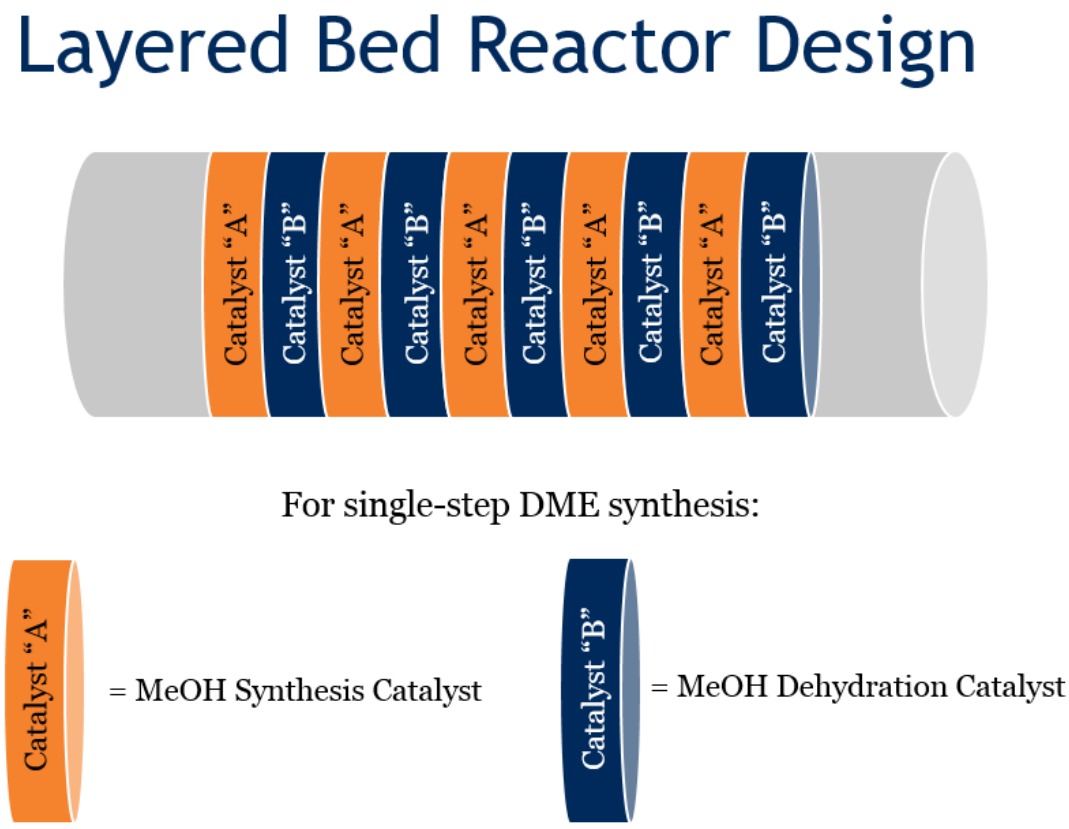

Figure 20. Visual depiction of the concept of a layered bed utilitzing discrete MFEC layers of different catalysts for the single-step DME reaction

While several kinetic models exist for the synthesis of methanol and dimethyl ether, the model developed by Aguayo et al. takes water inhibition on the catalyst into account as well as the formation of methane (Aguayo, et al., 2007). Generic equilibrium rate expressions were developed following the general expression Eqn. (15), and are shown below as Eqn. (16), Eqn. (17), Eqn. (18), and Eqn. (19). The temperature dependent reaction constants and equilibrium constants was determined using Eqn. (20) and Eqn. (21), respectively, and the values for equilibrium coefficients were determined by Aguayo et al. as shown in Table 5. Aguayo's water inhibition terms (Eqn. (22)) and Eqn. (23)) that quantifies the adsorption of water on the catalyst was also factored into Eqn. (16) and Eqn. (19).

$$r_i = k_i\left(\prod P_{Reactants}^{n} - \frac{\prod P_{Products}^{n}}{K_i}\right) \quad \text{Eqn. (15)}$$

$$r_{MeOH} = k_{MeOH}\left(P_{CO}P_{H_2}^2 - \frac{P_{MeOH}}{K_{MeOH}}\right)\theta \quad \text{Eqn. (16)}$$

$$r_{DME} = k_{DME}\left(P_{MeOH}^2 - \frac{P_{DME}P_{H_2O}}{K_{DME}}\right) \quad \text{Eqn. (17)}$$

$$r_{CO_2} = k_{CO_2}\left(P_{CO}P_{H_2O} - \frac{P_{CO_2}P_{H_2}}{K_{CO_2}}\right) \quad \text{Eqn. (18)}$$

$$r_{CH_4} = k_{CH_4}\left(P_{CO}P_{H_2}^3 - \frac{P_{CH_4}P_{H_2O}}{K_{CH_4}}\right)\theta \quad \text{Eqn. (19)}$$

$$k_i = k_i^*\exp\left(-\frac{E_a}{R}\left[\frac{1}{T} - \frac{1}{573.15}\right]\right) \quad \text{Eqn. (20)}$$

$$K_i = \exp\left(a + \frac{b}{T} + c\log_{10}T + dT + eT^2 + \frac{f}{T^2}\right) \quad \text{Eqn. (21)}$$

$$\theta = \frac{1}{1 + K_{H_2O}P_{H_2O}} \quad \text{Eqn. (22)}$$

$$K_{H_2O} = K_{H_2O}^*\exp\left(\frac{\Delta H_{H_2O}}{R}\left[\frac{1}{T} - \frac{1}{548}\right]\right) \quad \text{Eqn. (23)}$$

Table 5. Equilibrium constant coefficients determined by Aguayo et al. (Aguayo, et al., 2007).

K_i	**a**	**b * 10^{-3}**	**c**	**d * 10^{4}**	**e * 10^{8}**	**f * 10^{-3}**
K_{MeOH}	21.84	9.04	-7.66	54.07	-57.50	-6.75

K_{DME}	-9.76	3.20	1.07	-6.57	4.90	6.05
K_{CO2}	18.01	-5.87	-1.86	2.70	0	58.20
K_{CH4}	24.90	22.78	-7.95	43.54	-36.07	-4.85

After the kinetic information was programmed into Matlab, two different programs were developed. The "Packed Bed Model" simply allowed for all reactions to occur simultaneously in order to simulate a physically mixed catalyst bed. The "Layered Bed Model" program involved layers in which the first layer suppressed the production of dimethyl ether while the second layer suppressed the production of methanol. An example of the product formation inside the "Packed Bed Model" is shown in Figure 21, and a similar example of the "Layered Bed Model" is shown in Figure 22. The code for these models can be found in the appendix, in sections ix, x, and xi.

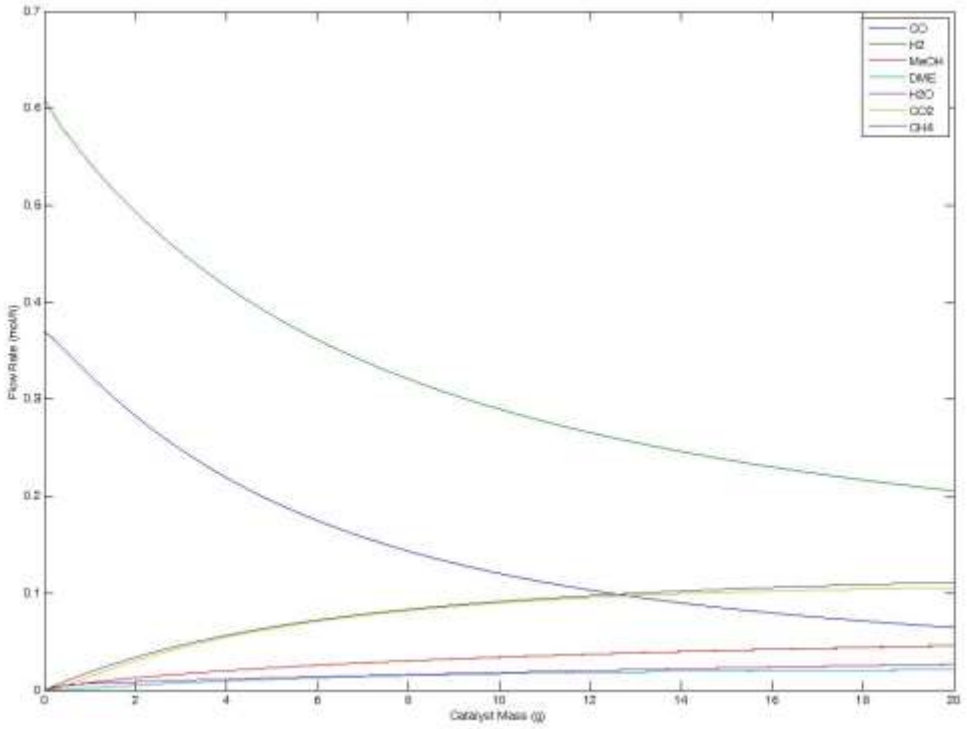

Figure 21. "Packed Bed Model" – CO conversion = 82.5% at outlet

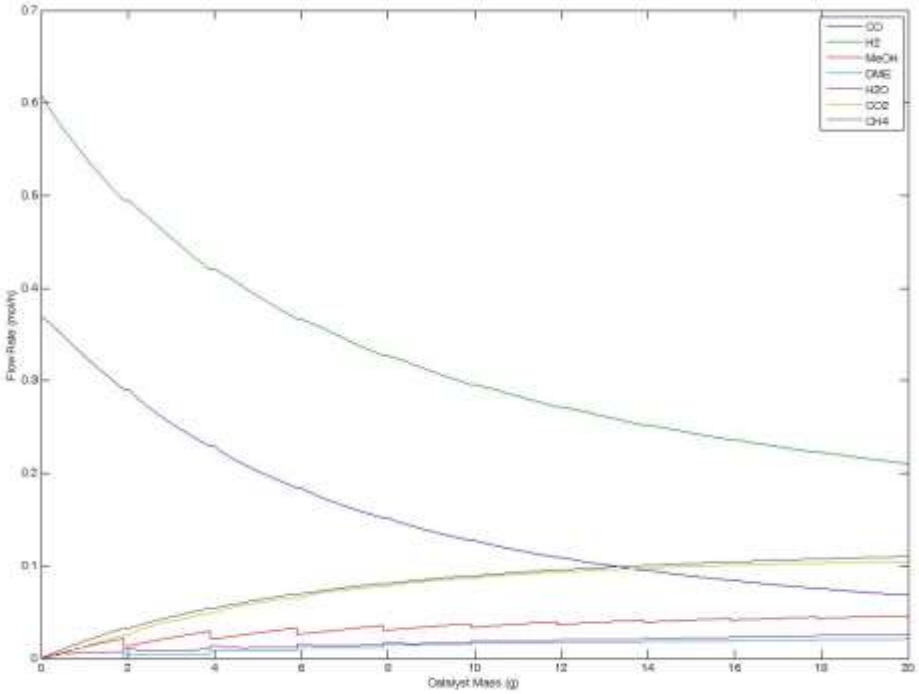

Figure 22. “Layered Bed Model” – CO conversion = 81.5% at outlet, 10 layers

The amount of layers was then increased, up to a maximum of 50 layers. The results indicated that as the layers increased, the overall CO conversion decreased. This result indicated that the extra addition of layers (while maintaining the same mass of catalyst) in essence diluted the reactor with a particular catalyst that was no longer able to be used. The results are tabulated below in Table 6.

Table 6. Flow rates and conversions comparing the multi-layered catalyst bed to a packed bed.

Variable	**Traditional PBR**	**5 Layers**	**10 Layers**	**20 Layers**	**30 Layers**	**50 Layers**
CO Conversion	82.5051	81.8336	81.5403	80.6415	79.5999	77.1135
H_2 Conversion	66.2995	65.9643	65.4419	64.4557	63.4024	61.0094

MeOH Outlet Flow	0.0458	0.0459	0.0452	0.0442	0.0432	0.0410
DME Outlet Flow	0.0211	0.0210	0.0209	0.0206	0.0203	0.0197
H_2O Outlet Flow	0.0267	0.0269	0.0262	0.0253	0.0245	0.0229
CO_2 Outlet Flow	0.1058	0.1045	0.1047	0.1041	0.1032	0.1009
CH_4 Outlet Flow	0.1114	0.1105	0.1100	0.1088	0.1074	0.1041

To summarize, the use of MFEC as a means to make a layered bed will not have a beneficial effect for this particular set of reactions. As can be seen from Table 6, as the total number of discrete layers is increased, the overall conversion decreases. This indicates that catalysts should be intimately close to one another in order to obtain the highest overall conversion.

4.3 Experimental Setup

Stainless steel reactors were employed to run both the packed bed and MFEC experiments. Initially, a 15mm ID stainless steel tube with a wall thickness of 2.05 mm was used to ensure that the target reaction is occurring, as well as being used to compare the heat generation resulting from the packed bed and MFEC reactor configurations. The reactor was later scaled up to a 29mm ID stainless steel tube to test for the scalability of the target reaction under the packed bed and MFEC designs.

A schematic of the overall reactor setup can be seen in Figure 23. For the methanol synthesis and dimethyl ether synthesis reactions, only hydrogen, helium, and syngas were required. Each of these gases was controlled by mass flow controllers that were adjusted through a PLC (programmable logic controller). The pressure of the reaction was controlled manually

through a back pressure regulator that is located physically after the reactor. After passing through the back pressure regulator, the effluent first passed through a hot trap that typically ran at a temperature of 150°C. The effluent then continued through a cooling unit and cold trap that typically ran at a temperature of 4°C. The remaining effluent that is still in the gas phase was then split to be analyzed in an online gas chromatograph before being vented. All compounds detected by the GC were calibrated with pure compounds.

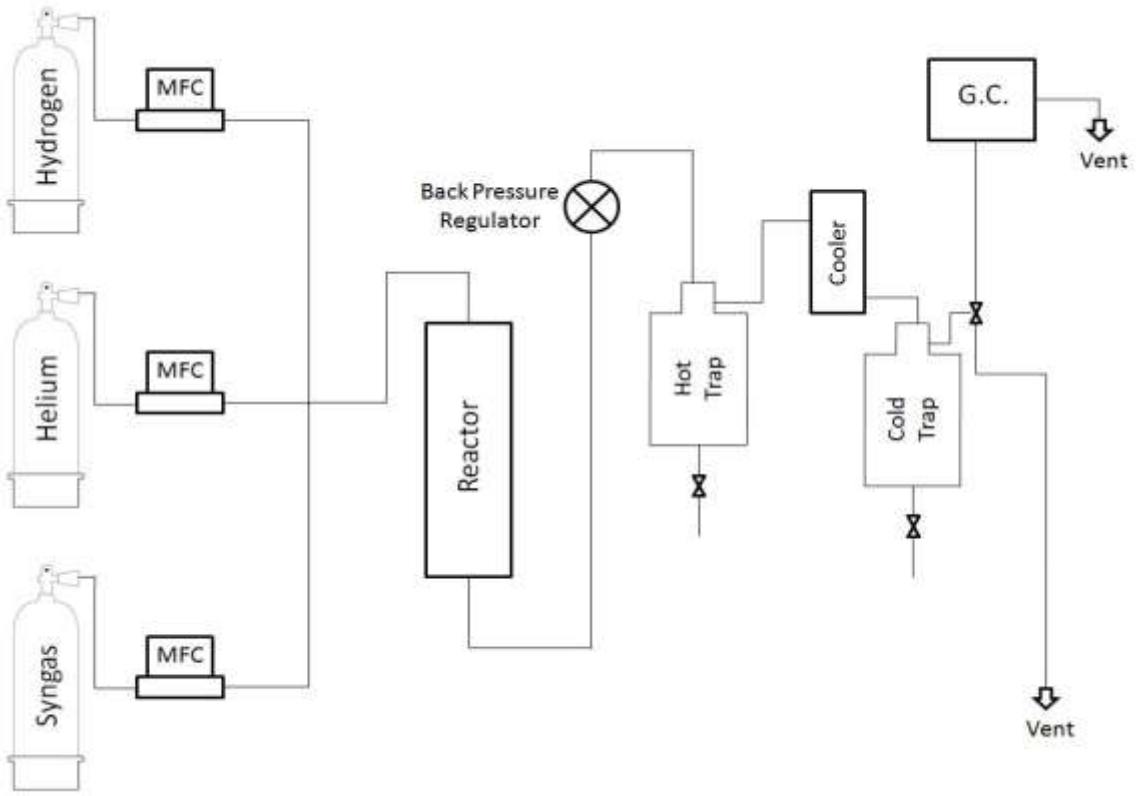

Figure 23. Schematic of the single-step dimethyl ether experimental setup

An online Agilent 6890A gas chromatograph (GC) installed with a thermal conductivity detector (TCD) in conjunction with a capillary column is used to analyze the gas samples of the effluent. The same GC is also installed with a flame ionization detector (FID) in conjunction with a packed column in order to analyze the liquid samples from the effluent.

In addition to controlling the flow rates of the reactants, the PLC also functions as a temperature controller for the hot trap and reactor. It will also record the temperature measurements that are obtained from inside the reactor. A thin sheath multipoint thermocouple (Omega, 316SS probe, k-type, 1.59mm OD, 0.15mm wall thickness, 6 measurement points spaced 25.4mm apart) is used to measure the temperature inside the reactor at 6 different points. The thermocouple itself has a low thermal mass and low axial thermal conductivity. The thermocouple was inserted across constant temperature baths at different points with the bathes differing in temperature by over 200 °C, and negligible conduction down the thermocouple was observed. A schematic of a reactor with the multipoint thermocouple in use is shown in Figure 14.

The temperature of the reactor itself is controlled by the PLC through the use of heating tape wrapped around the location of the catalyst bed inside the reactor in conjuction with a thermocouple on the outside wall of the reactor. The reactor is also wrapped with insulation to try and maintain a uniform reactor surface temperature. The tubing leading into and out of the reactor is also insulted to reduce heat losses to the surroundings.

4.4 15mm ID Single-Step Dimethyl Ether Synthesis Results

Single-step dimethyl ether synthesis, meaning dimethyl ether that is produced from the conversion of syngas to methanol, and the subsequent dehydration of methanol to dimethyl ether in the same reactor, was carried out initially in a 15mm ID reactor. As can be seen from Figure 12, the effect of temperature on single-step dimethyl ether synthesis can be significant. Not only can an increase in temperature produce a drop in theoretical conversion of carbon monoxide, an increase in temperature also has the potential to form methane. The presence of methane can

actually be a qualitative indicator that the reactor has hot spots, even if they are not detected with a thermocouple.

Since temperature is crucial to single-step dimethyl ether synthesis, the temperature profiles as a function of time should be monitored. The 15mm ID reactor was run at varying inlet temperatures (215°C, 230°C, 245°C, 260°C) with a MFEC bed, and those profiles are shown in Figure 24, Figure 25, Figure 26, and Figure 27, respectively. The same reactor inlet temperatures were run for a packed bed of equivalent volumetric catalyst loading (diluted with inert material). The packed bed temperature profiles are shown in Figure 28, Figure 29, Figure 30, and Figure 31. Overall, the temperature profiles exhibit a trend in which the MFEC beds are able to maintain a temperature without drifting like their packed bed counterparts.

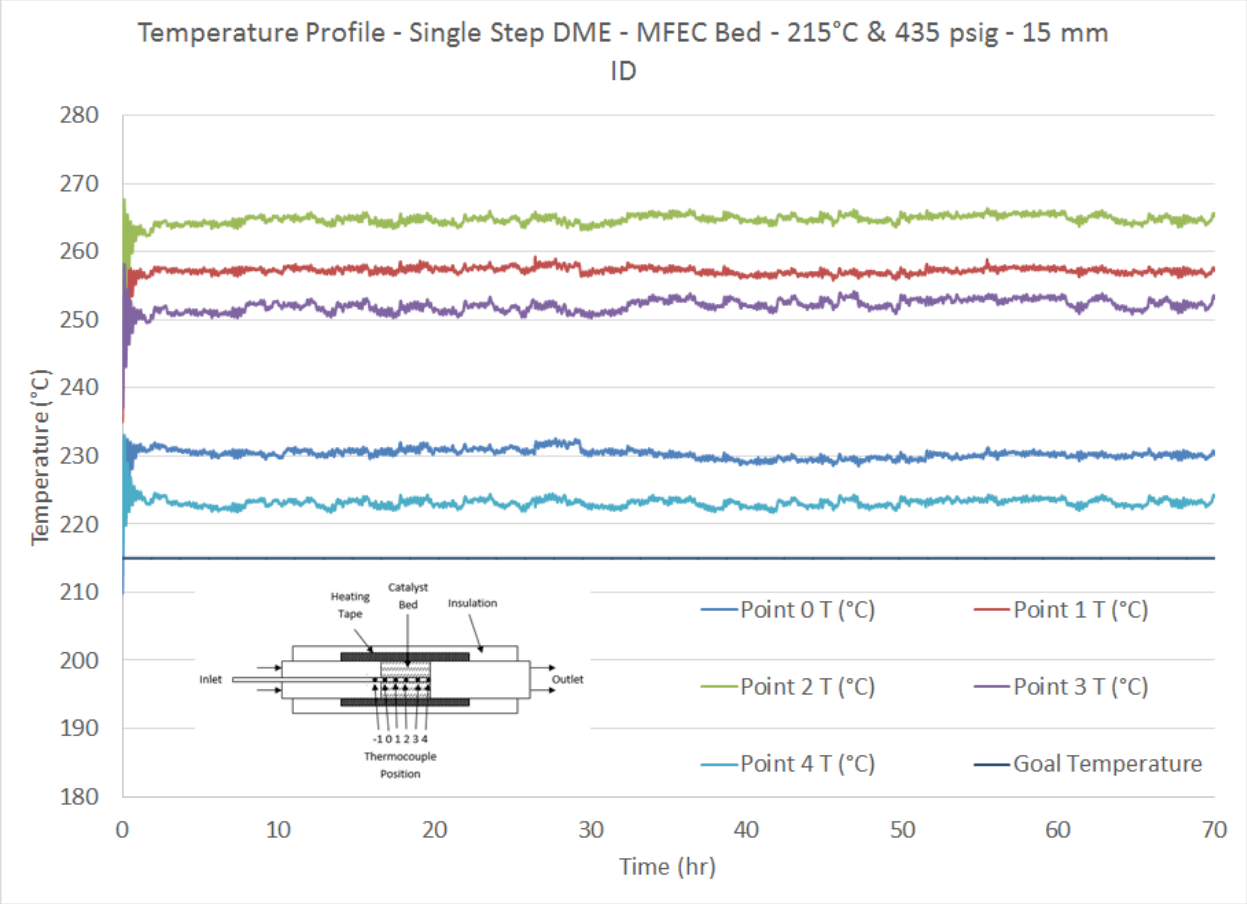

Figure 24. Temperature profile as a function of time for single-step dimethyl ether synthesis with MFEC reactor conditions of ID=15mm, P=435psig, T_{Inlet}=215°C, H_2:CO ratio of 3:1, and GHSV=1880 h^{-1}. Catalyst (60-80 mesh, or 180-250 μm) is HiFuelR120 and γ-Al_2O_3 in a 2:1 ratio by mass

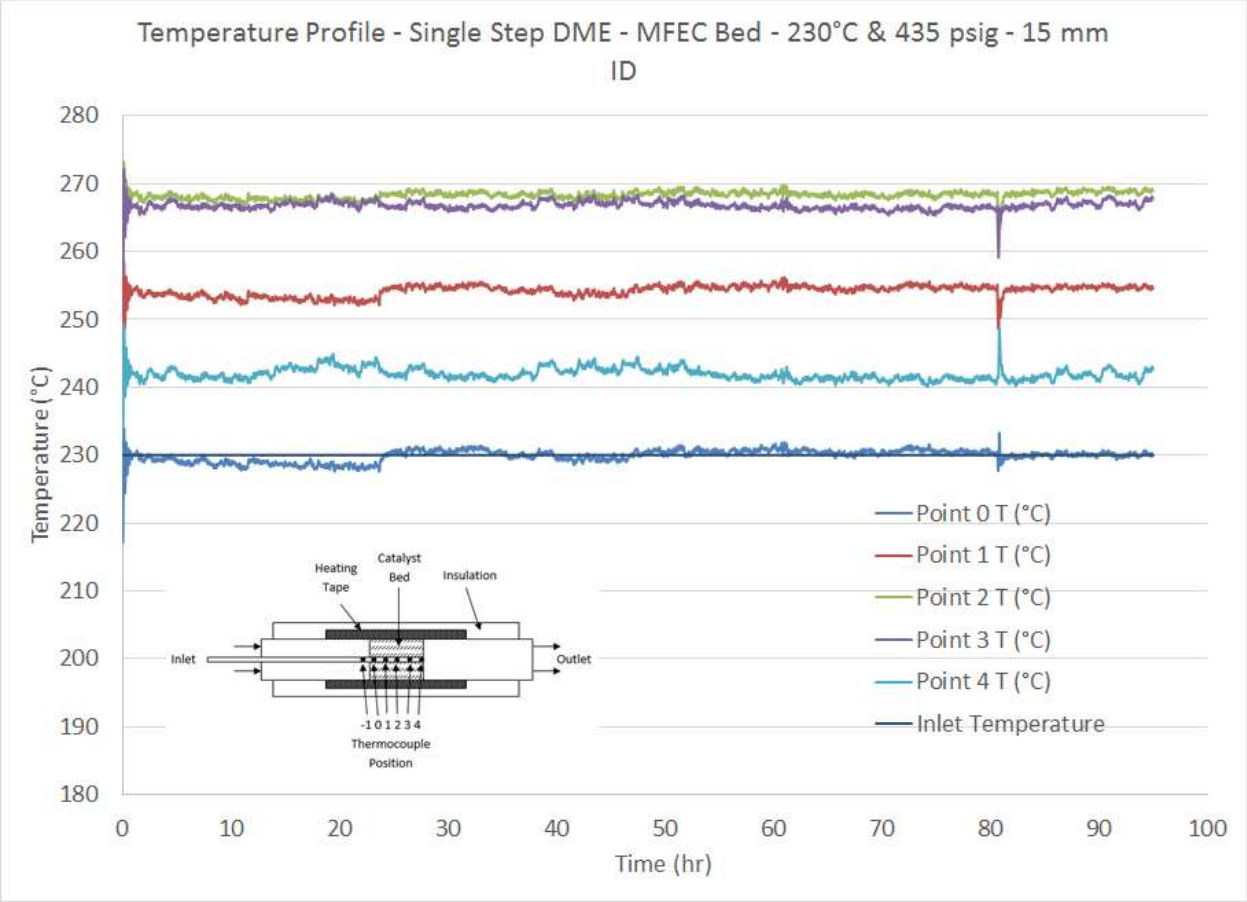

Figure 25. Temperature profile as a function of time for single-step dimethyl ether synthesis with MFEC reactor conditions of ID=15mm, P=435psig, T_{Inlet}=230°C, H_2:CO ratio of 3:1, and GHSV=1880 h^{-1}. Catalyst (60-80 mesh, or 180-250 μm) is HiFuelR120 and γ-Al_2O_3 in a 2:1 ratio by mass

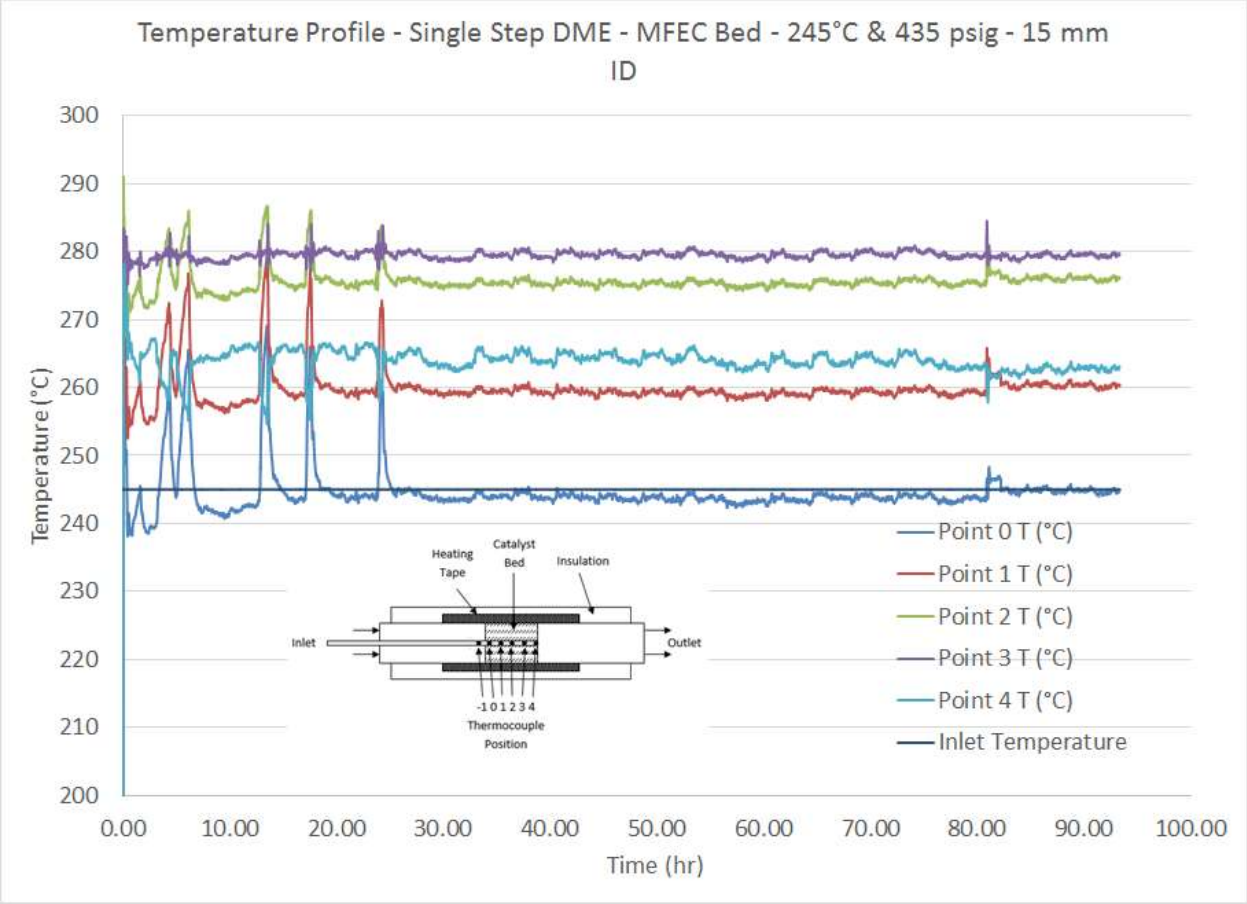

Figure 26. Temperature profile as a function of time for single-step dimethyl ether synthesis with MFEC reactor conditions of ID=15mm, P=435psig, T_{Inlet}=245°C, H_2:CO ratio of 3:1, and GHSV=1880 h^{-1}. Catalyst (60-80 mesh, or 180-250 μm) is HiFuelR120 and γ-Al_2O_3 in a 2:1 ratio by mass

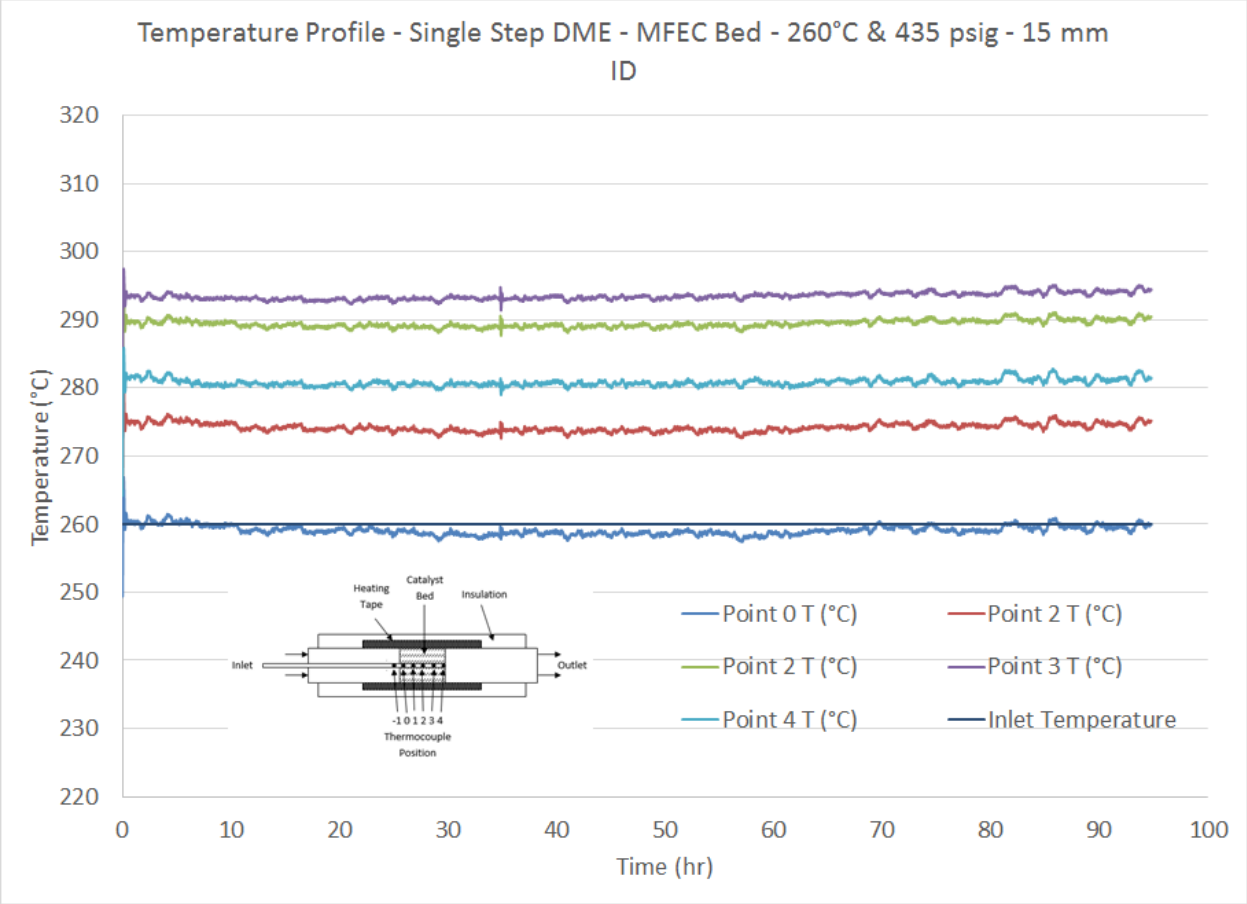

Figure 27. Temperature profile as a function of time for single-step dimethyl ether synthesis with MFEC reactor conditions of ID=15mm, P=435psig, T_{Inlet}=260°C, H_2:CO ratio of 3:1, and GHSV=1880 h^{-1}. Catalyst (60-80 mesh, or 180-250 μm) is HiFuelR120 and γ-Al_2O_3 in a 2:1 ratio by mass

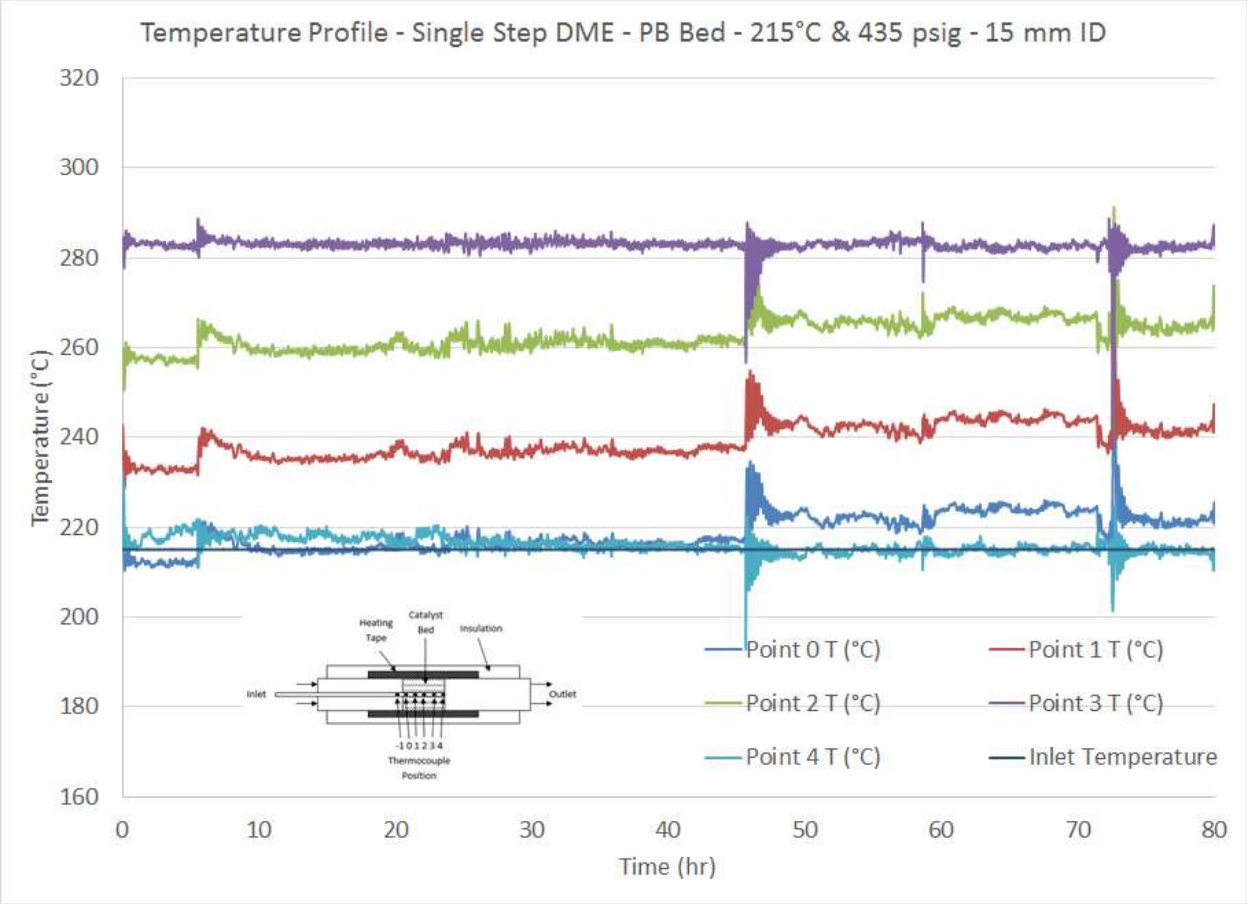

Figure 28. Temperature profile as a function of time for single-step dimethyl ether synthesis with PB reactor conditions of ID=15mm, P=435psig, T_{Inlet}=215°C, H_2:CO ratio of 3:1, and GHSV=1880 h^{-1}. Catalyst (60-80 mesh, or 180-250 μm) is HiFuelR120 and γ-Al_2O_3 in a 2:1 ratio by mass

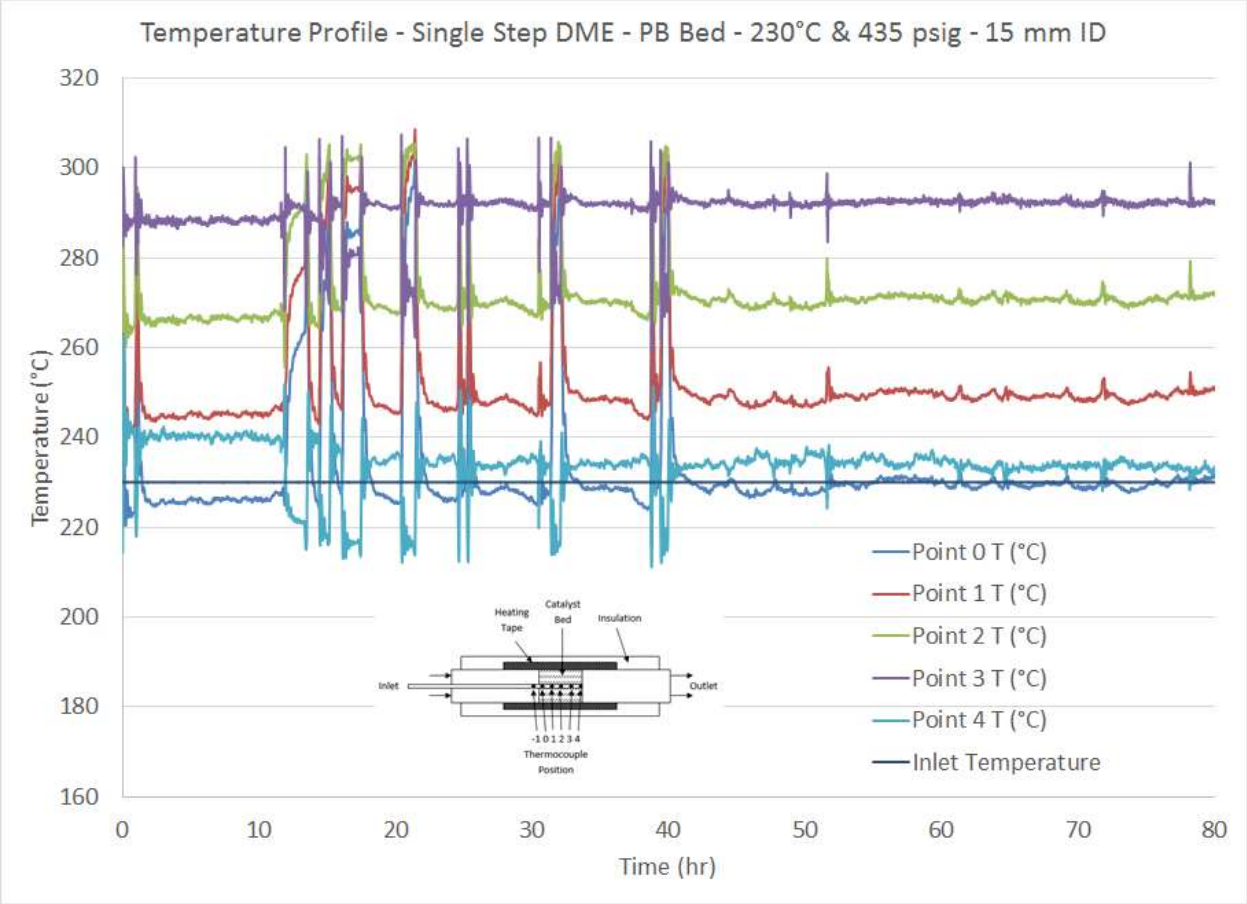

Figure 29. Temperature profile as a function of time for single-step dimethyl ether synthesis with PB reactor conditions of ID=15mm, P=435psig, T_{Inlet}=230°C, H_2:CO ratio of 3:1, and GHSV=1880 h^{-1}. Catalyst (60-80 mesh, or 180-250 μm) is HiFuelR120 and γ-Al_2O_3 in a 2:1 ratio by mass

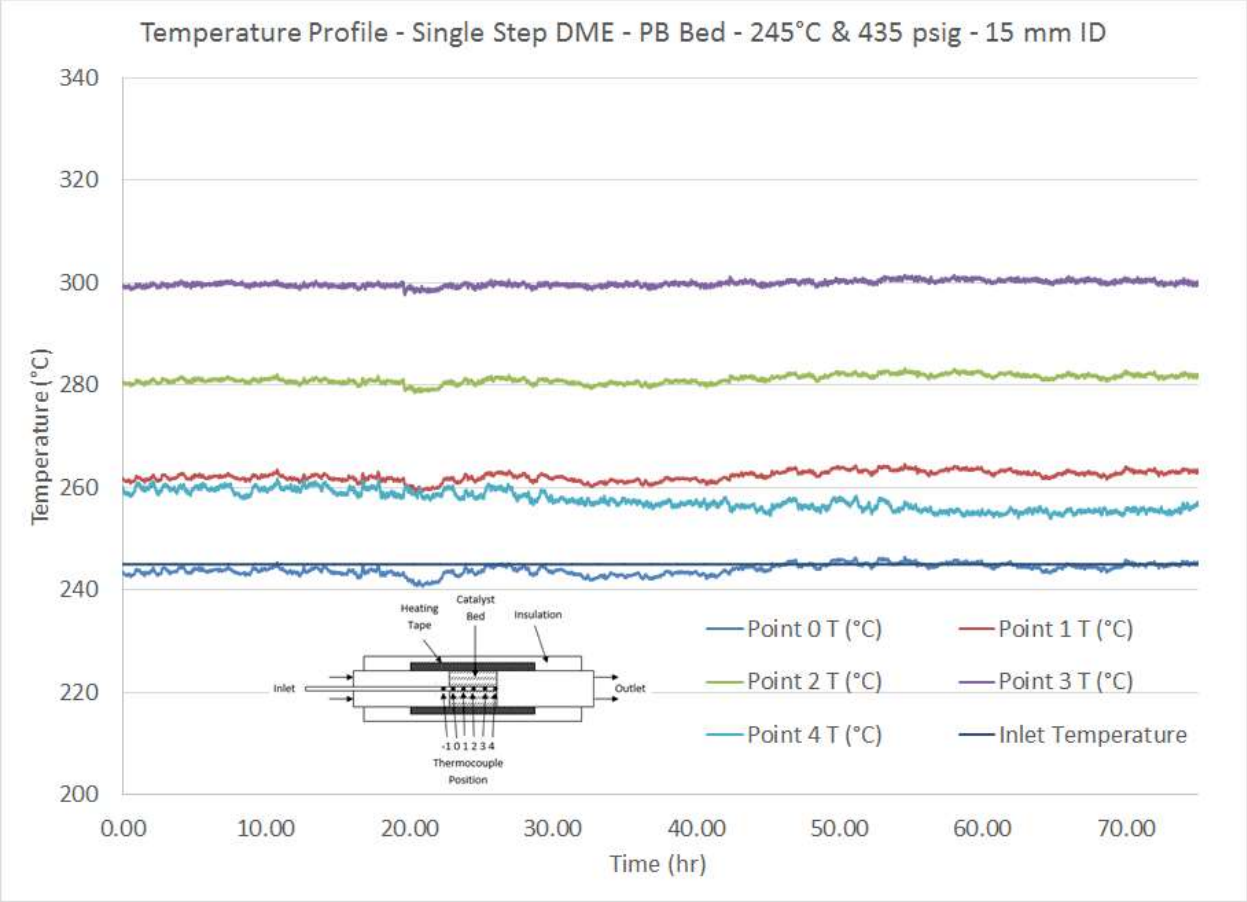

Figure 30. Temperature profile as a function of time for single-step dimethyl ether synthesis with PB reactor conditions of ID=15mm, P=435psig, T_{Inlet}=245°C, H_2:CO ratio of 3:1, and GHSV=1880 h^{-1}. Catalyst (60-80 mesh, or 180-250 μm) is HiFuelR120 and γ-Al_2O_3 in a 2:1 ratio by mass

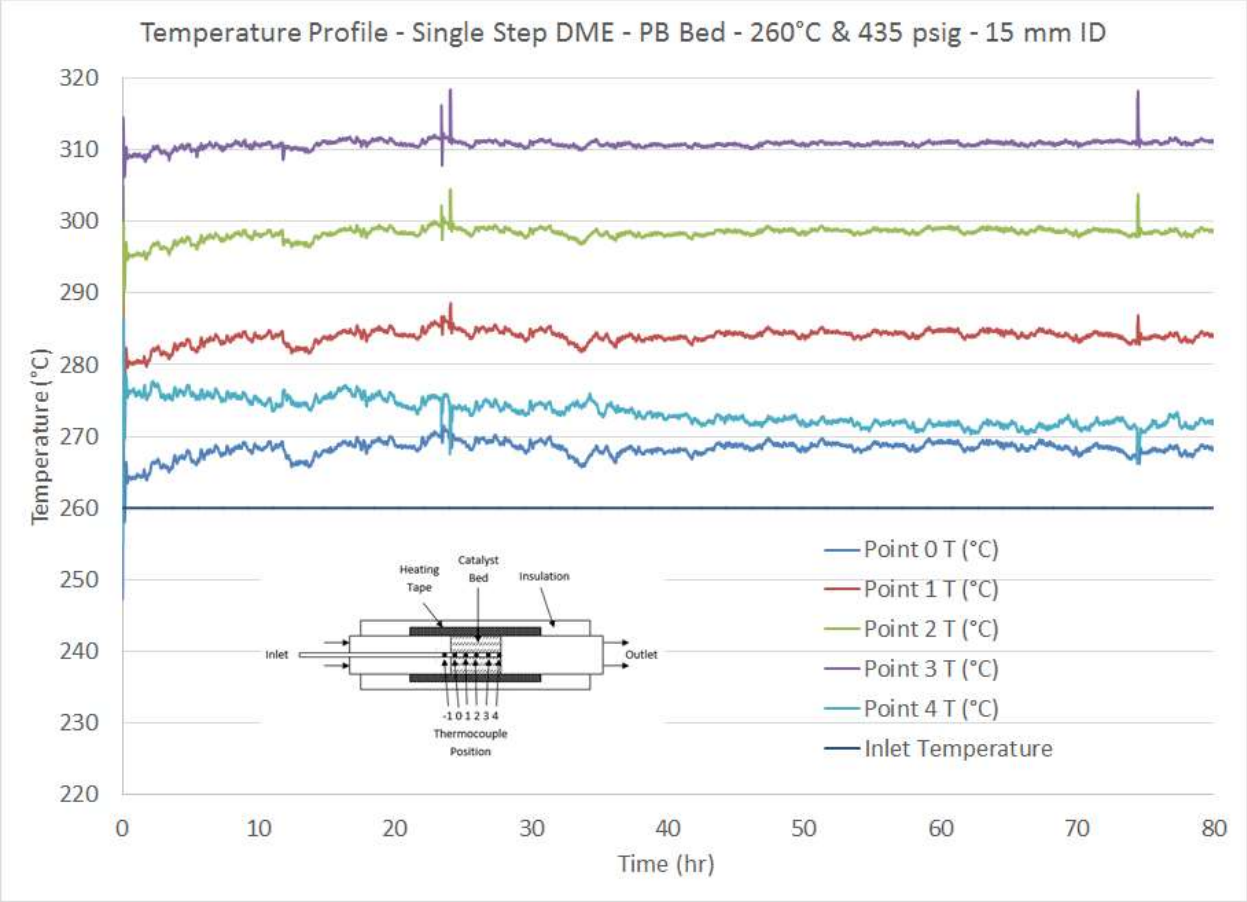

Figure 31. Temperature profile as a function of time for single-step dimethyl ether synthesis with PB reactor conditions of ID=15mm, P=435psig, T_{Inlet}=260°C, H_2:CO ratio of 3:1, and GHSV=1880 h^{-1}. Catalyst (60-80 mesh, or 180-250 μm) is HiFuelR120 and γ-Al_2O_3 in a 2:1 ratio by mass

Since it is difficult to compare the temperature profiles as currently presented, axial temperature profiles can better show the difference in how the MFEC vs. PB reactors are able to remove heat. The comparisons for each inlet temperature are shown in Figure 32, Figure 33, Figure 34, and Figure 35. It should be noted that in each figure, the packed bed obtains a higher increase in temperature compared to the MFEC bed. Furthermore, the MFEC bed seems to have

a broader temperature profile, which corresponds with the increased thermal conductivity of the MFEC bed compared to the packed bed.

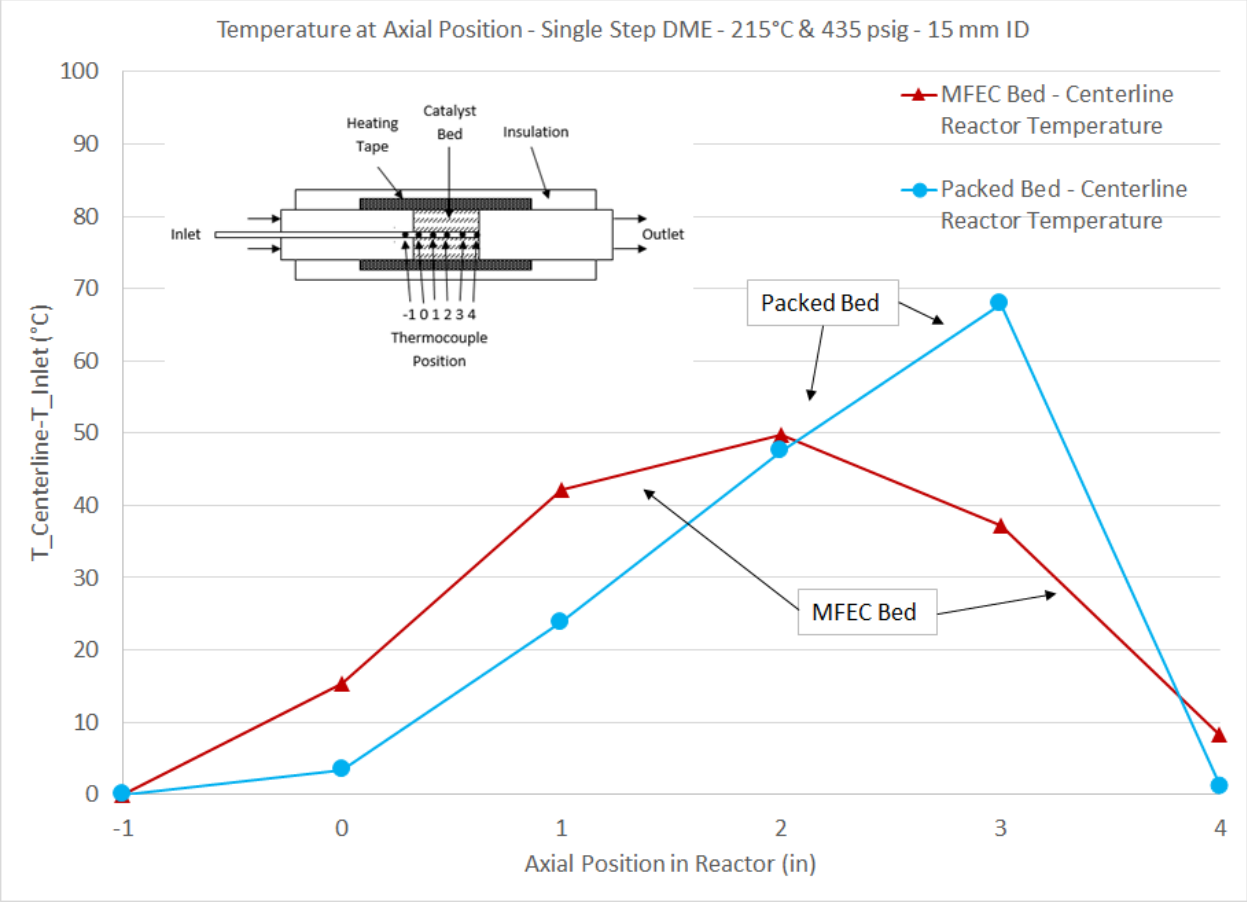

Figure 32. Axial temperature profile comparison for the 15mm ID reactors with T_{Inlet}=215°C.

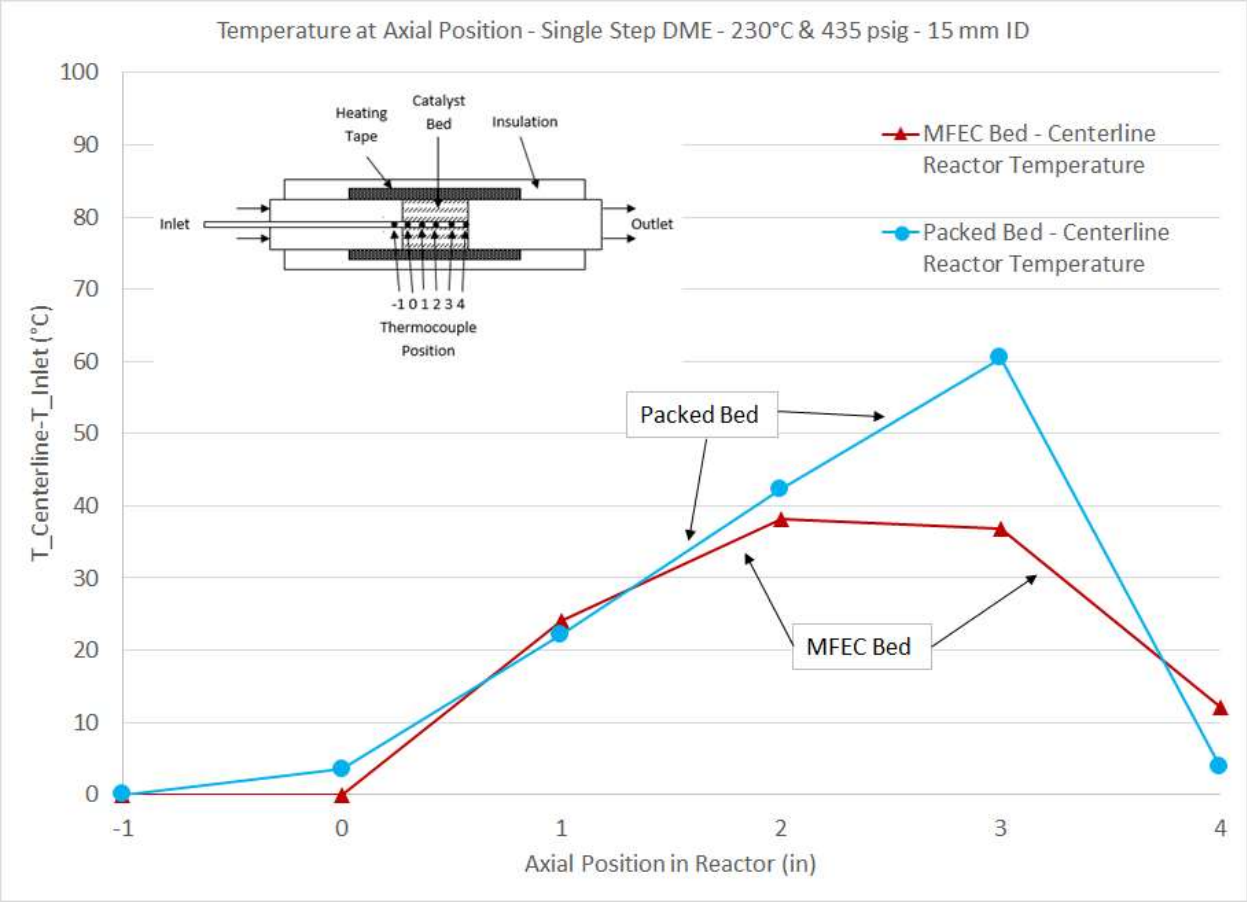

Figure 33. Axial temperature profile comparison for the 15mm ID reactors with T_{Inlet}=230°C.

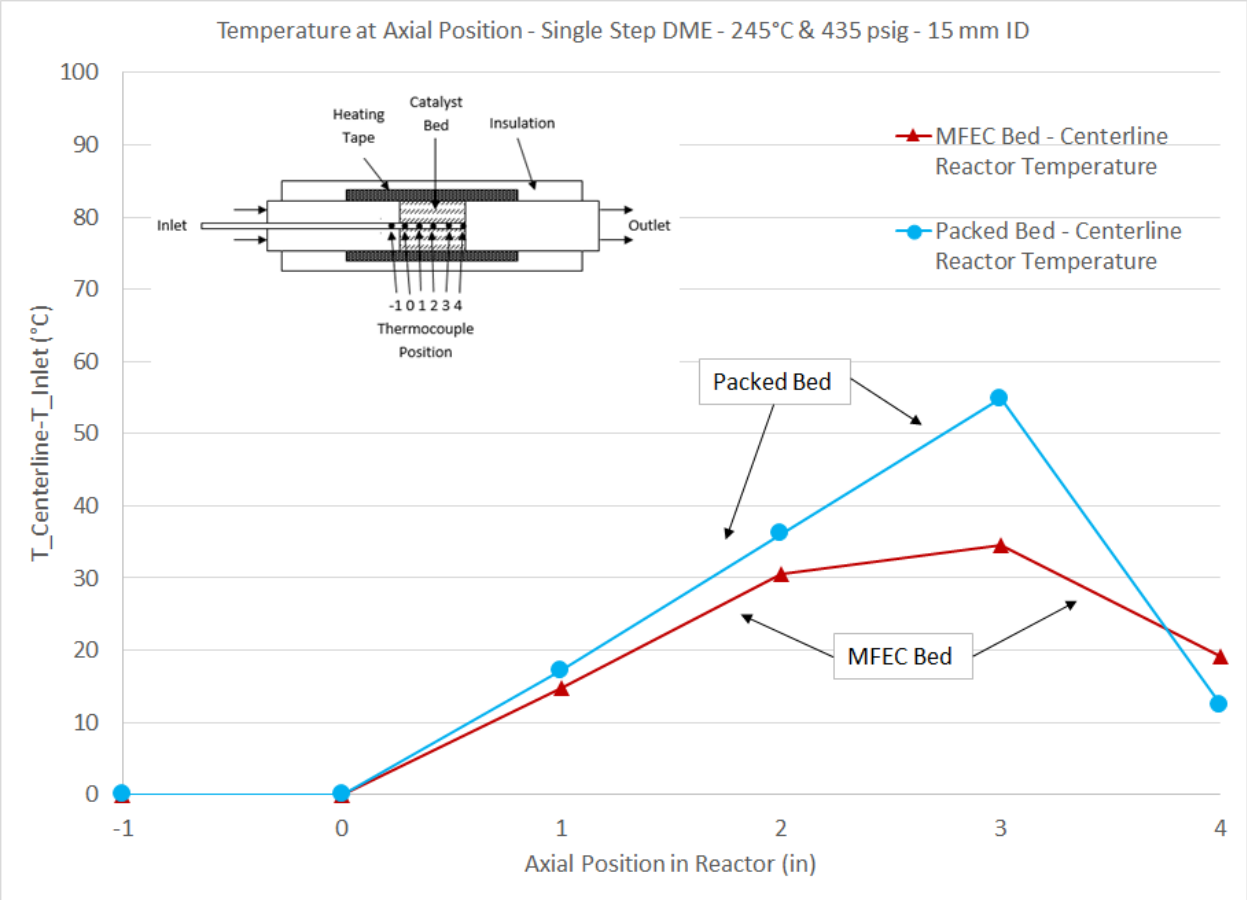

Figure 34. Axial temperature profile comparison for the 15mm ID reactors with T_{Inlet}=245°C.

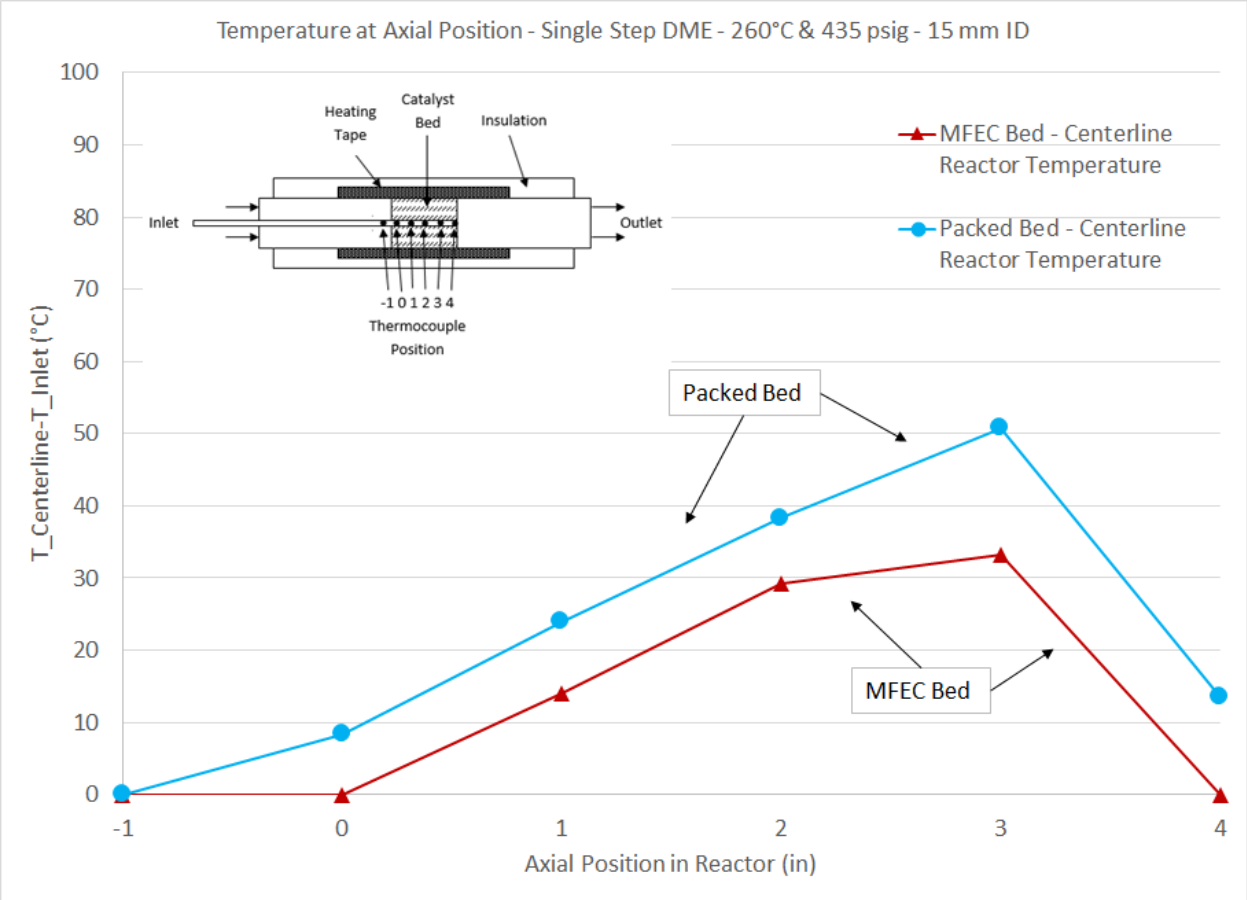

Figure 35. Axial temperature profile comparison for the 15mm ID reactors with T_{Inlet}=260°C.

To visualize the difference in heat generation between the MFEC and PB reactors, Figure 36 should be referenced. In the figure, one can graphically see the difference in centerline temperature increases for both the 15 mm ID MFEC and PB reactors. In each pair of bar graphs, the gray bar to the left shows the maximum temperature increase along the centerline for the MFEC bed. In contrast, the PB maximum temperature increase is shown in the red bar to the right. Across all the various inlet temperatures, the MFEC had a lower increase in temperature. Further, as the inlet temperature increased, the PB deviation became more apparent, going from a 1.36 fold increase to a 1.52 fold increase. These temperature increases can have negative side effects that typically result in unwanted products and/or a loss of carbon monoxide conversion.

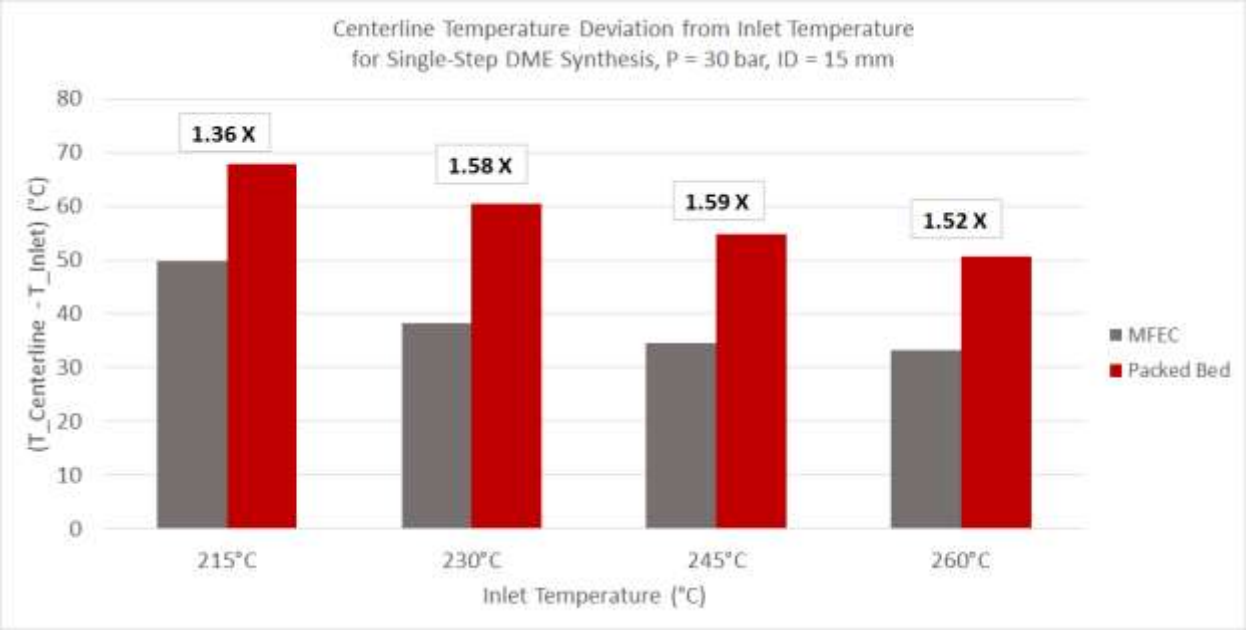

Figure 36. Comparison of the extent of temperature increase within the 15 mm ID reactor for both the MFEC and PB reactors.

In order to understand how the temperature deviations shown in Figure 36 affected the product quality, the overall carbon monoxide conversion must be evaluated. In Figure 37, the trend can be seen that the MFEC reactor outperformed the PB as the inlet temperature increased. As an aside, it should be noted that both reactors did overcome the methanol equilibrium constraints due to using the single-step dimethyl ether synthesis route.

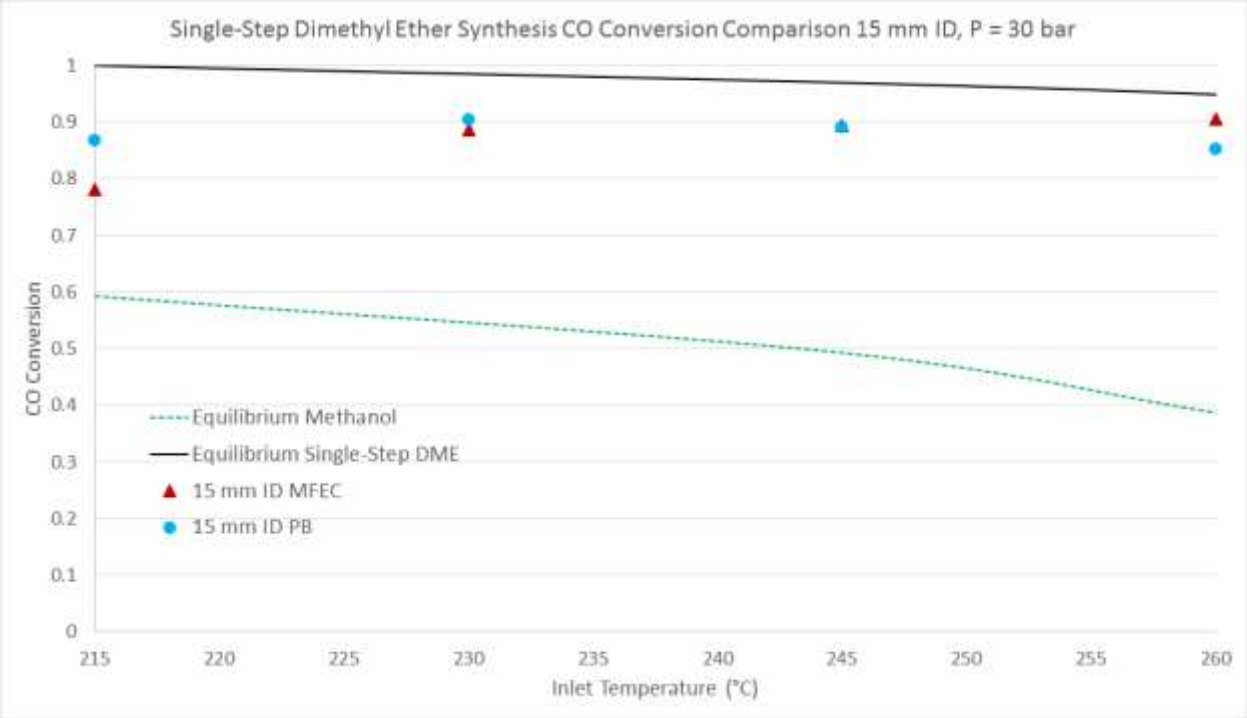

Figure 37. Overall carbon monoxide conversion for single-step dimethyl ether synthesis at varying temperatures for the 15mm ID reactors with a H_2:CO ratio of 3:1, and GHSV=1880 h^{-1}. Catalyst (60-80 mesh, or 180-250 μm) is HiFuelR120 and γ-Al_2O_3 in a 2:1 ratio by mass

However, overall carbon monoxide conversion does not necessarily indicate a more productive reactor. The products that are ultimately produced are the most crucial indication of a profitable chemical conversion process. The goal of this reaction was to produce the most dimethyl ether possible, and the mass fraction of dimethyl ether in the effluent can be seen in Figure 38. The MFEC reactor does consistently produce more dimethyl ether in the product than its PB counterpart.

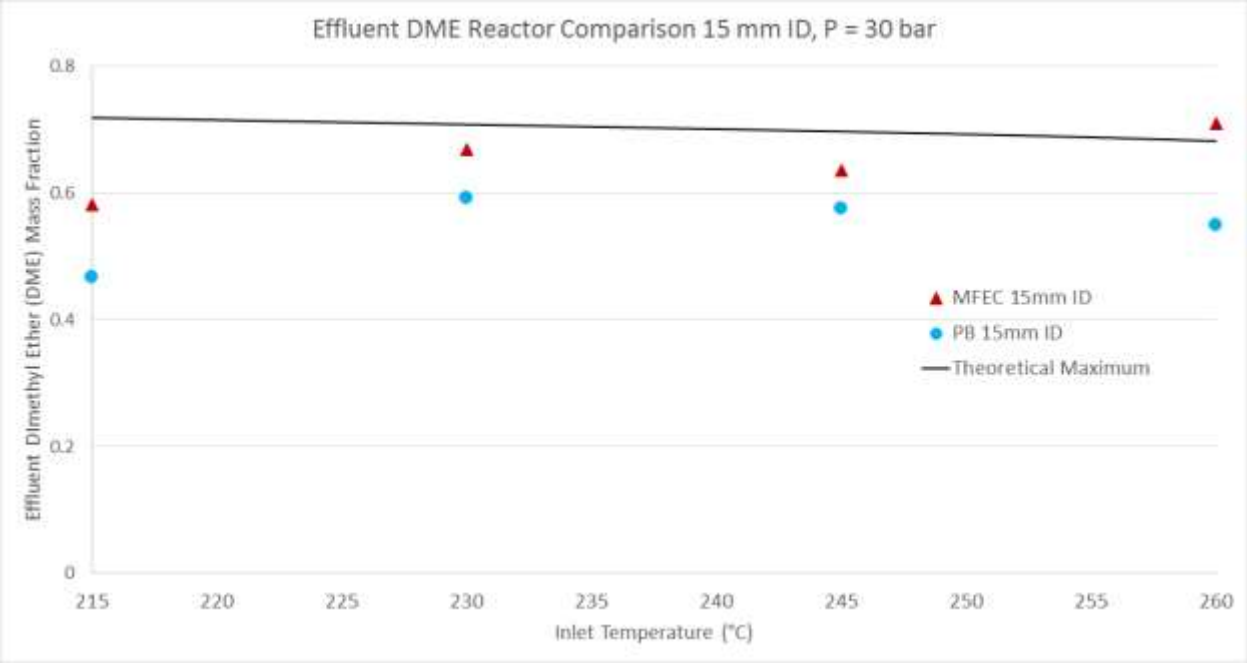

Figure 38. Effluent mass fraction of dimethyl ether for single-step dimethyl ether synthesis at varying temperatures for the 15mm ID reactors with a H_2:CO ratio of 3:1, and GHSV=1880 h^{-1}. Catalyst (60-80 mesh, or 180-250 μm) is HiFuelR120 and γ-Al_2O_3 in a 2:1 ratio by mass

The last main component of comparing the reactor schemes is to compare the overall products generated and their relative amounts. In Figure 39, Figure 40, Figure 41, and Figure 42 the overall effluent mass fractions (ignoring hydrogen since it was run in excess) are shown for the MFEC reactors at 215°C, 230°C, 245°C, and 260°C, respectively. The comparable PB reactor effluent mass fractions can be viewed in Figure 43, Figure 44, Figure 45, and Figure 46 for 215°C, 230°C, 245°C, and 260°C, respectively. As mentioned previously, methane can be an indirect indicator of an increase in temperature that promotes the dissociative absorption of carbon monoxide. In these 15 mm ID studies, no methane was observed in any of the product streams. This is not a surprising result though since none of the reactors maintained a temperature well above 300°C.

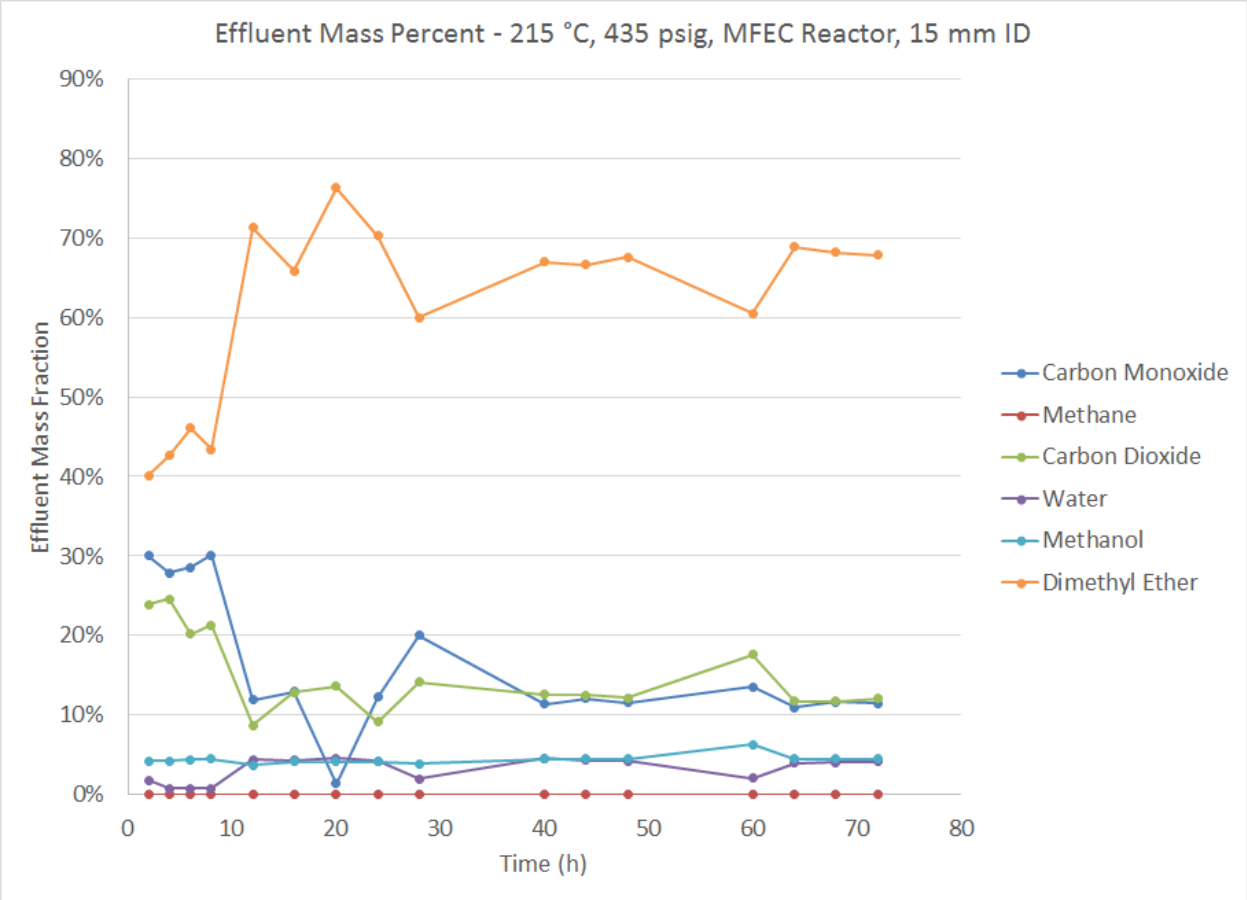

Figure 39. Product distribution as a mass perfect for single-step dimethyl ether synthesis with MFEC reactor conditions of ID=15mm, P=435psig, T_{Inlet}=215°C, H_2:CO ratio of 3:1, and GHSV=1880 h^{-1}. Catalyst (60-80 mesh, or 180-250 μm) is HiFuelR120 and γ-Al_2O_3 in a 2:1 ratio by mass

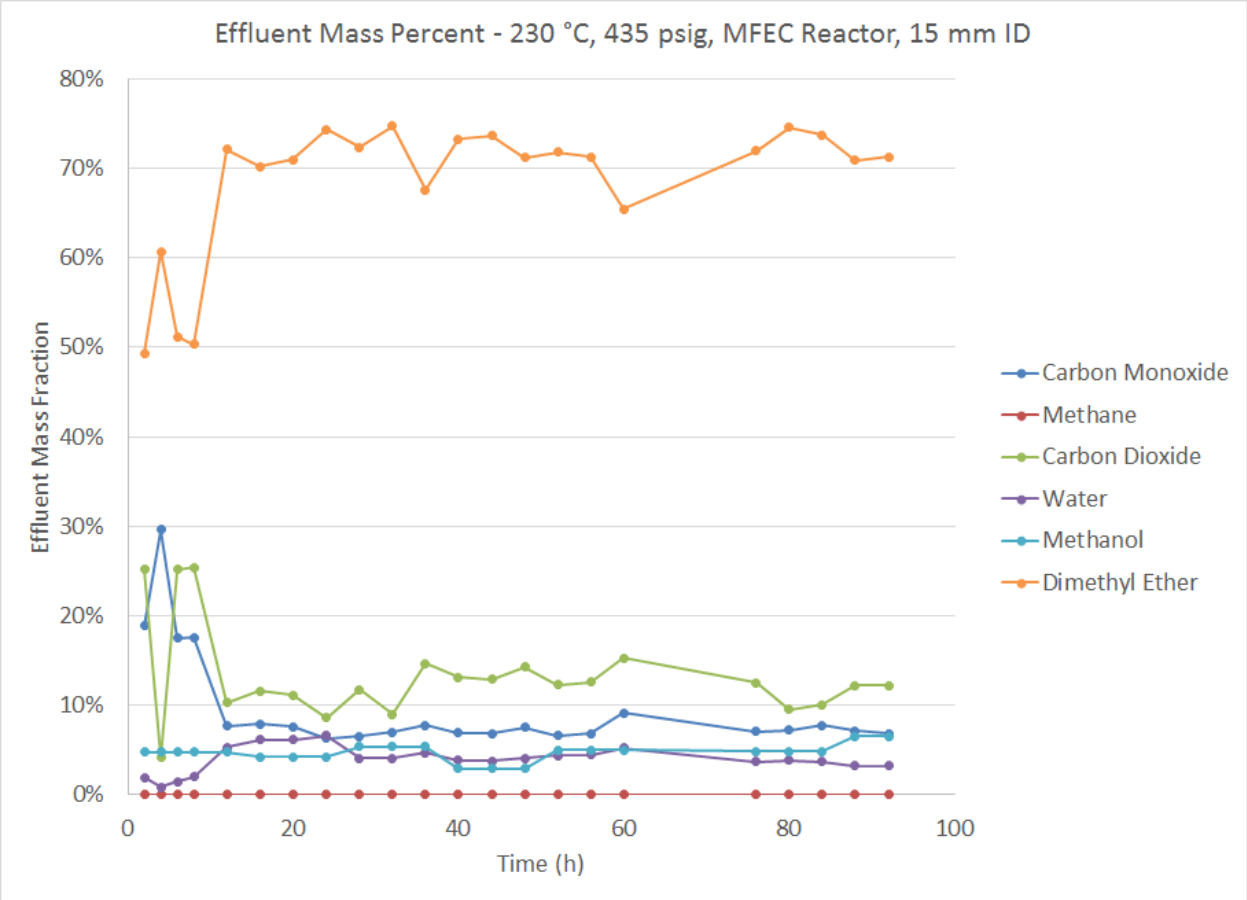

Figure 40. Product distribution as a mass perfect for single-step dimethyl ether synthesis with MFEC reactor conditions of ID=15mm, P=435psig, T_{Inlet}=230°C, H_2:CO ratio of 3:1, and GHSV=1880 h^{-1}. Catalyst (60-80 mesh, or 180-250 μm) is HiFuelR120 and γ-Al_2O_3 in a 2:1 ratio by mass

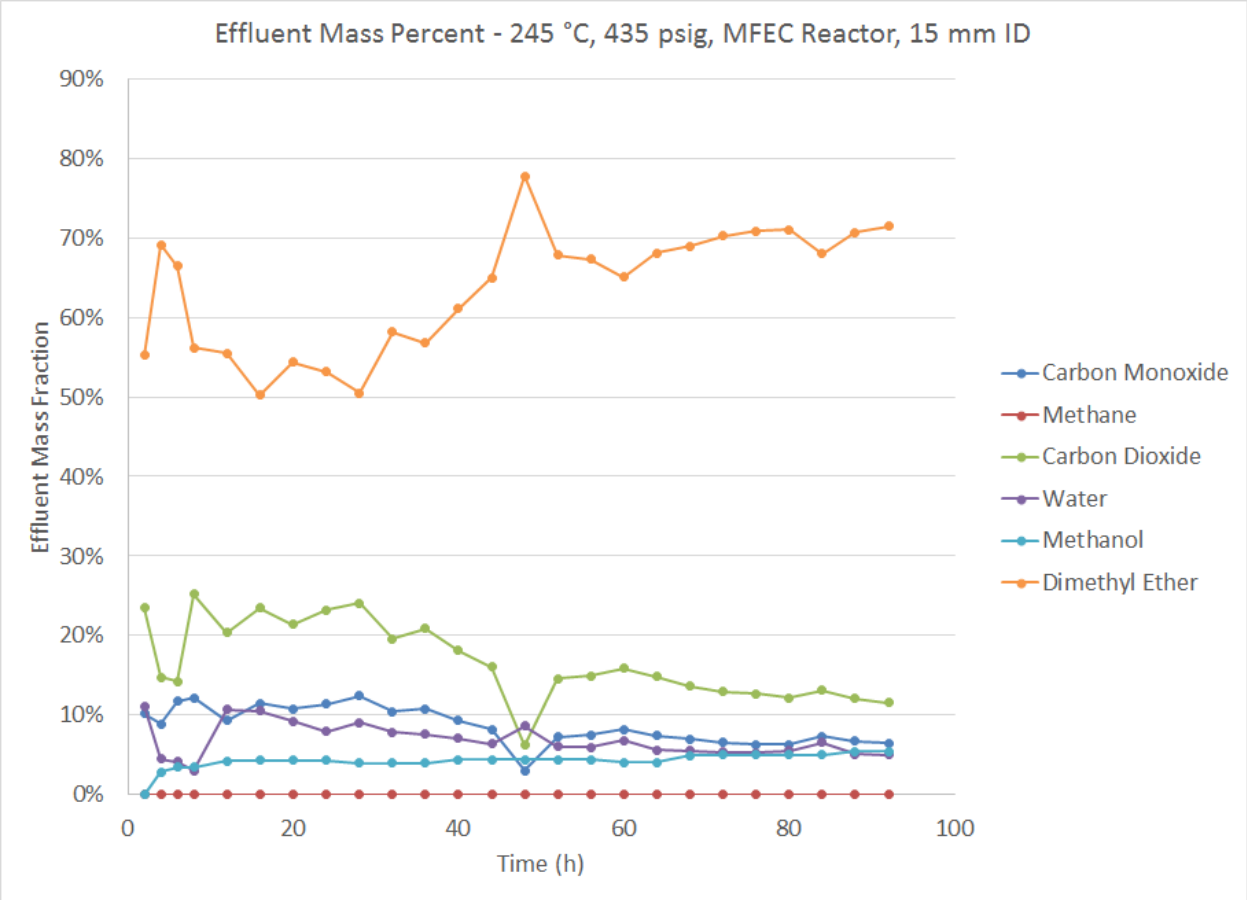

Figure 41. Product distribution as a mass perfect for single-step dimethyl ether synthesis with MFEC reactor conditions of ID=15mm, P=435psig, T_{Inlet}=245°C, H_2:CO ratio of 3:1, and GHSV=1880 h^{-1}. Catalyst (60-80 mesh, or 180-250 μm) is HiFuelR120 and γ-Al_2O_3 in a 2:1 ratio by mass

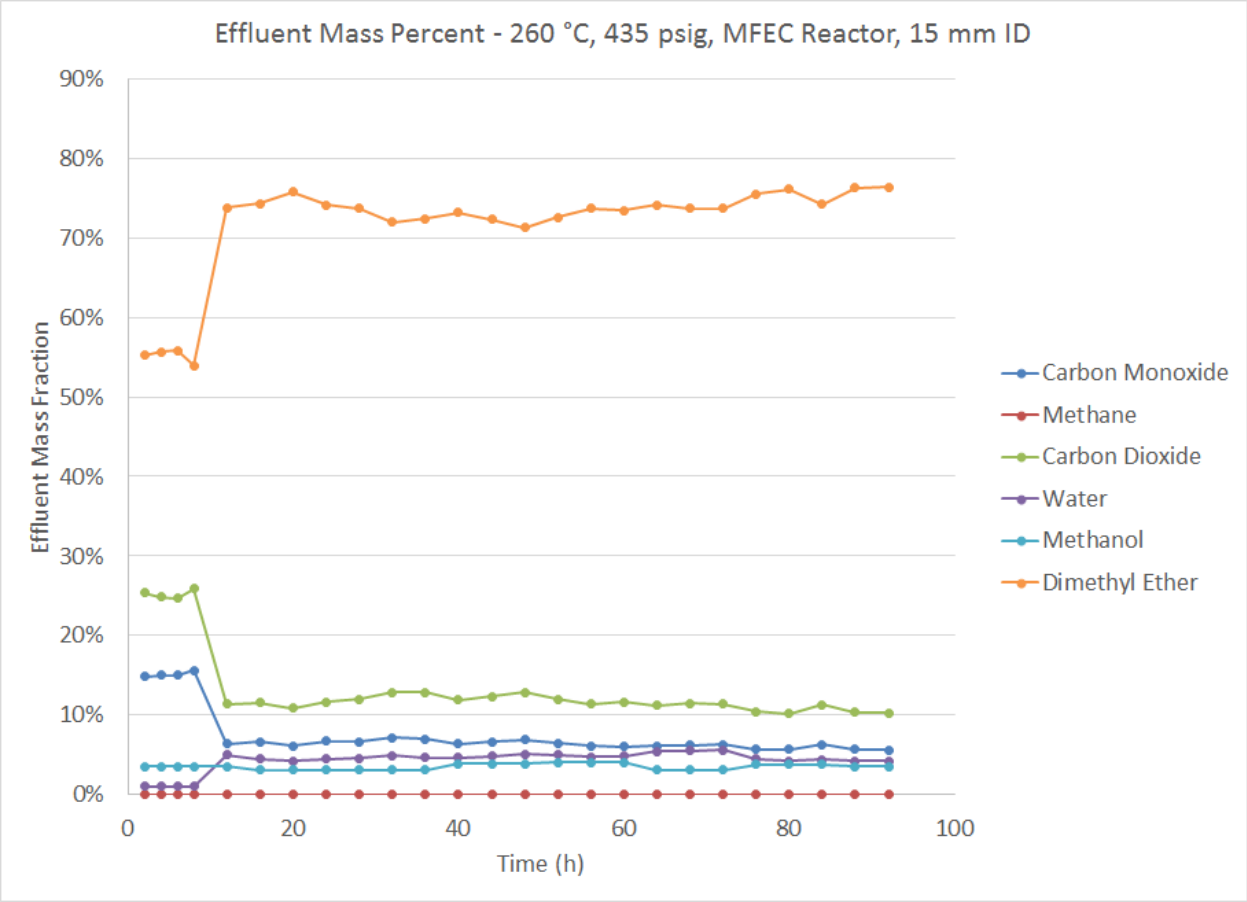

Figure 42. Product distribution as a mass perfect for single-step dimethyl ether synthesis with MFEC reactor conditions of ID=15mm, P=435psig, T_{Inlet}=260°C, H_2:CO ratio of 3:1, and GHSV=1880 h^{-1}. Catalyst (60-80 mesh, or 180-250 μm) is HiFuelR120 and γ-Al_2O_3 in a 2:1 ratio by mass

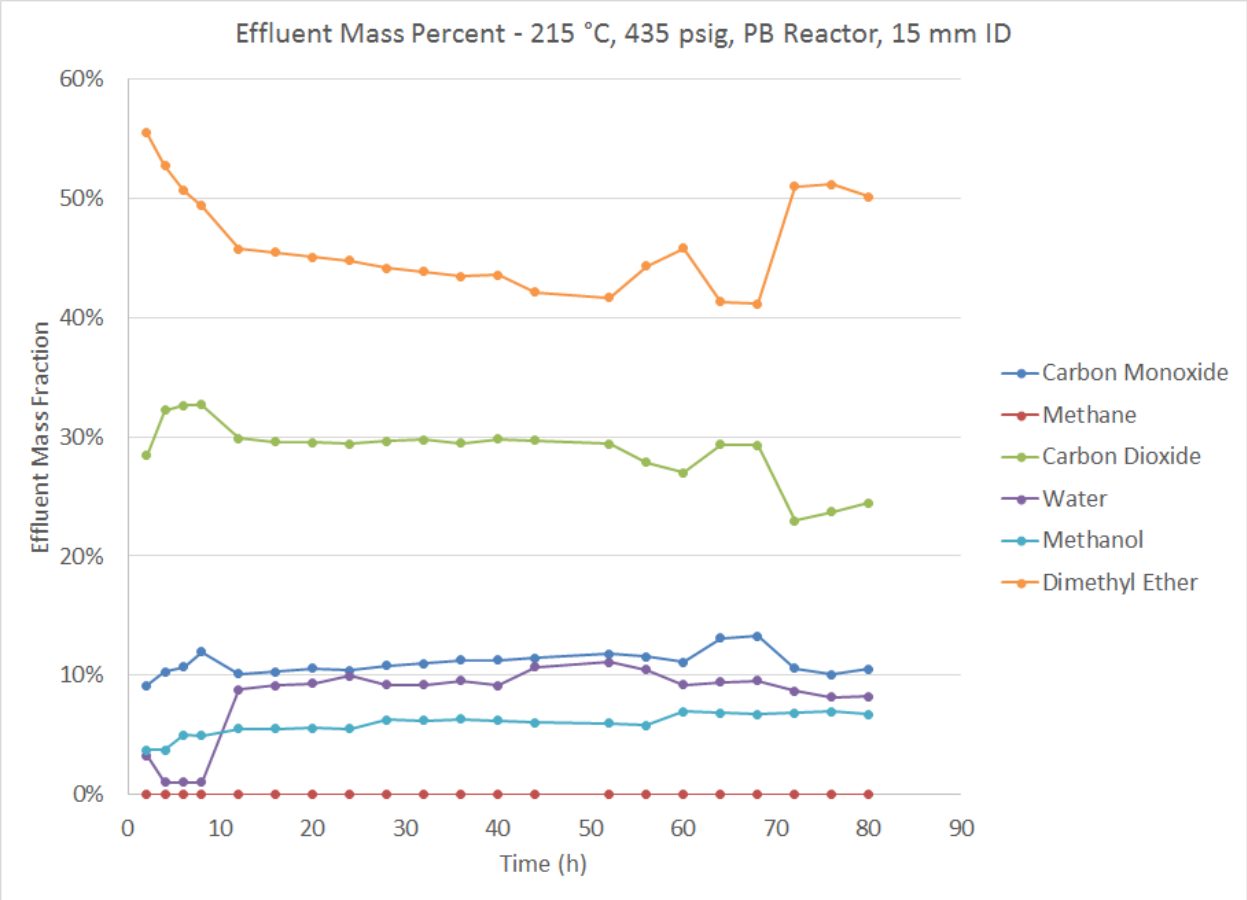

Figure 43. Product distribution as a mass perfect for single-step dimethyl ether synthesis with PB reactor conditions of ID=15mm, P=435psig, T_{Inlet}=215°C, H_2:CO ratio of 3:1, and GHSV=1880 h^{-1}. Catalyst (60-80 mesh, or 180-250 μm) is HiFuelR120 and γ-Al_2O_3 in a 2:1 ratio by mass

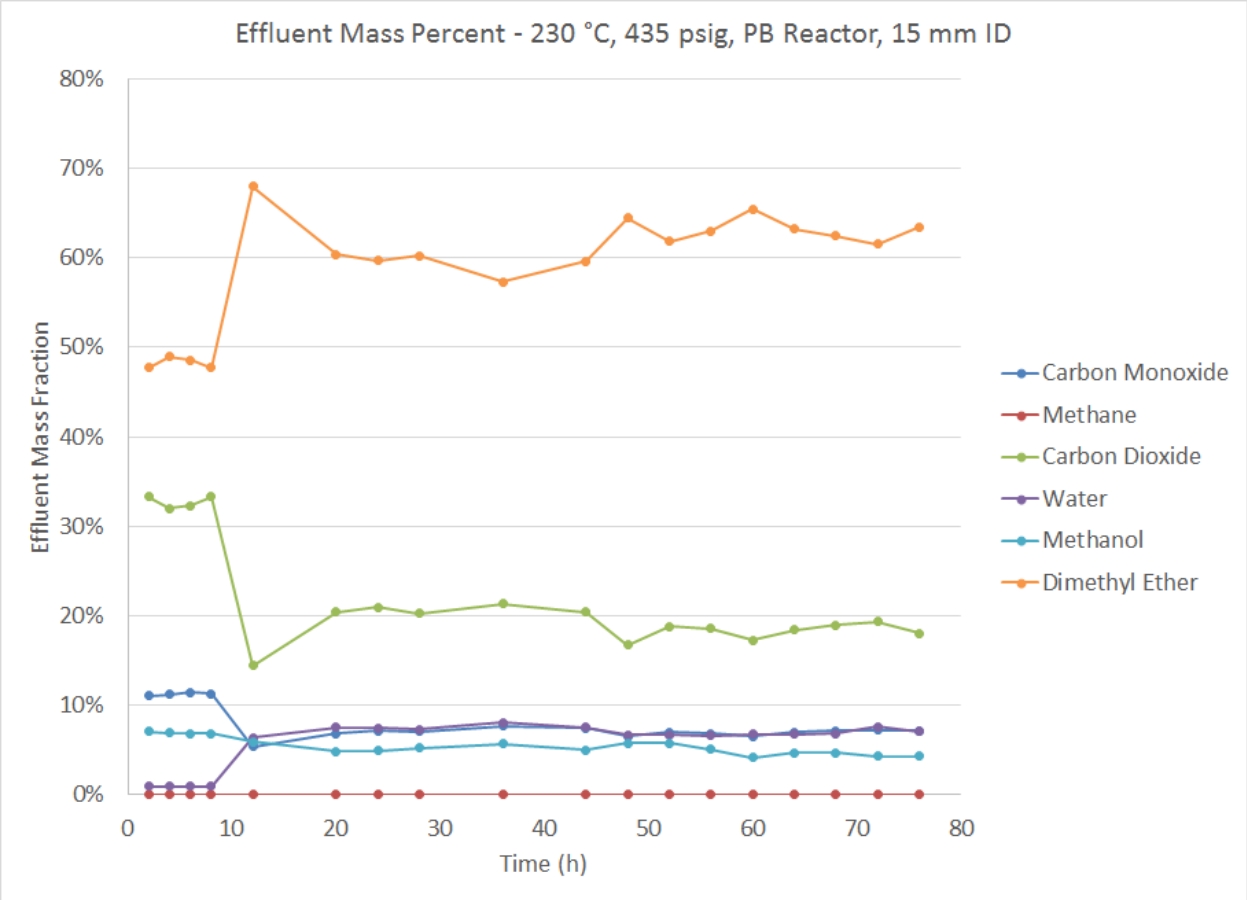

Figure 44. Product distribution as a mass perfect for single-step dimethyl ether synthesis with PB reactor conditions of ID=15mm, P=435psig, T_{Inlet}=230°C, H_2:CO ratio of 3:1, and GHSV=1880 h^{-1}. Catalyst (60-80 mesh, or 180-250 μm) is HiFuelR120 and γ-Al_2O_3 in a 2:1 ratio by mass

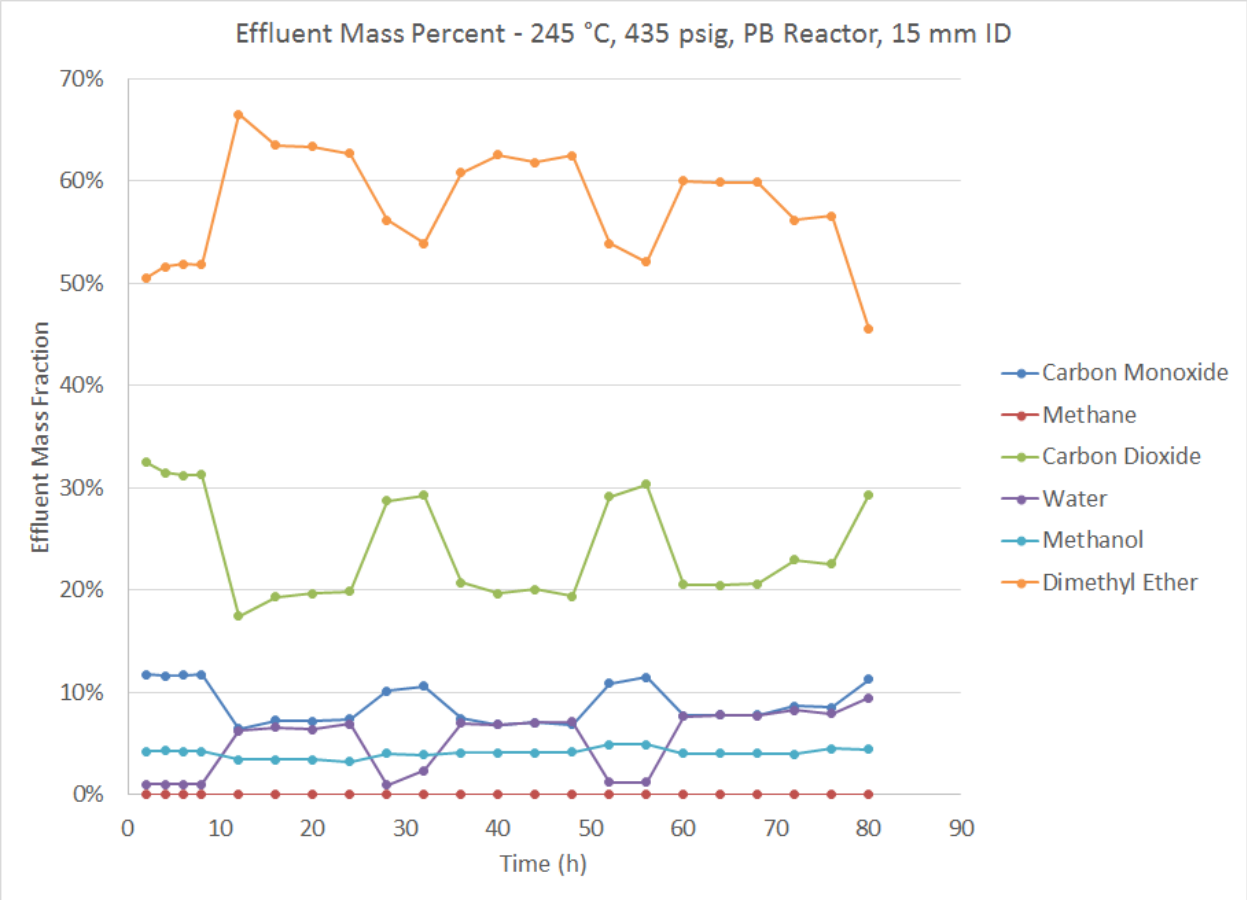

Figure 45. Product distribution as a mass perfect for single-step dimethyl ether synthesis with PB reactor conditions of ID=15mm, P=435psig, T_{Inlet}=245°C, H_2:CO ratio of 3:1, and GHSV=1880 h^{-1}. Catalyst (60-80 mesh, or 180-250 μm) is HiFuelR120 and γ-Al_2O_3 in a 2:1 ratio by mass

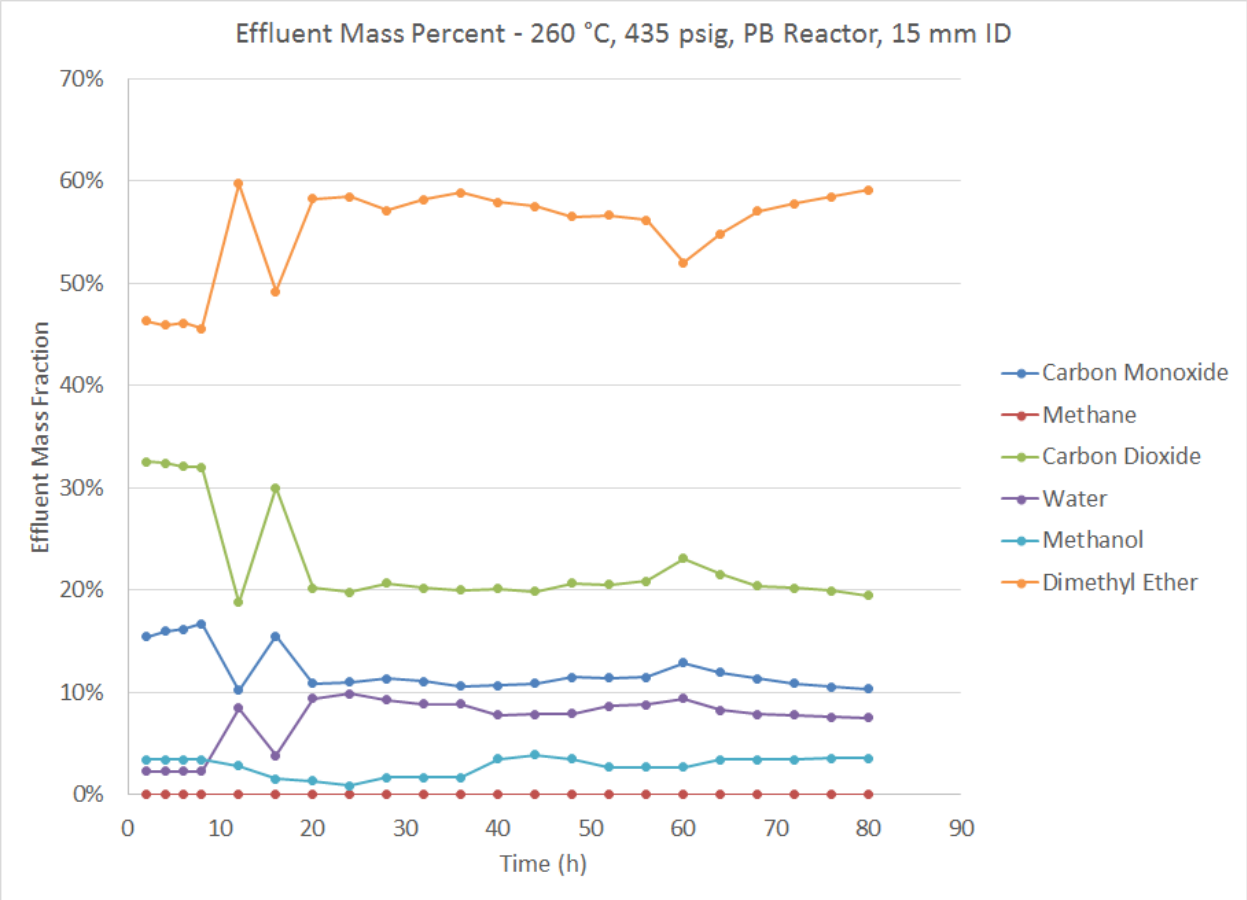

Figure 46. Product distribution as a mass perfect for single-step dimethyl ether synthesis with PB reactor conditions of ID=15mm, P=435psig, T_{Inlet}=260°C, H_2:CO ratio of 3:1, and GHSV=1880 h^{-1}. Catalyst (60-80 mesh, or 180-250 μm) is HiFuelR120 and γ-Al_2O_3 in a 2:1 ratio by mass

4.5 29mm ID Single-Step Dimethyl Ether Synthesis Results

Since the single-step dimethyl ether synthesis results in a 15mm ID reactor indicated an improved performance for the MFEC reactor over the PB reactor, the reactor was enlarged to a 29mm ID reactor. As can be seen from Figure 12, the effect of temperature on single-step dimethyl ether synthesis can be significant, and this was expected to be more pronounced in the larger scale reactor. Not only can an increase in temperature produce a drop in theoretical conversion of carbon monoxide, an increase in temperature also has the potential to form

methane. Though methane was not seen in the 15mm ID runs, it was hypothesized that the larger scale reactor would allow for the temperature rise to be significant for methane to be formed.

The 29mm ID reactor was run at varying inlet temperatures (245°C, 260°C, 275°C, 290°C) with a MFEC bed, and those profiles are shown in Figure 47, Figure 48, Figure 49, and Figure 50, respectively. The same reactor inlet temperatures were run for a packed bed of equivalent volumetric catalyst loading (diluted with inert material). The packed bed temperature profiles are shown in Figure 51, Figure 52, Figure 53, and Figure 54. Overall, the temperature profiles exhibit a trend in which the MFEC beds are able to maintain a temperature without drifting like their packed bed counterparts. Furthermore, the MFEC beds also do not reach as high of a centerline temperature as their PB counterparts.

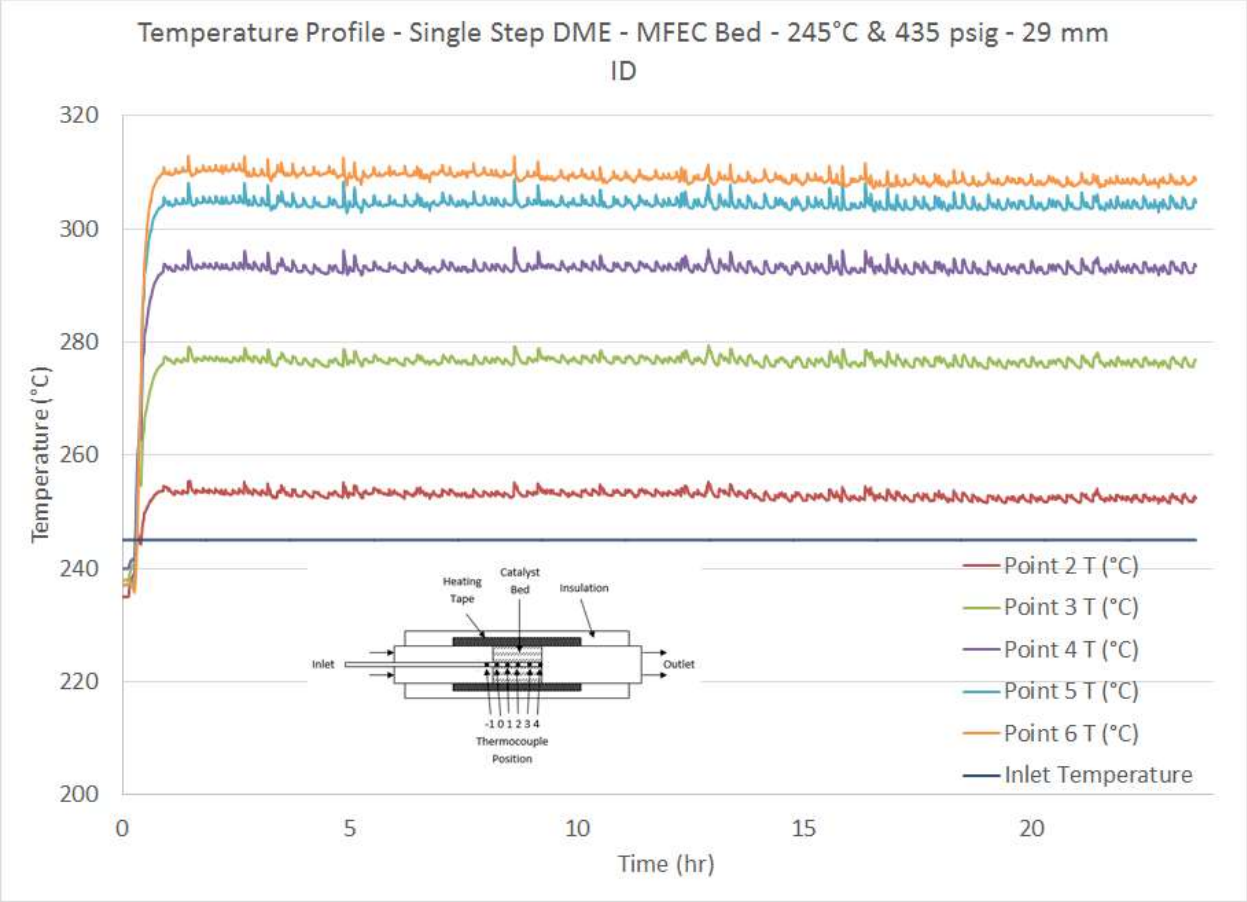

Figure 47. Temperature profile as a function of time for single-step dimethyl ether synthesis with MFEC reactor conditions of ID=29mm, P=435psig, T_{Inlet}=245°C, H_2:CO ratio of 3:1, and GHSV=1880 h^{-1}. Catalyst (60-80 mesh, or 180-250 μm) is HiFuelR120 and γ-Al_2O_3 in a 2:1 ratio by mass

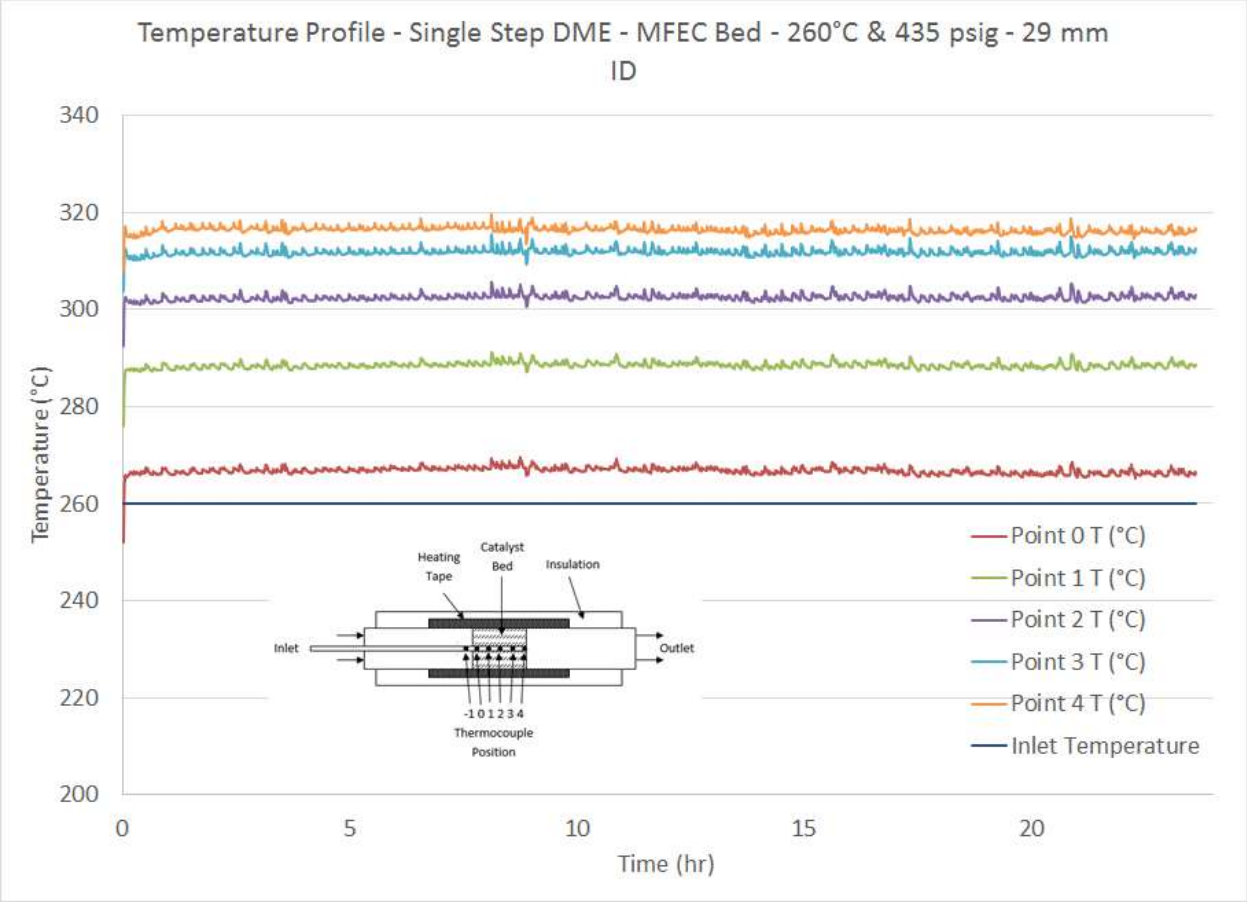

Figure 48. Temperature profile as a function of time for single-step dimethyl ether synthesis with MFEC reactor conditions of ID=29mm, P=435psig, T_{Inlet}=260°C, H_2:CO ratio of 3:1, and GHSV=1880 h^{-1}. Catalyst (60-80 mesh, or 180-250 μm) is HiFuelR120 and γ-Al_2O_3 in a 2:1 ratio by mass

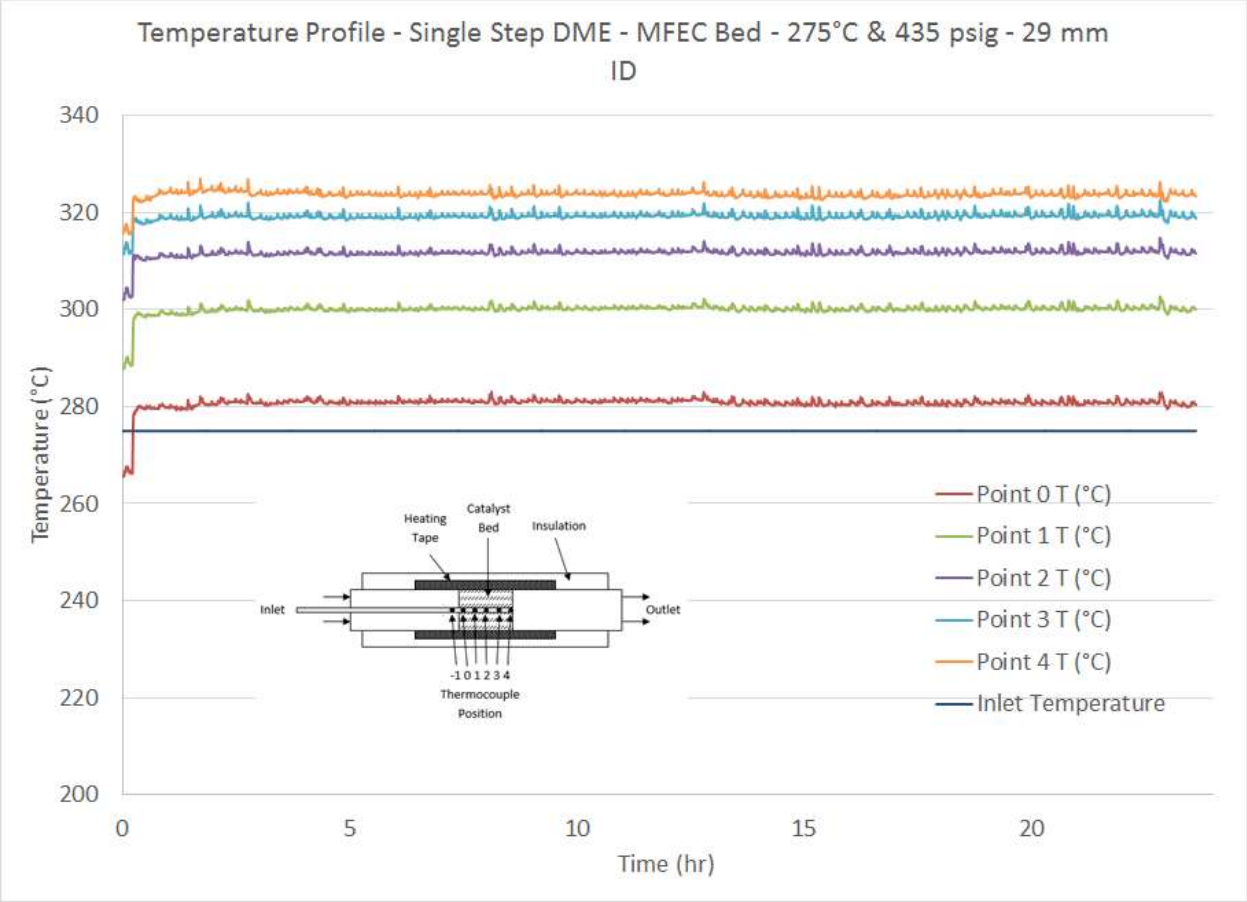

Figure 49. Temperature profile as a function of time for single-step dimethyl ether synthesis with MFEC reactor conditions of ID=29mm, P=435psig, T_{Inlet}=275°C, H_2:CO ratio of 3:1, and GHSV=1880 h^{-1}. Catalyst (60-80 mesh, or 180-250 μm) is HiFuelR120 and γ-Al_2O_3 in a 2:1 ratio by mass

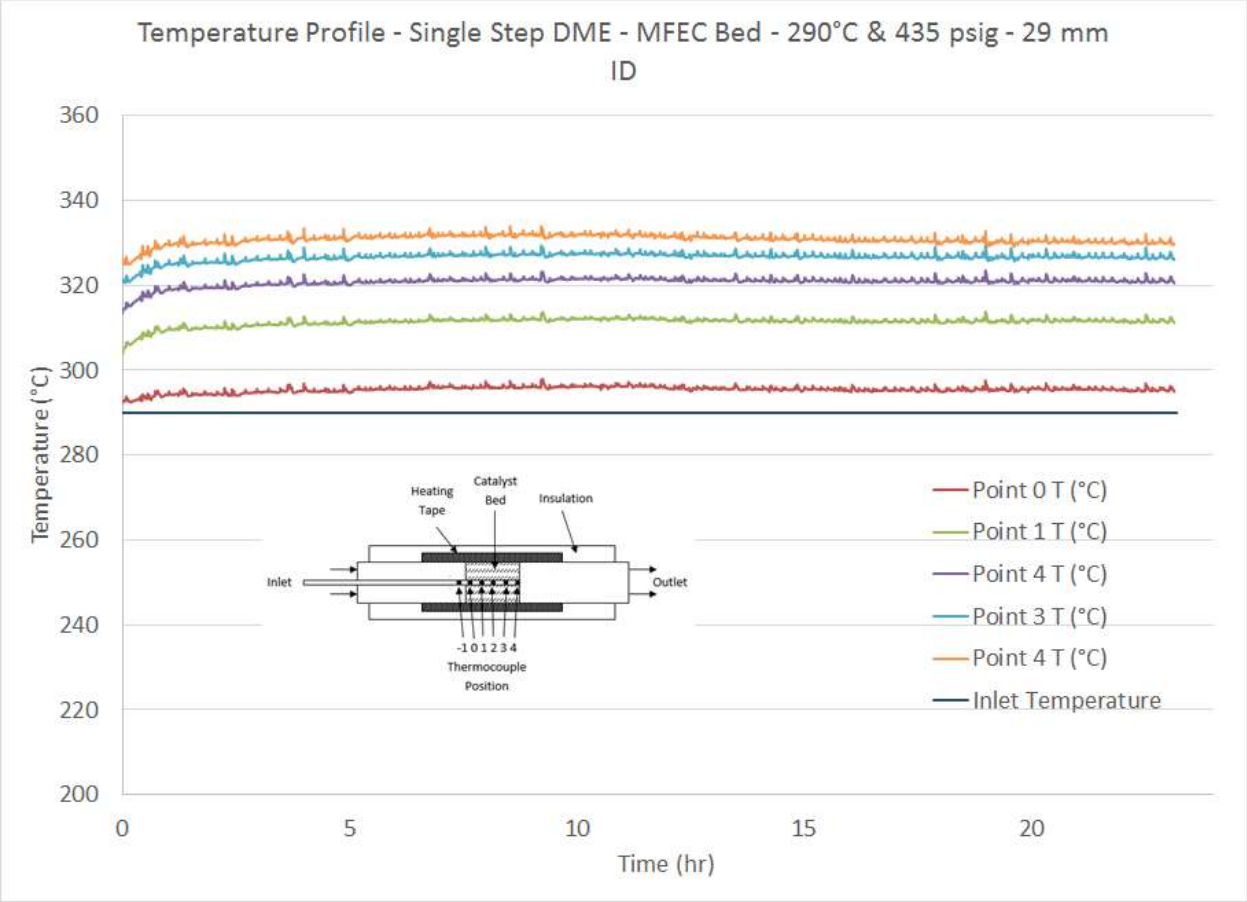

Figure 50. Temperature profile as a function of time for single-step dimethyl ether synthesis with MFEC reactor conditions of ID=29mm, P=435psig, T_{Inlet}=290°C, H_2:CO ratio of 3:1, and GHSV=1880 h^{-1}. Catalyst (60-80 mesh, or 180-250 μm) is HiFuelR120 and γ-Al_2O_3 in a 2:1 ratio by mass

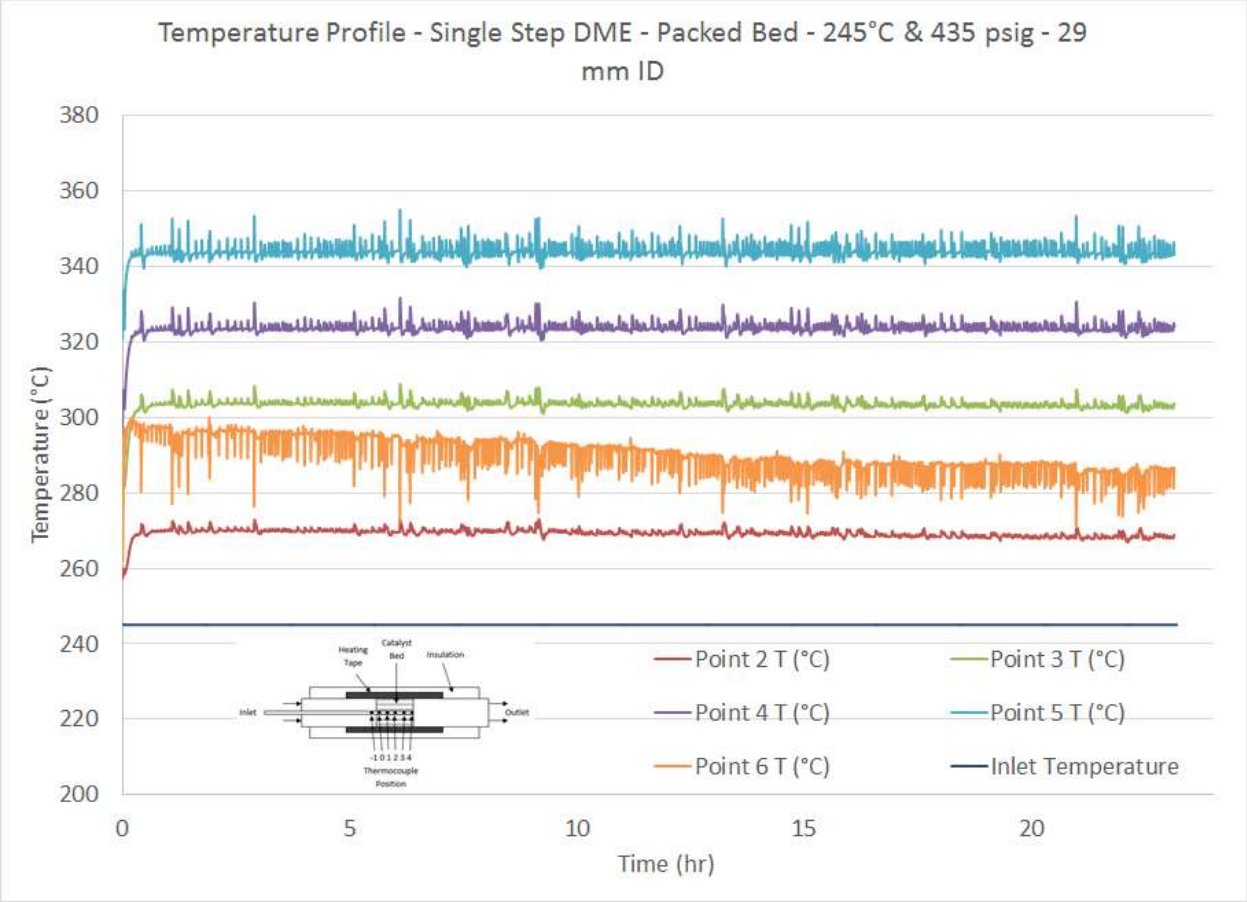

Figure 51. Temperature profile as a function of time for single-step dimethyl ether synthesis with PB reactor conditions of ID=29mm, P=435psig, T_{Inlet}=245°C, H_2:CO ratio of 3:1, and GHSV=1880 h^{-1}. Catalyst (60-80 mesh, or 180-250 μm) is HiFuelR120 and γ-Al_2O_3 in a 2:1 ratio by mass

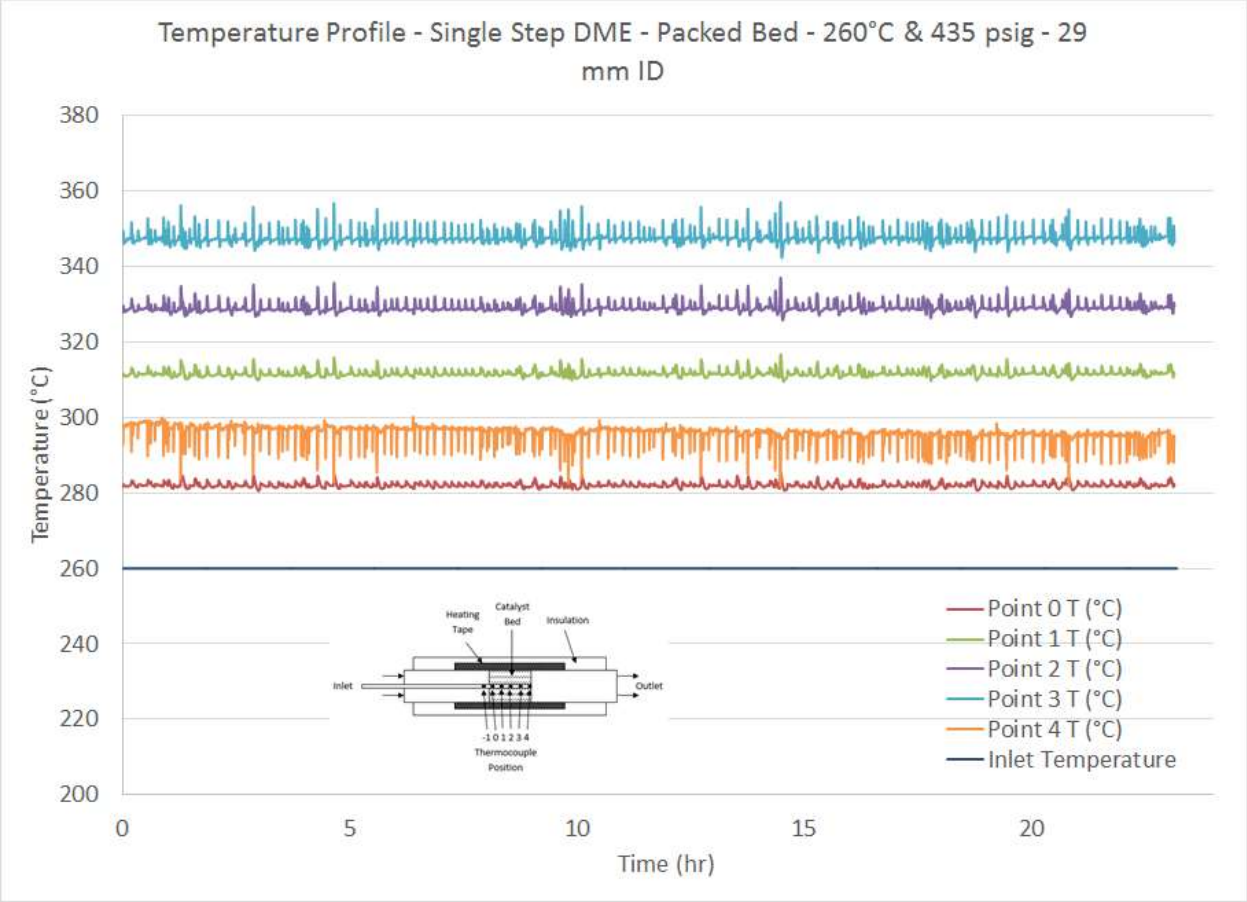

Figure 52. Temperature profile as a function of time for single-step dimethyl ether synthesis with PB reactor conditions of ID=29mm, P=435psig, T_{Inlet}=260°C, H_2:CO ratio of 3:1, and GHSV=1880 h^{-1}. Catalyst (60-80 mesh, or 180-250 μm) is HiFuelR120 and γ-Al_2O_3 in a 2:1 ratio by mass

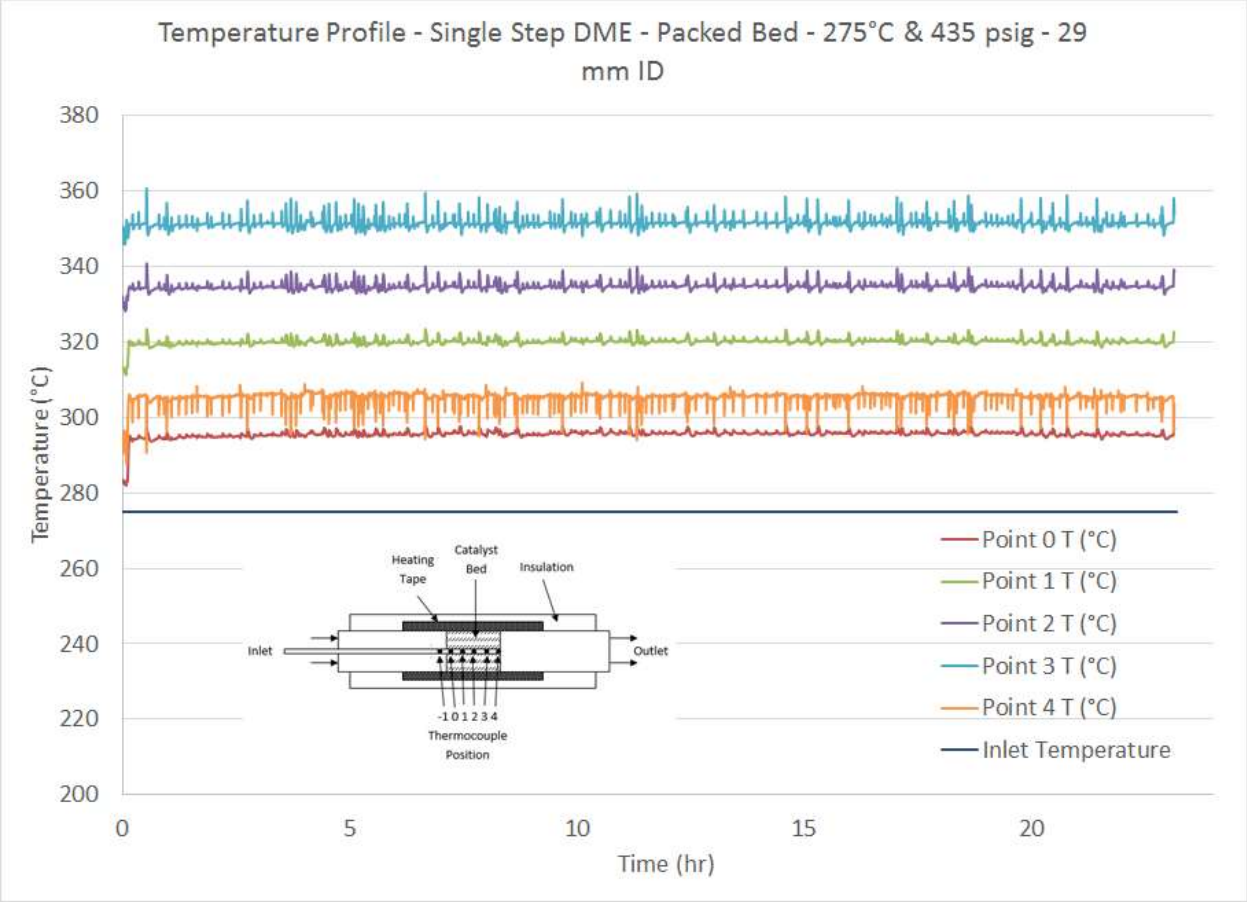

Figure 53. Temperature profile as a function of time for single-step dimethyl ether synthesis with PB reactor conditions of ID=29mm, P=435psig, T_{Inlet}=275°C, H_2:CO ratio of 3:1, and GHSV=1880 h^{-1}. Catalyst (60-80 mesh, or 180-250 μm) is HiFuelR120 and γ-Al_2O_3 in a 2:1 ratio by mass

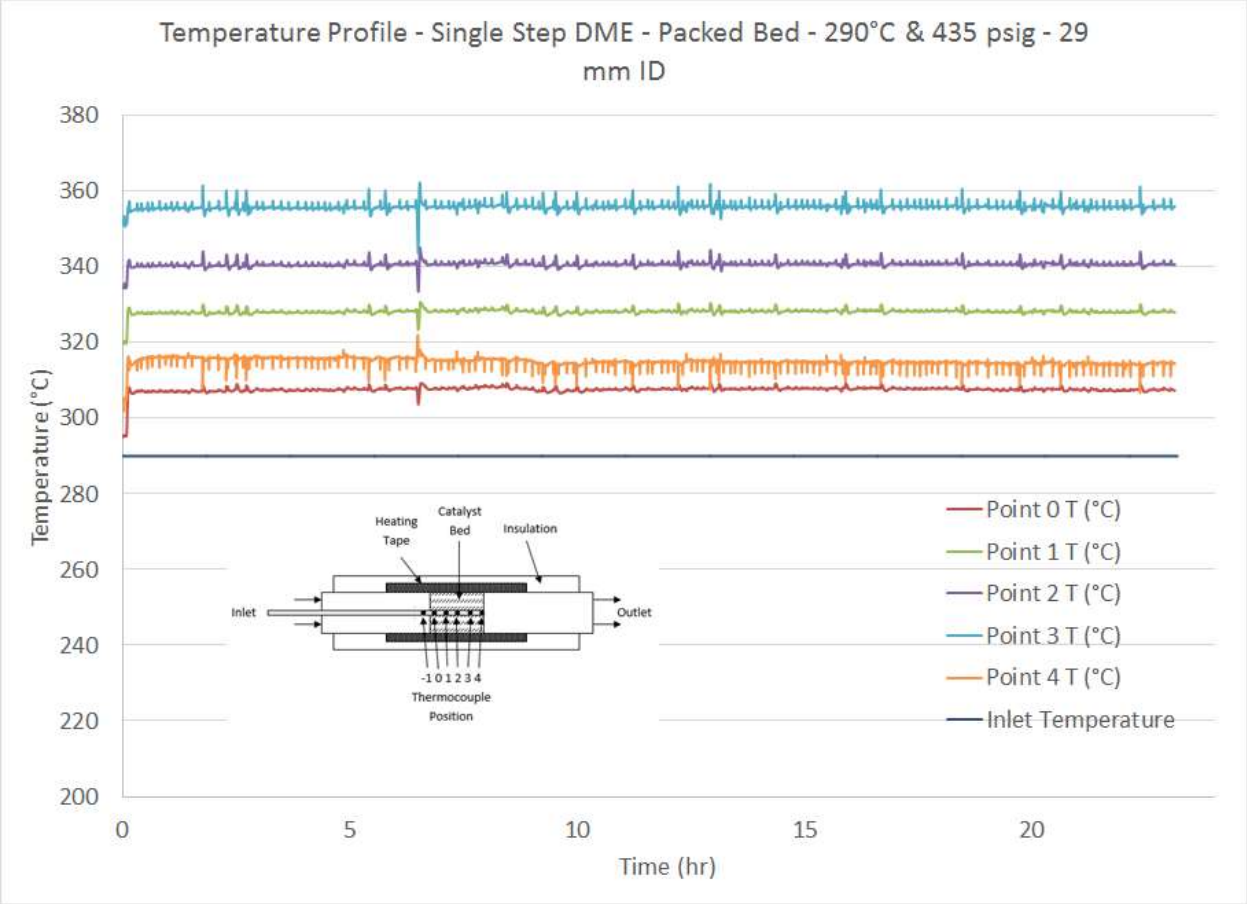

Figure 54. Temperature profile as a function of time for single-step dimethyl ether synthesis with PB reactor conditions of ID=29mm, P=435psig, T_{Inlet}=290°C, H_2:CO ratio of 3:1, and GHSV=1880 h^{-1}. Catalyst (60-80 mesh, or 180-250 μm) is HiFuelR120 and γ-Al_2O_3 in a 2:1 ratio by mass

Since it is difficult to compare the temperature profiles as currently presented, axial temperature profiles can better show the difference in how the MFEC vs. PB reactors are able to remove heat. The comparisons for each inlet temperature are shown in Figure 55, Figure 56, Figure 57, and Figure 58. It should be noted that in each figure, the packed bed obtains a higher increase in temperature compared to the packed bed. Further, the MFEC bed seems to have a

broader temperature profile, which corresponds with the increased thermal conductivity of the MFEC bed compared to the packed bed.

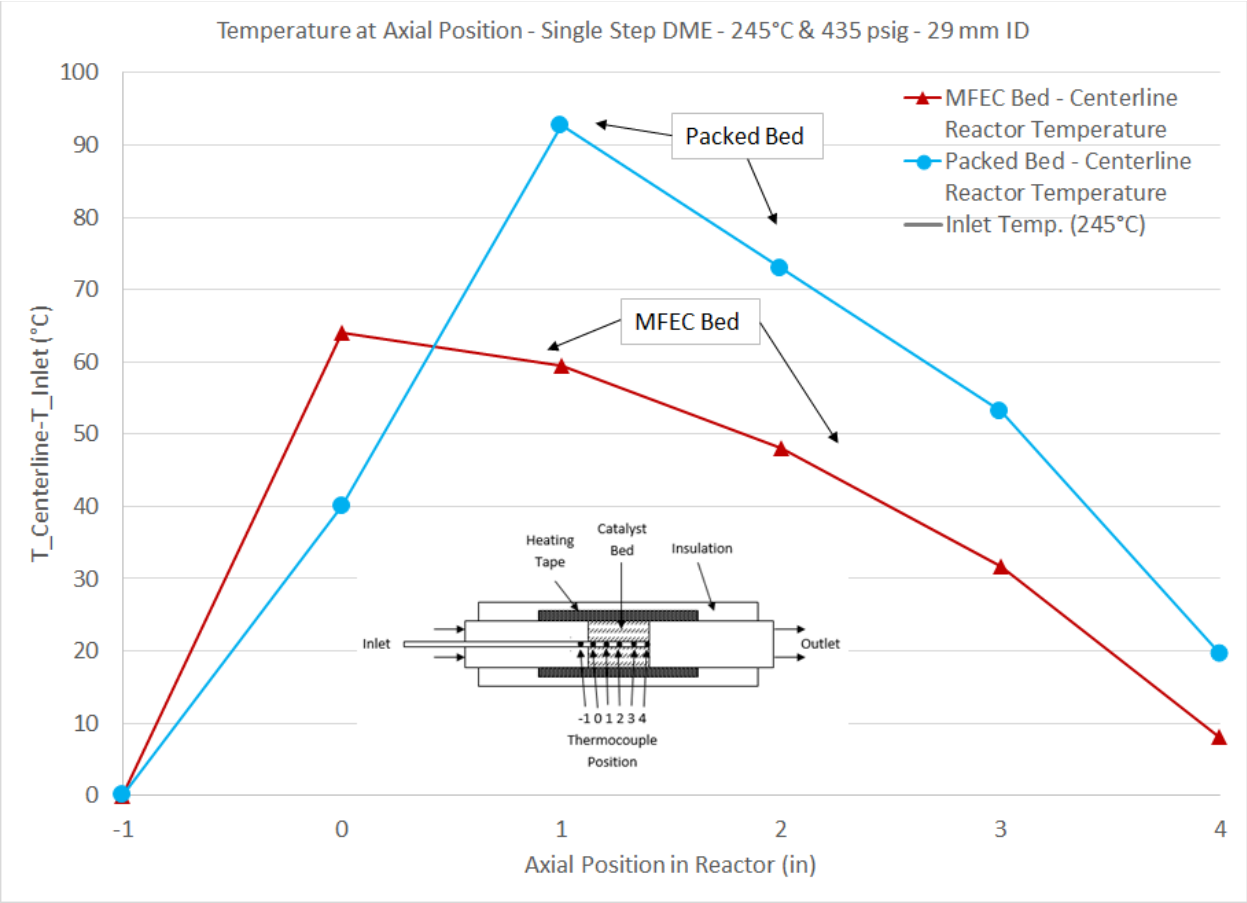

Figure 55. Axial temperature profile comparison for the 29mm ID reactors with T_{Inlet}=245°C.

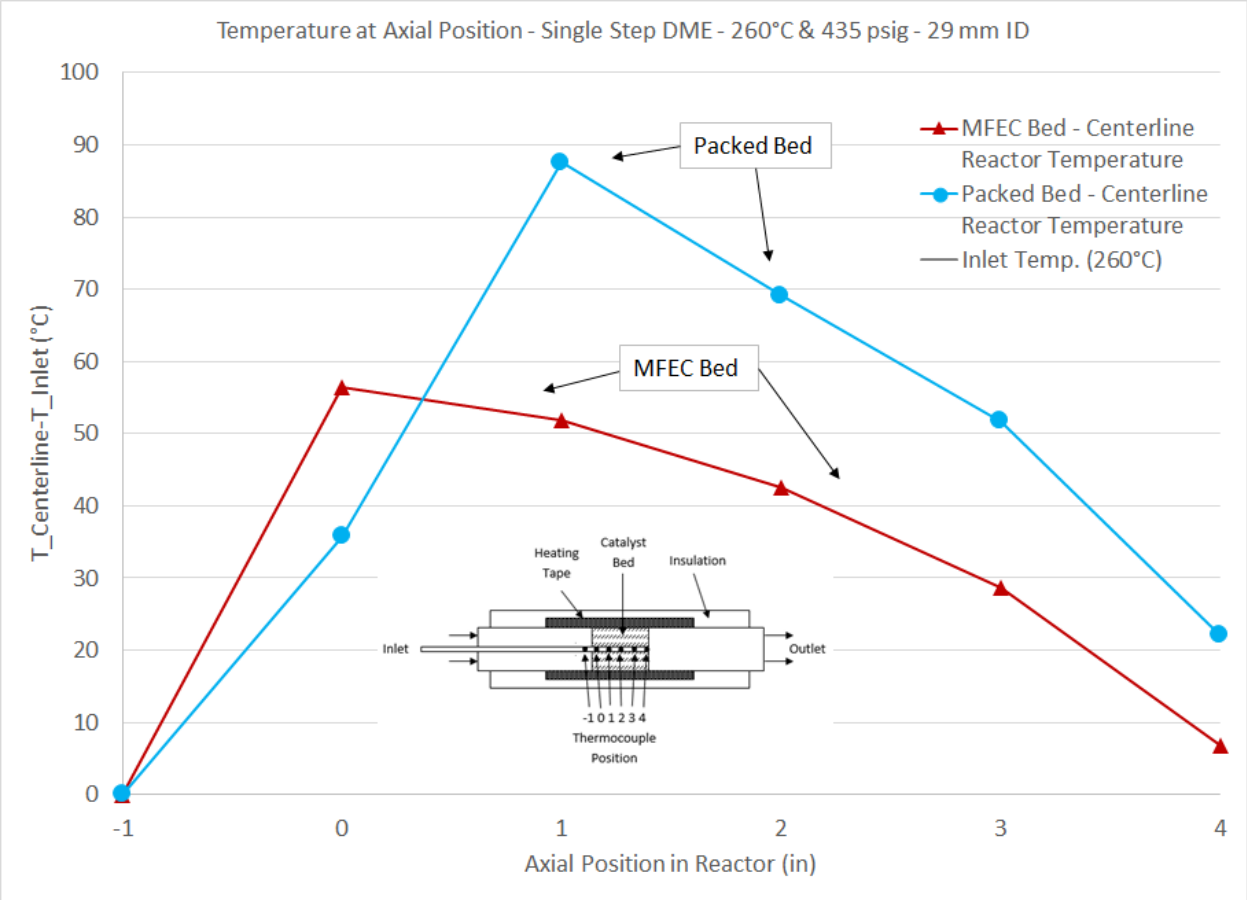

Figure 56. Axial temperature profile comparison for the 29mm ID reactors with T_{Inlet}=260°C.

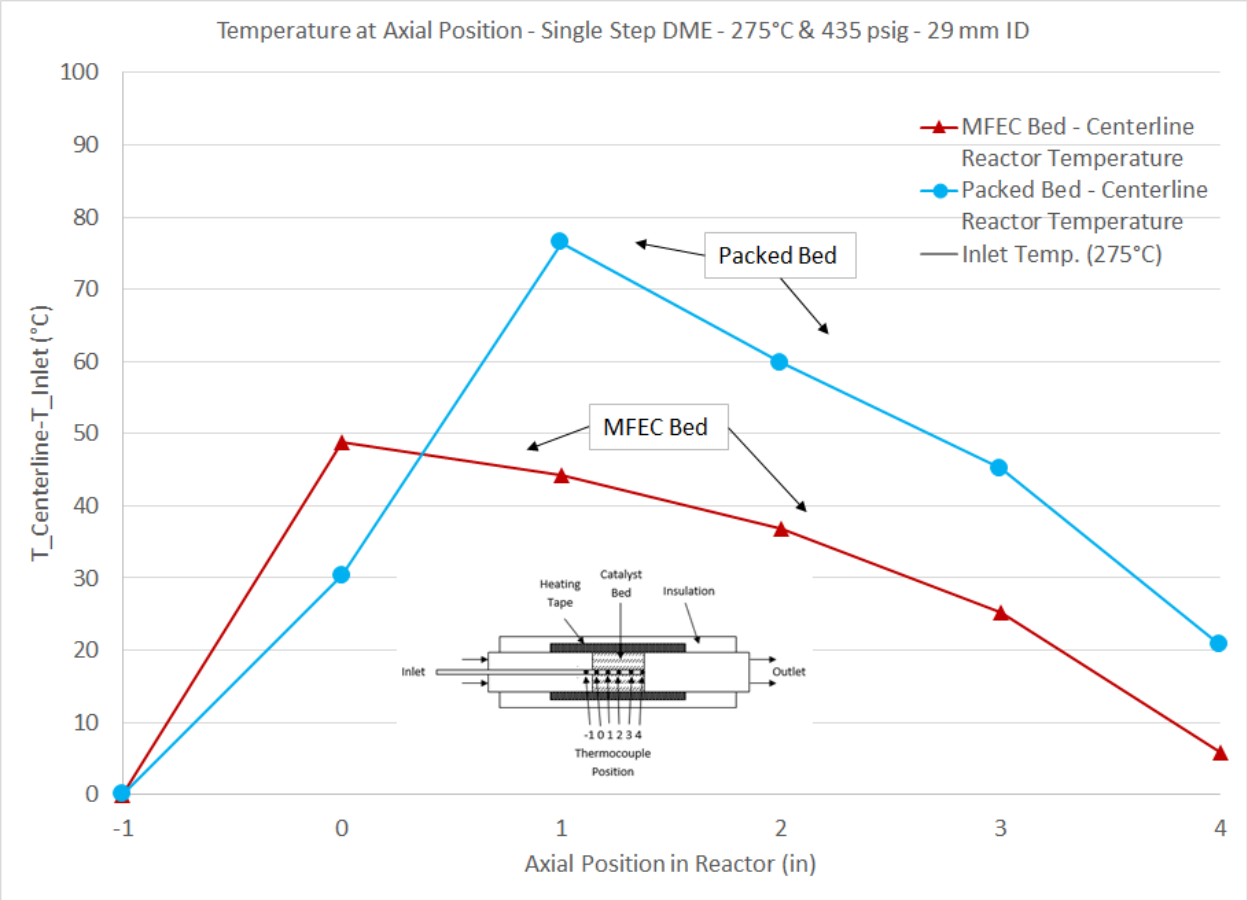

Figure 57. Axial temperature profile comparison for the 29mm ID reactors with T_{Inlet}=275°C.

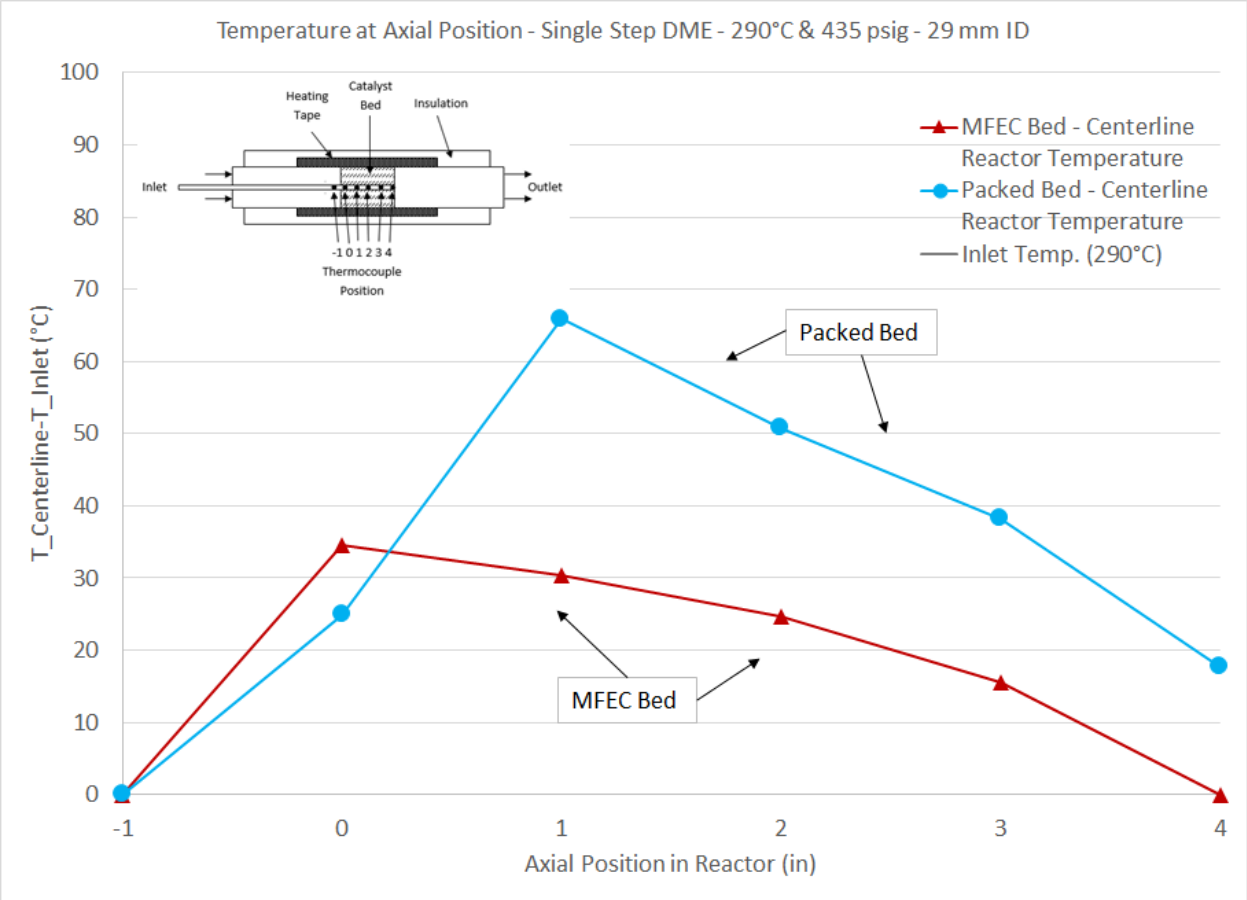

Figure 58. Axial temperature profile comparison for the 29mm ID reactors with T_{Inlet}=290°C.

To get a complete picture on the extent to which each reactor had an increase in temperature, Figure 59 was developed. In the figure, one can graphically see the difference in centerline temperature increases for both the 29 mm ID MFEC and PB reactors. In each pair of bar graphs, the gray bar to the left shows the maximum temperature increase along the centerline for the MFEC bed. In contrast, the PB maximum temperature increase is shown in the red bar to the right. Across all the various inlet temperatures, the MFEC had a lower increase in temperature. Further, as the inlet temperature increased, the PB deviation became more apparent, going from a 1.45 fold increase to a 1.91 fold increase. These temperature increases can have

negative side effects that typically result in unwanted products and/or a loss of carbon monoxide conversion.

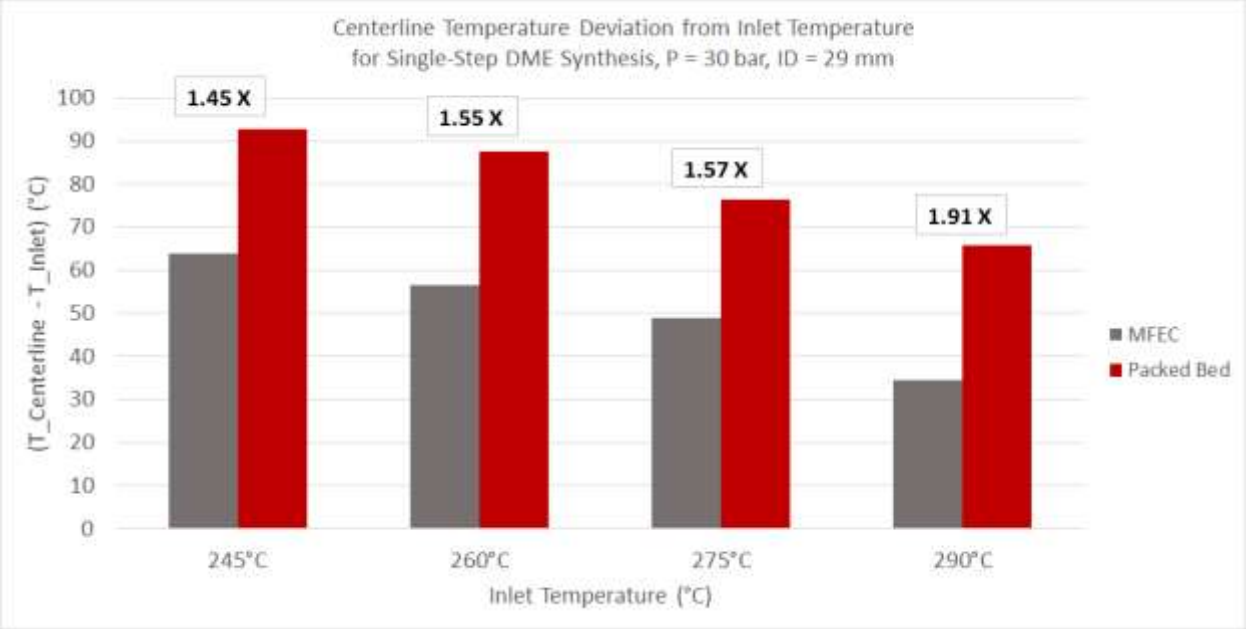

Figure 59. Comparison of the extent of temperature increase within the 29 mm ID reactor for both the MFEC and PB reactors.

In order to get a picture of how the temperature deviations shown in Figure 59 effected the product quality, the overall carbon monoxide conversion must be determined. In Figure 60, the trend can be seen that the MFEC reactor outperformed the PB by converting more of the carbon monoxide. This directly translates to a more profitable reactor due to less recycled carbon monoxide. As an aside, it should be noted that both reactors did overcome the methanol equilibrium constraints due to using the single-step dimethyl ether synthesis route.

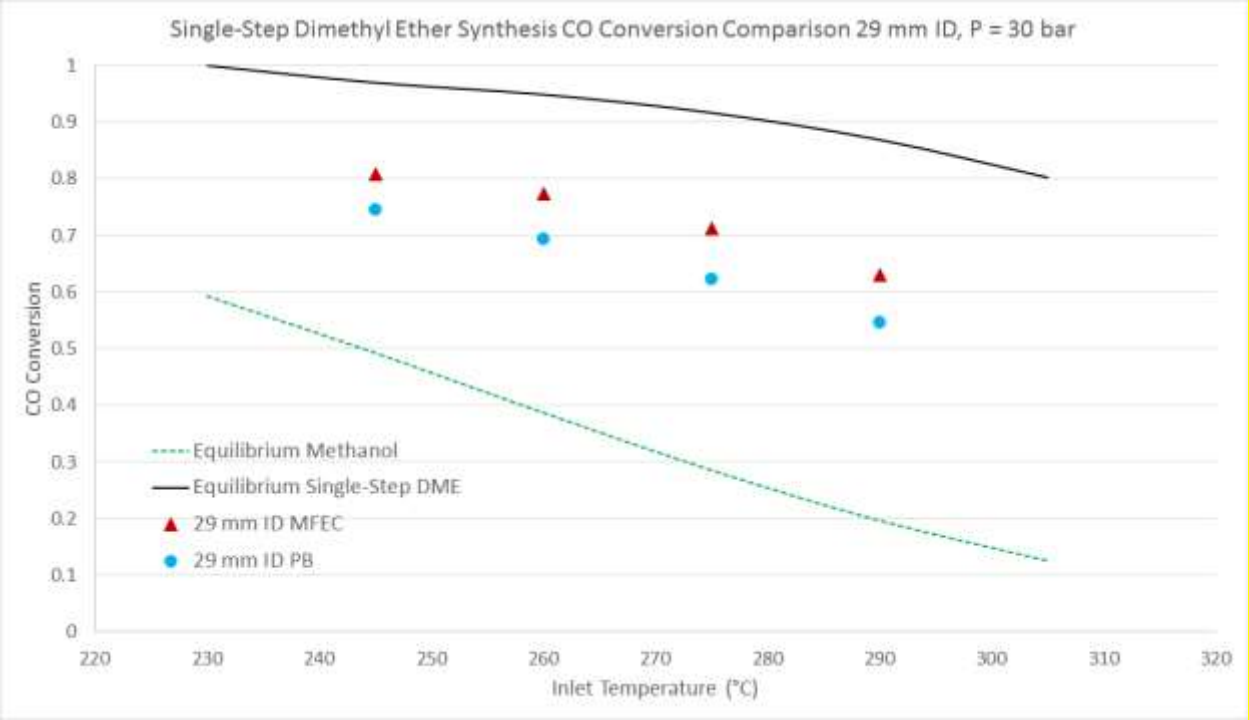

Figure 60. Overall carbon monoxide conversion for single-step dimethyl ether synthesis at varying temperatures for the 29mm ID reactors with a H_2:CO ratio of 3:1, and GHSV=1880 h^{-1}. Catalyst (60-80 mesh, or 180-250 μm) is HiFuelR120 and γ-Al_2O_3 in a 2:1 ratio by mass

However, as with the 15mm ID reactor studies, overall carbon monoxide conversion does not tell the entire story. The products that are ultimately produced are the most important part of a chemical conversion process. The goal of this reaction was to produce the most dimethyl ether possible, and the mass fraction of dimethyl ether in the effluent can be seen in Figure 61. Once again, the MFEC reactor does consistently produce more dimethyl ether in the product than its PB counterpart.

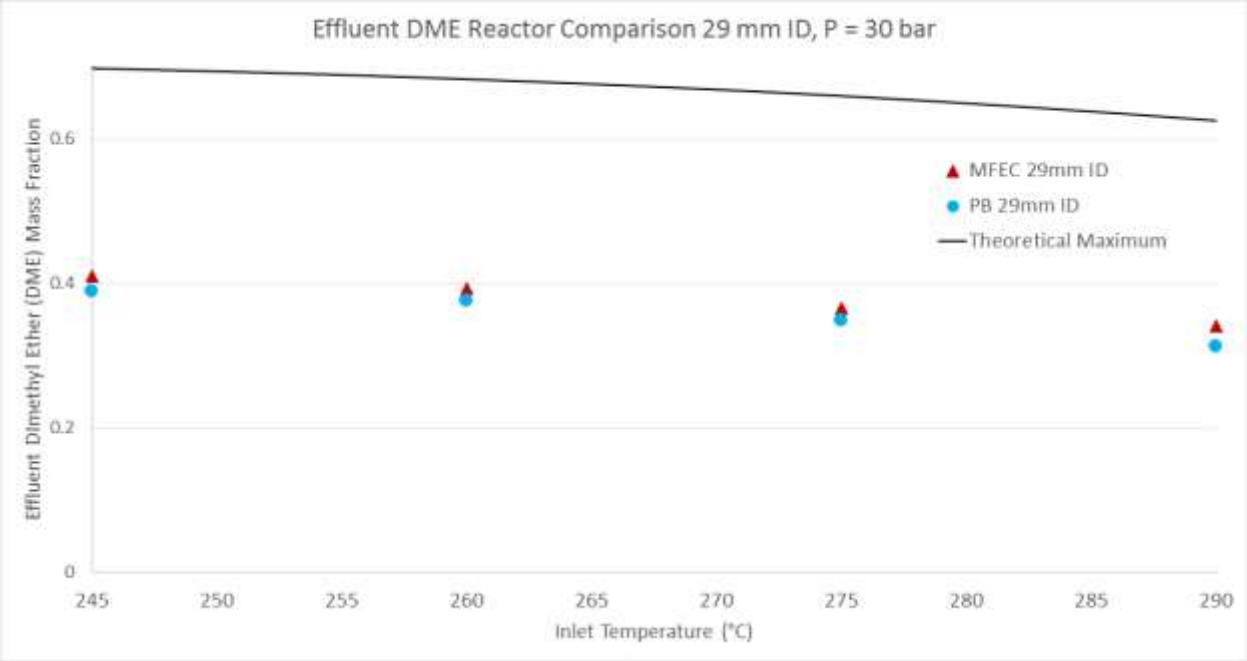

Figure 61. Effluent mass fraction of dimethyl ether for single-step dimethyl ether synthesis at varying temperatures for the 29mm ID reactors with a H_2:CO ratio of 3:1, and GHSV=1880 h^{-1}. Catalyst (60-80 mesh, or 180-250 μm) is HiFuelR120 and γ-Al_2O_3 in a 2:1 ratio by mass

The last main component of comparing the reactor schemes is to compare the overall products generated. In Figure 62, Figure 63, Figure 64, and Figure 65 the overall effluent mass fractions (ignoring hydrogen since it was run in excess) are shown for the MFEC reactors at 245°C, 260°C, 275°C, and 290°C, respectively. The comparable PB reactor effluent mass fractions can be viewed in Figure 66, Figure 67, Figure 68, and Figure 69 for 245°C, 260°C, 275°C, and 290°C, respectively. As mentioned previously, methane can be an indirect indicator of an increase in temperature that promotes the dissociative absorption of carbon monoxide. One very important difference between the MFEC reactor and PB reactors, is that the PB generated methane for each inlet temperature while the MFEC did not. Furthermore, as the inlet temperature of the PB increased, so too did the methane generation.

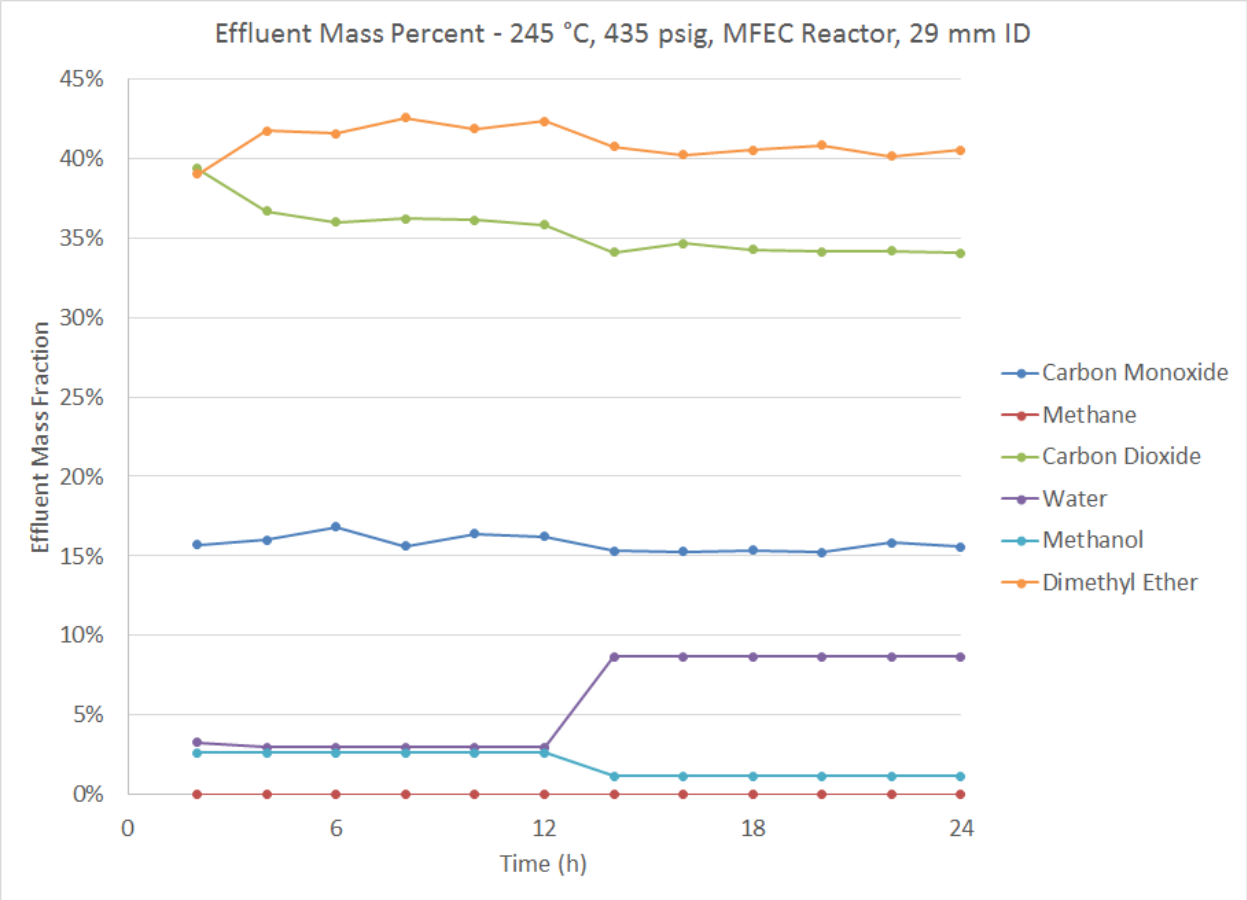

Figure 62. Product distribution as a mass perfect for single-step dimethyl ether synthesis with MFEC reactor conditions of ID=29mm, P=435psig, T_{Inlet}=245°C, H_2:CO ratio of 3:1, and GHSV=1880 h^{-1}. Catalyst (60-80 mesh, or 180-250 μm) is HiFuelR120 and γ-Al_2O_3 in a 2:1 ratio by mass

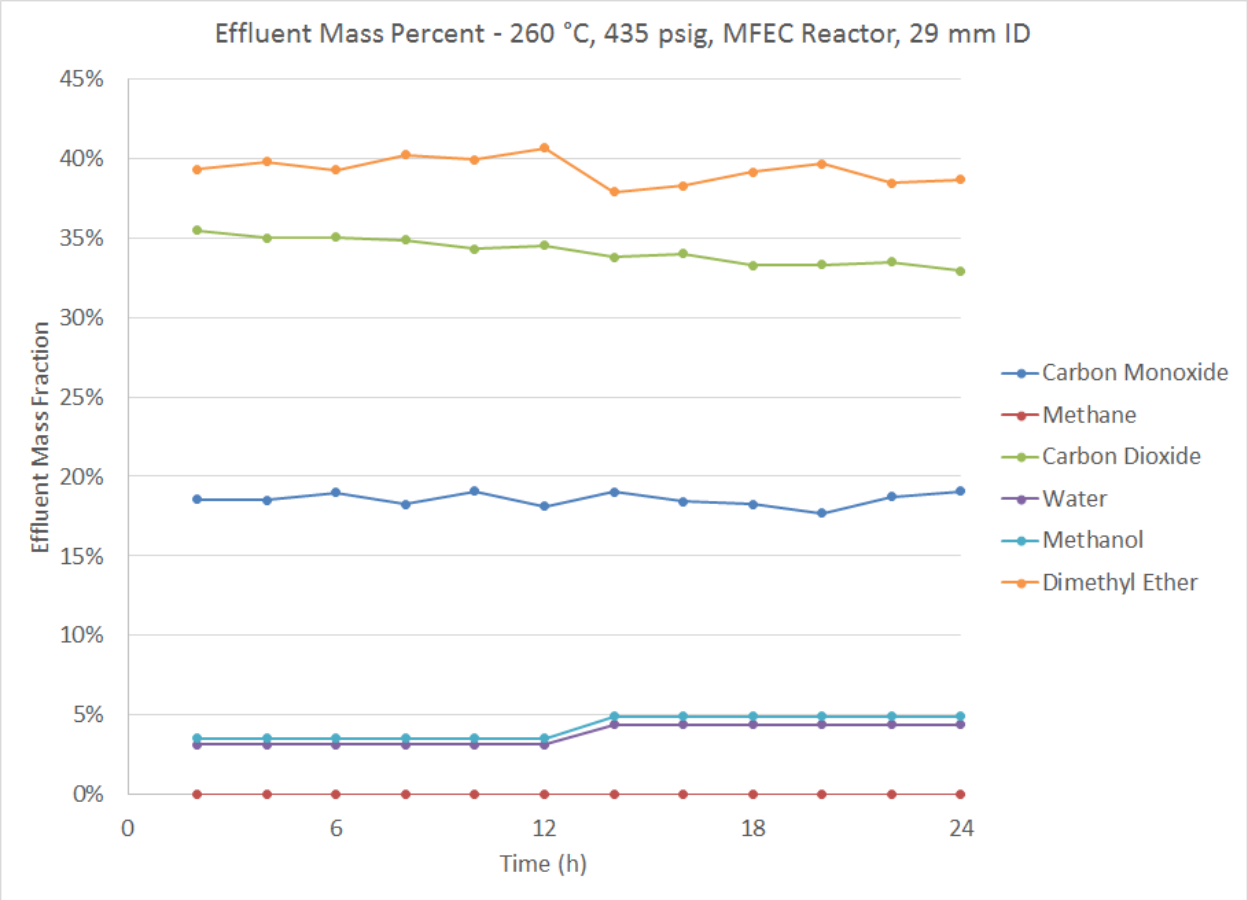

Figure 63. Product distribution as a mass perfect for single-step dimethyl ether synthesis with MFEC reactor conditions of ID=29mm, P=435psig, T_{Inlet}=260°C, H_2:CO ratio of 3:1, and GHSV=1880 h^{-1}. Catalyst (60-80 mesh, or 180-250 μm) is HiFuelR120 and γ-Al_2O_3 in a 2:1 ratio by mass

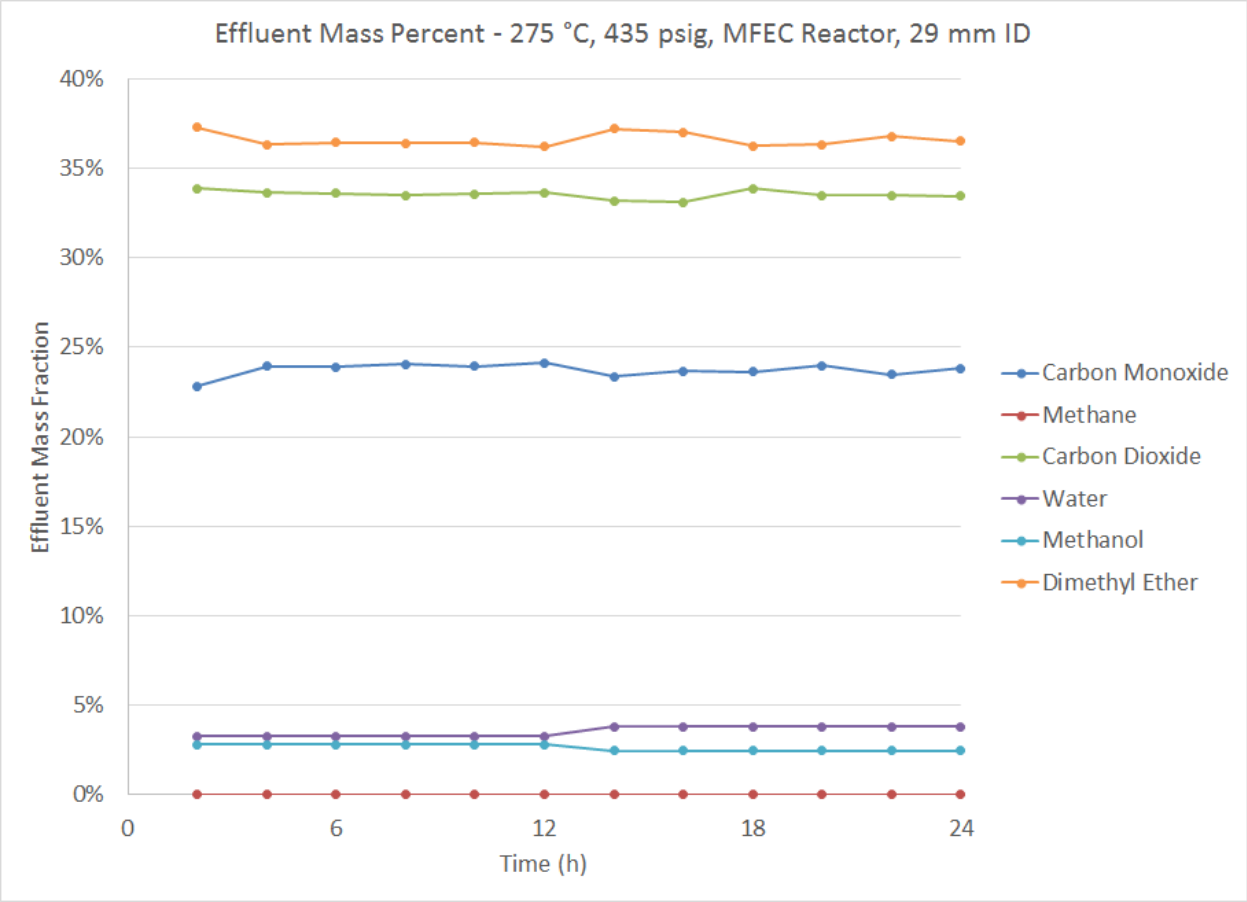

Figure 64. Product distribution as a mass perfect for single-step dimethyl ether synthesis with MFEC reactor conditions of ID=29mm, P=435psig, T_{Inlet}=275°C, H_2:CO ratio of 3:1, and GHSV=1880 h^{-1}. Catalyst (60-80 mesh, or 180-250 μm) is HiFuelR120 and γ-Al_2O_3 in a 2:1 ratio by mass

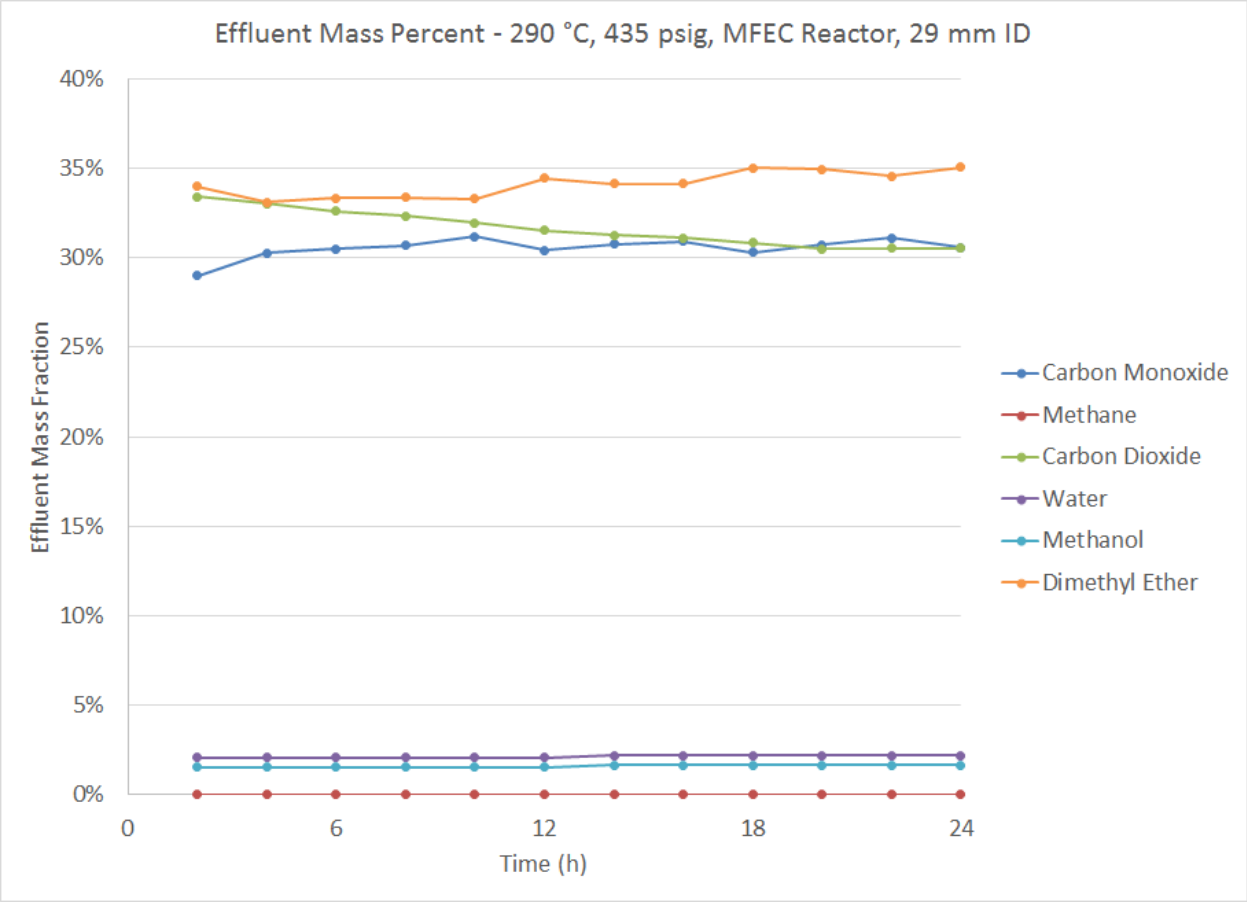

Figure 65. Product distribution as a mass perfect for single-step dimethyl ether synthesis with MFEC reactor conditions of ID=29mm, P=435psig, T_{Inlet}=290°C, H_2:CO ratio of 3:1, and GHSV=1880 h^{-1}. Catalyst (60-80 mesh, or 180-250 μm) is HiFuelR120 and γ-Al_2O_3 in a 2:1 ratio by mass

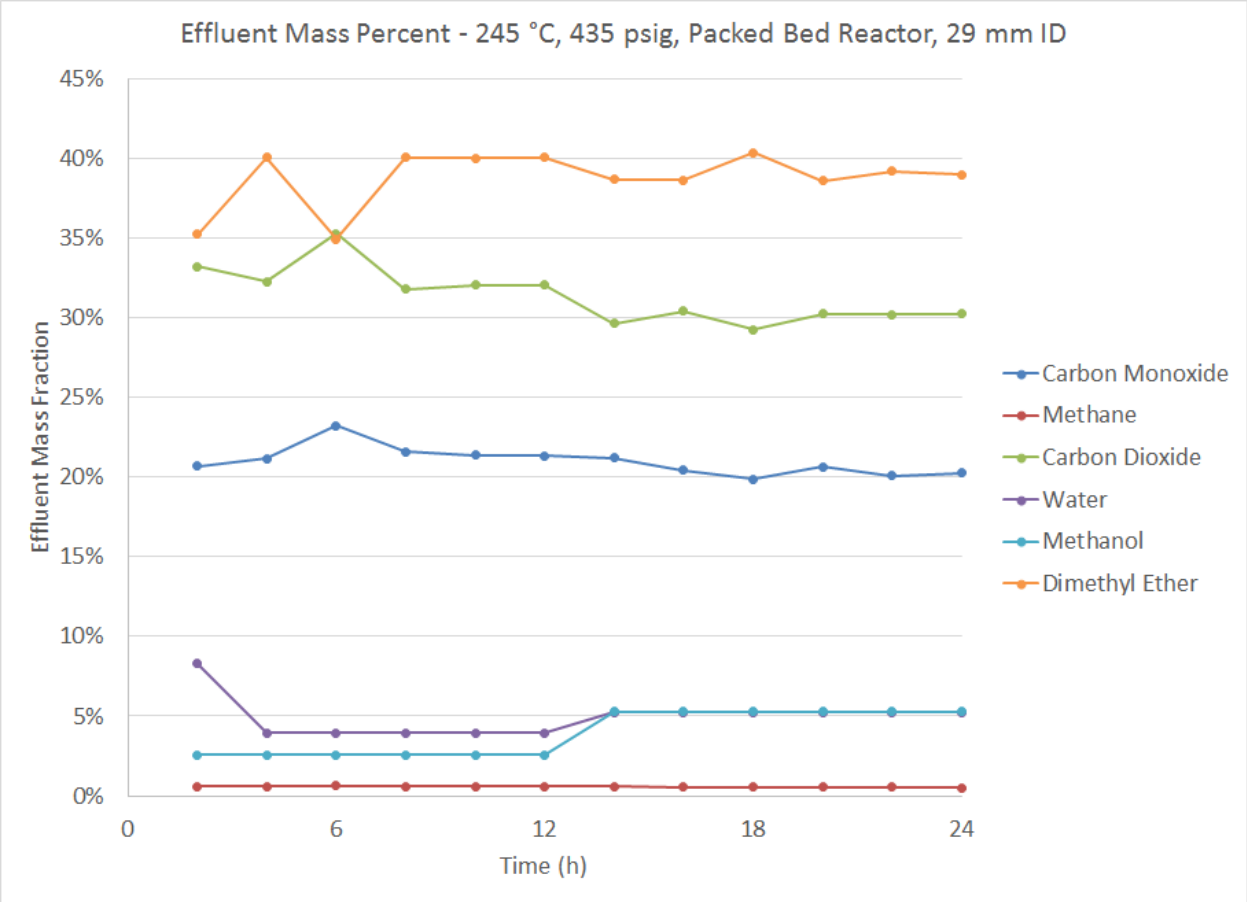

Figure 66. Product distribution as a mass perfect for single-step dimethyl ether synthesis with PB reactor conditions of ID=29mm, P=435psig, T_{Inlet}=245°C, H_2:CO ratio of 3:1, and GHSV=1880 h^{-1}. Catalyst (60-80 mesh, or 180-250 μm) is HiFuelR120 and γ-Al_2O_3 in a 2:1 ratio by mass

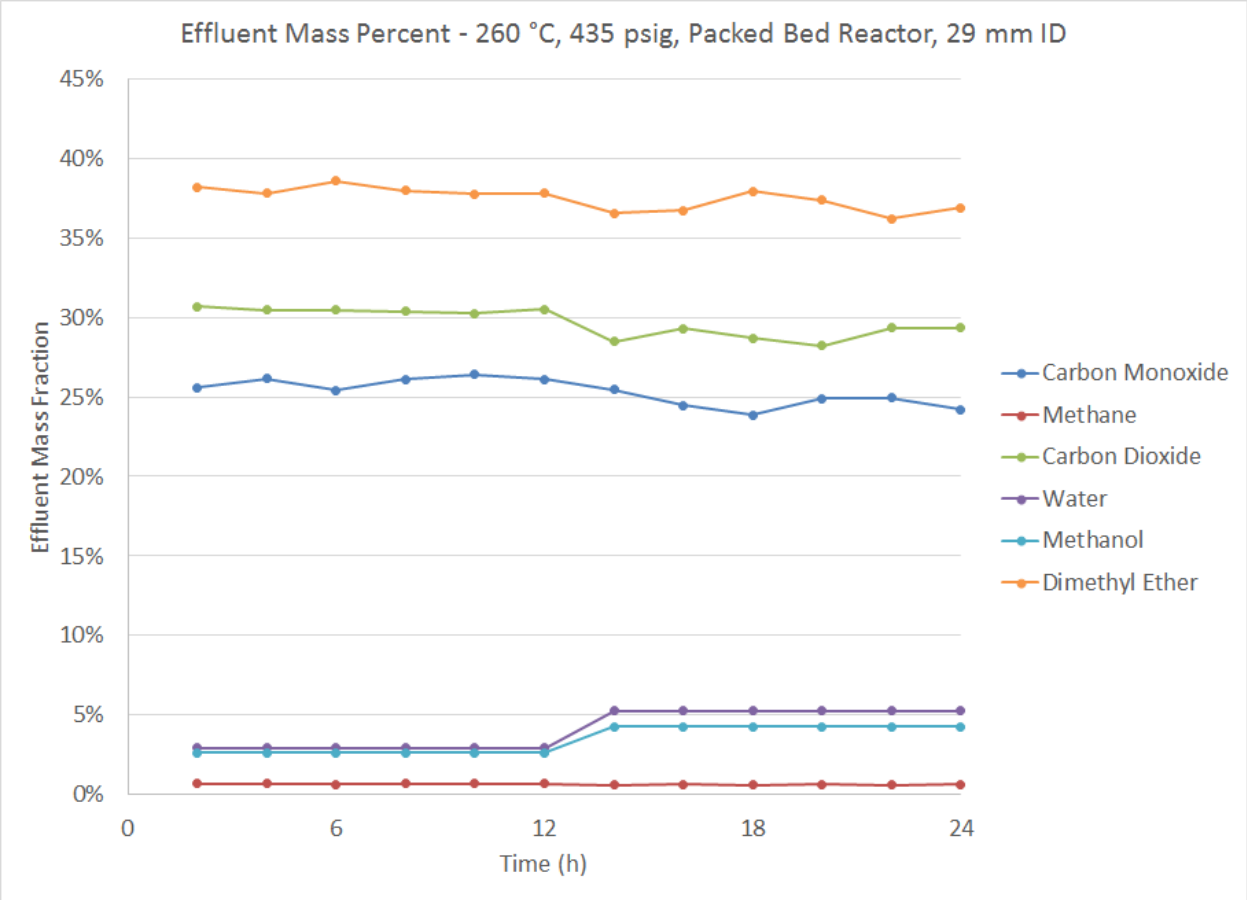

Figure 67. Product distribution as a mass perfect for single-step dimethyl ether synthesis with PB reactor conditions of ID=29mm, P=435psig, T_{Inlet}=260°C, H_2:CO ratio of 3:1, and GHSV=1880 h^{-1}. Catalyst (60-80 mesh, or 180-250 μm) is HiFuelR120 and γ-Al_2O_3 in a 2:1 ratio by mass

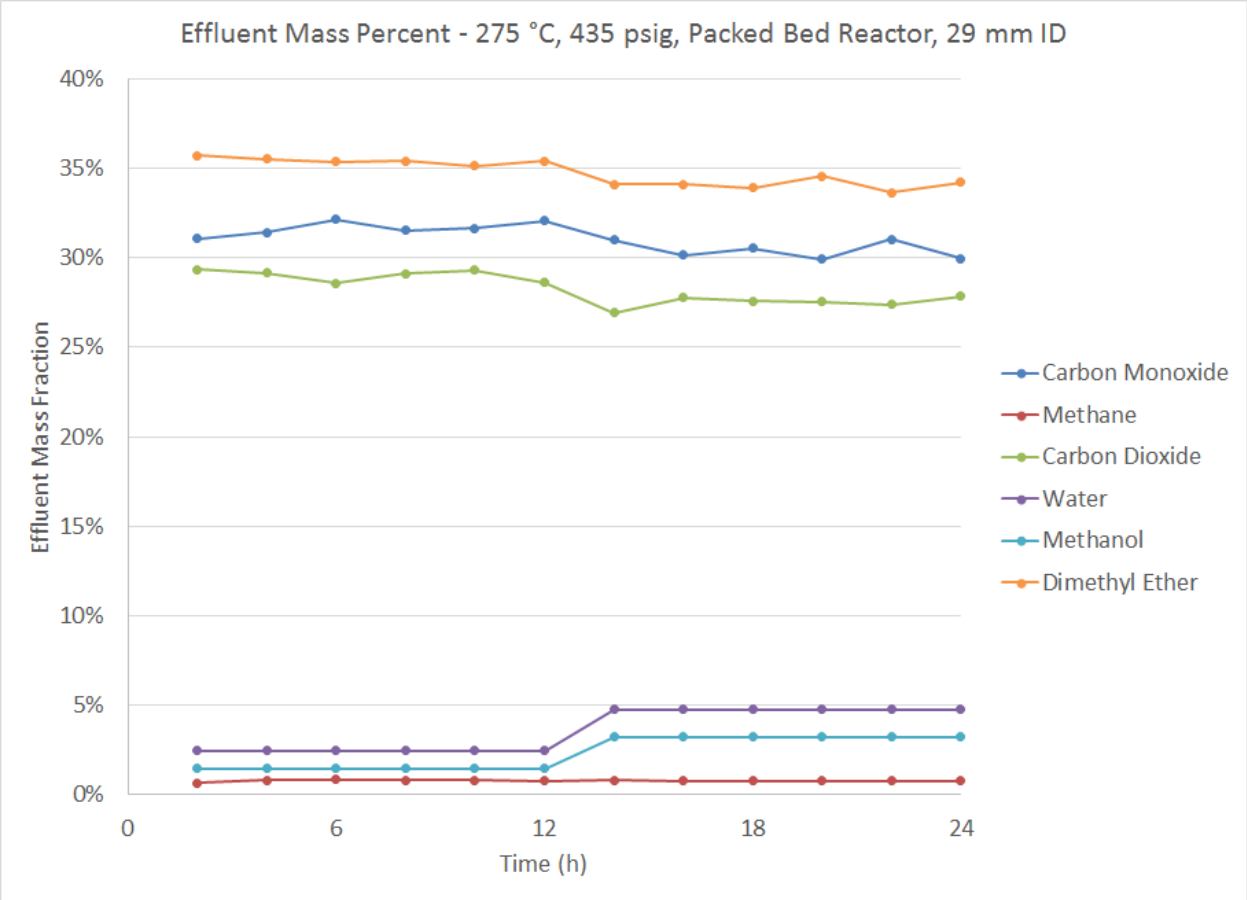

Figure 68. Product distribution as a mass perfect for single-step dimethyl ether synthesis with PB reactor conditions of ID=29mm, P=435psig, T_{Inlet}=275°C, H_2:CO ratio of 3:1, and GHSV=1880 h^{-1}. Catalyst (60-80 mesh, or 180-250 μm) is HiFuelR120 and γ-Al_2O_3 in a 2:1 ratio by mass

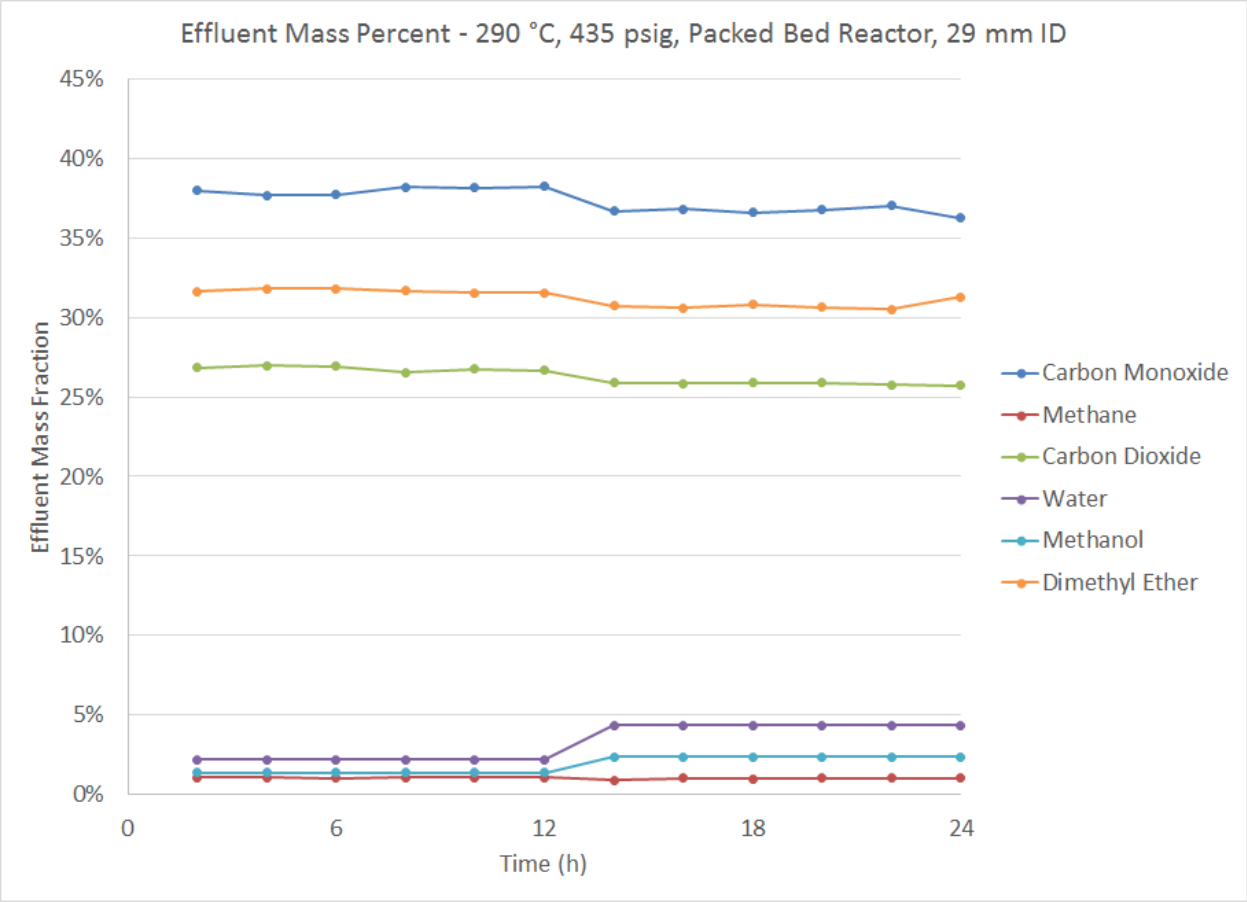

Figure 69. Product distribution as a mass perfect for single-step dimethyl ether synthesis with PB reactor conditions of ID=29mm, P=435psig, T_{Inlet}=290°C, H_2:CO ratio of 3:1, and GHSV=1880 h^{-1}. Catalyst (60-80 mesh, or 180-250 μm) is HiFuelR120 and γ-Al_2O_3 in a 2:1 ratio by mass

4.6 Summary of Results

Briefly, the sources of potential error in measurements should be noted. While care is taken in recovering and analyzing liquid samples, it is all done by hand, which can result in slight loses of product. That in turn could artificially increase the overall gas to liquid product ratios. Another potential source of error is in the controlling of the reactor pressure. Since it is controlled with a back-pressure regulator by hand, it can fluctuate slightly (+/- 15 psi) throughout

the course of a run. Though this pressure fluctuation is low compared to the reactor pressure, it can still have an influence on the products that are formed.

In general, the summary of the single-step dimethyl ether synthesis results can be placed into three categories: catalyst proximity, heat generation with subsequent mitigation, and overall product generation. As far as catalyst proximity is concerned, the simulated results indicated that the two catalyst should be quite close to one another. If the catalysts are separated into distinct layers, then the overall conversion of methane seems to suffer.

The heat generation within the single-step dimethyl ether synthesis reaction cannot be ignored, and is one of the problems with scaling up this reaction. With an overall ΔH_R = -246 kJ/mol, it should come as no surprise that a reactor that can mitigate the heat generation is necessary. The MFEC reactor does seem to fit this criterion, as it had an overall lower centerline temperature when compared to its PB counterpart. This trend was noticed across all inlet temperatures, as well as each reactor diameter. This result suggests that the reactor can be scaled up to allow for higher throughputs, but without the negative side effect of heat building up in the reactor.

The centerline temperature deviation in the 15mm ID reactor was 1.36 to 1.52 times lower in the MFEC when compared the a PB. When scaled up to a 29mm ID reactor, the centerline temperature deviation was 1.45 to 1.91 times lower for the MFEC when compared to its equivalent PB. While these temperature deviations are important due to reactor stability and product generation, the differences in temperature deviations are not as significant as expected. This suggests that while the MFEC reactor is better able to remove heat from the catalyst, there is still a chokepoint on removing the heat from the reactor itself to its surrounding. Since the reactor does not have a phase change material on to effectively remove heat (such as a steam

jacket), it seems likely that this is why the centerline temperature deviations are not as significant as expected.

Finally, since the MFEC was able to better control the heat generation within the reactor, the MFEC reactors were able to outperform the PB reactors with higher carbon monoxide conversion and greater conversion of carbon monoxide ultimately to dimethyl ether. Additionally, the MFEC was able to prevent the formation of methane as it was scaled up. The PB reactor was not able to prevent the creation of methane, and this problem was more pronounced as the inlet temperature of the reactor increased. Methane is the least desirable product during single-step dimethyl ether synthesis since the required syngas would more than likely be generated from steam reforming of methane.

Chapter 5: COMSOL Studies

5.1 Previous MFEC COMSOL research

Due to the uniqueness of microfibrous entrapped materials, very little published literature exists in the area of computational fluid dynamics. All of the literature comes from Dr. Tatarchuk's group out of Auburn University in Auburn, AL. In 2008, simulations were conducted to look into mass transfer within a microfibrous material (Duggirala, 2008). Further simulations were conducted concerning the pressure drop (Qiang Gu, 2015), and later the heat transfer within the fluid of a microfibrous material (Sheng Et Al, 2013). To date, no simulations concerning the catalyst surface temperatures have been published.

5.2 Experimental Equipment

All COMSOL (version 4.3a) simulations were performed on a HP Z600 Workstation equipped with an Intel® Xeon® CPU (E5645 @ 2.40GHz, 2 Processors). The system was also equipped with 24.0 GB of error-correcting code memory.

5.3 Results and Conclusions

One of the goals of this dissertation was to determine the role that MFEC plays in mitigating the surface temperature of a catalyst. While sticking thermocouples in a reactor does tell one what the temperature is at that point, it does not indicate the temperature at the surface of the catalyst. Ultimately, the surface temperature of the catalyst is what will play a major role in the reactions that take place on its surface. Since the MFEC has superior heat transfer properties compared to a packed bed, it is hypothesized that the MFEC simulation will show a reduced surface temperature when compared to a packed bed. The characteristics of each reactor are shown in Table 7.

Table 7. Properties of MFEC and PB reactors as simulated in COMSOL

Property	**MFEC**	**PB**
Voidage	70% (Vol.)	80% (Vol.)
Catalyst Loading	20% (Vol.)	20% (Vol.)
Fiber Loading	10% (Vol.)	N/A
Inlet Temperature (K)	473.15	473.15
Initial Surface Temp. (K)	473.15	473.15
Wall Temperature (K)	473.15	473.15
Flow Rate (mm/s)	10	10

As shown in Table 7, all the initial temperatures are set to the same value. This was intentionally done in order to determine what effect a heat flux has from the catalyst surface. Various heat fluxes (25, 50, 75, and 100 kW/m^s) were simulated at the surface of the catalyst. An example of the simulation result for a PB reactor can be seen in Figure 70 and an example of the MFEC reactor can be seen in Figure 71.

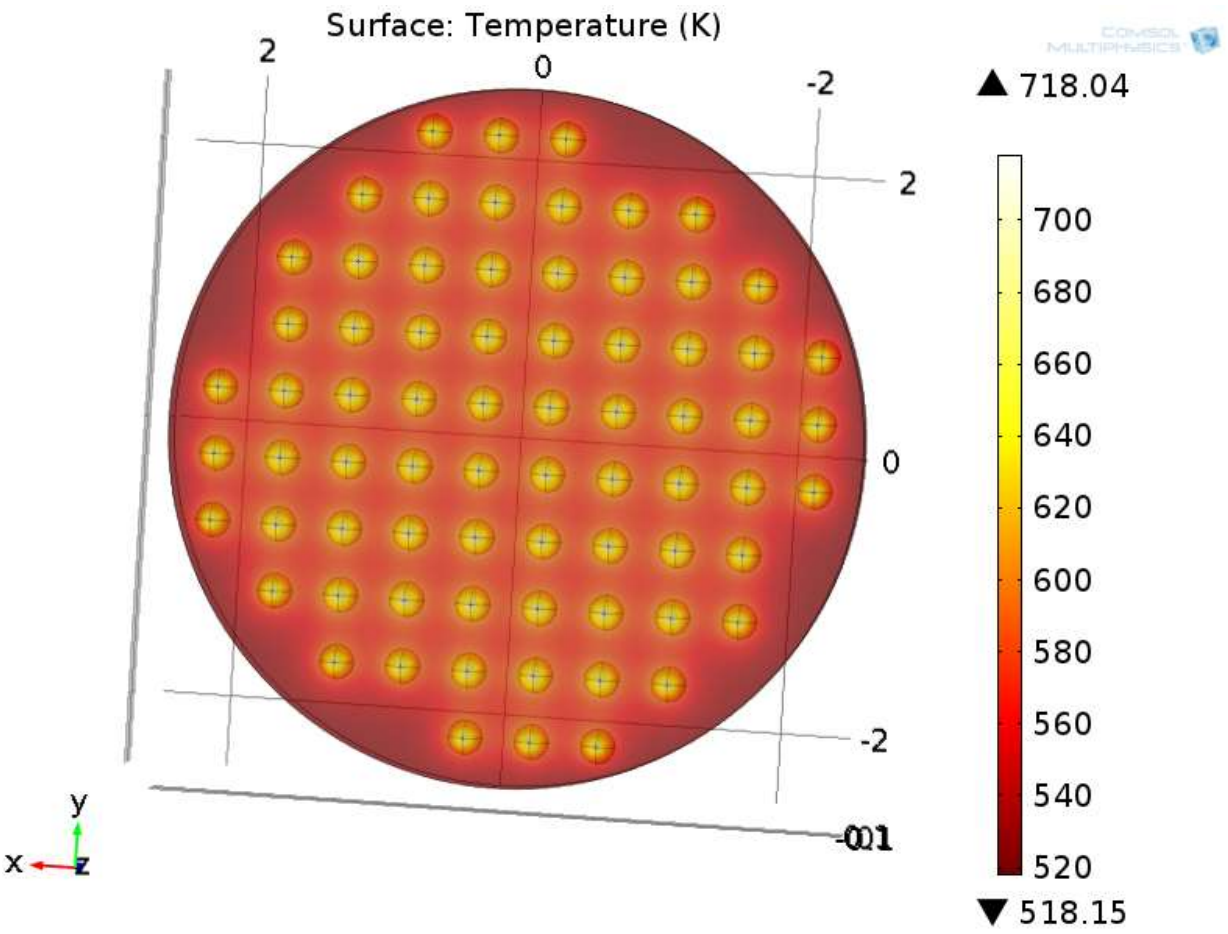

Figure 70. Example of a simulated PB reactor in COMSOL with a catalyst surface as the source of heat.

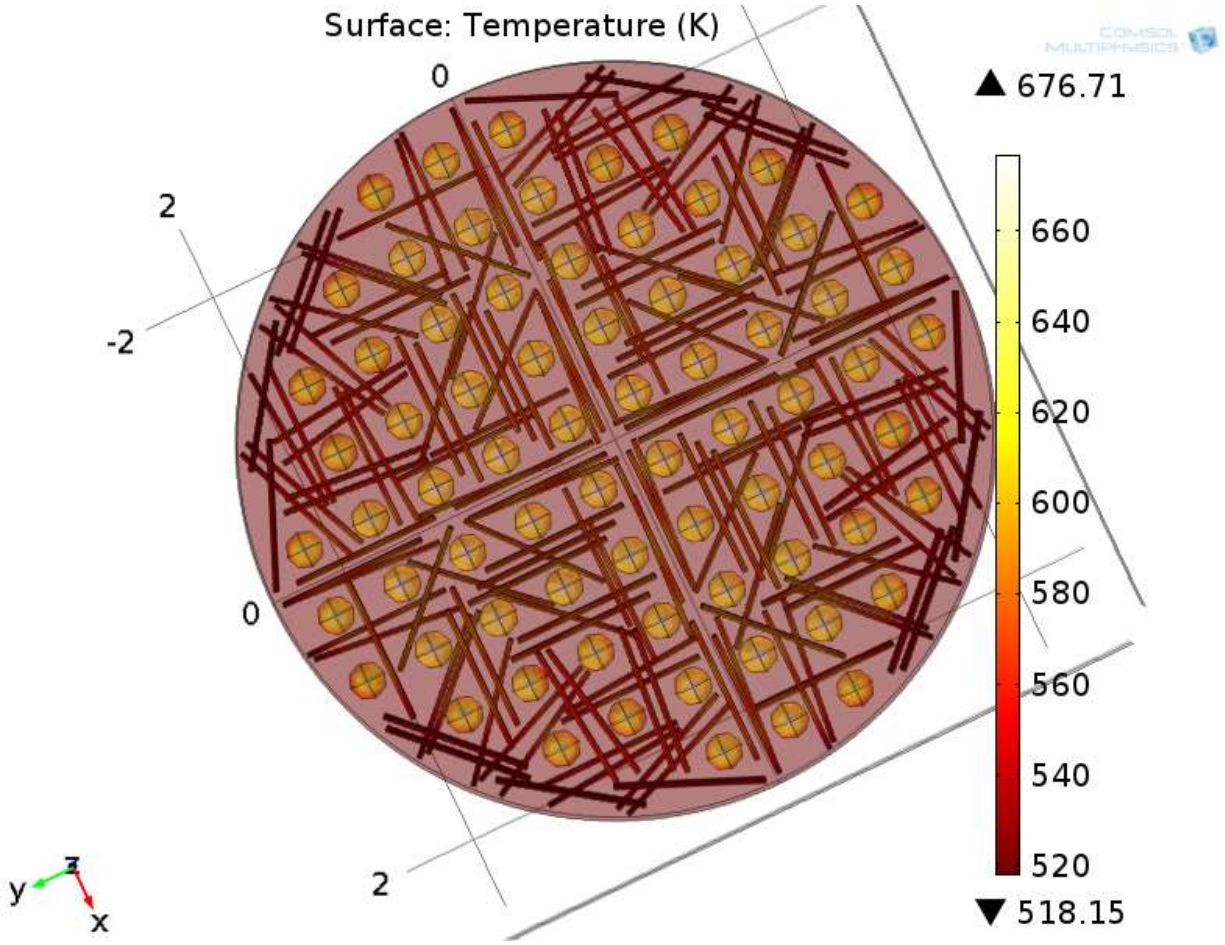

Figure 71. Example of a simulated MFEC reactor in COMSOL with a catalyst surface as the source of heat.

In order to see the effect of the MFEC on the mitigation of the catalyst surface temperature, the average catalyst surface temperature was plotted as a function of the catalyst heat flux as shown in Figure 72 for both reactor types. Since the overall surface temperature ranged over a few hundred degrees, the net difference between both reactors was plotted against the catalyst heat flux as shown in Figure 73. For each simulation, the PB had a higher average catalyst surface temperature. As previously seen in this dissertation, higher temperatures can lead to a loss of conversion and/or the production of undesired side products. Due to these COMSOL

simulations, it can be seen that the MFEC reactor does mitigate the heat generation of the reaction by removing the heat more efficiently than the PB reactor.

While it is important to notice that the average surface temperature is lower in the MFEC simulations, it should be noted that the individual fiber contacts that are present in reality, are nonexistent within this COMSOL model. However, despite the lack of these point-to-point contacts that would allow for greater thermal conduction, one still sees a difference in surface temperature. The lowered average catalyst surface temperature should be attributed at least partly to an increase in surface area for heat to be transferred through convection. If further work is done to allow for fibers to contact one another (as well as catalysts and walls), one should see further improvement to the model by allowed more realistic pathways for heat to transfer.

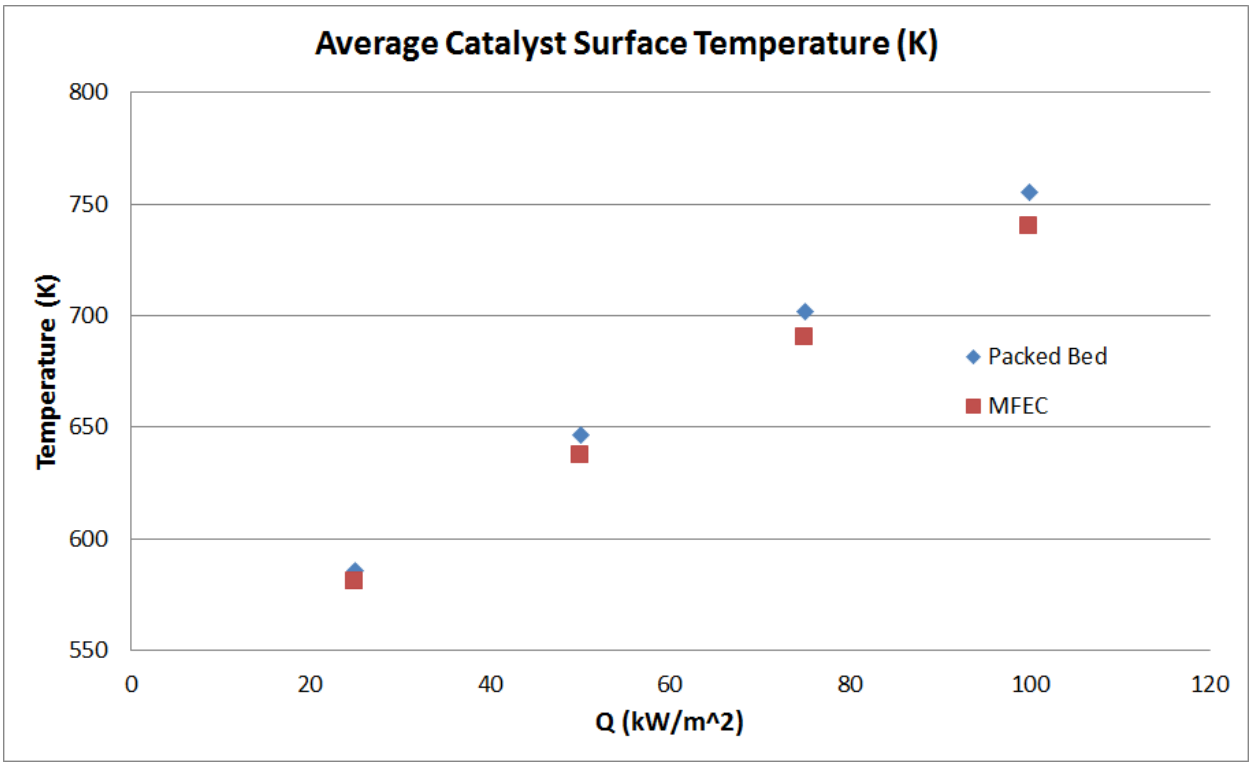

Figure 72. Average catalyst surface temperature as a function of catalyst surface heat flux as determined by COMSOL simulations

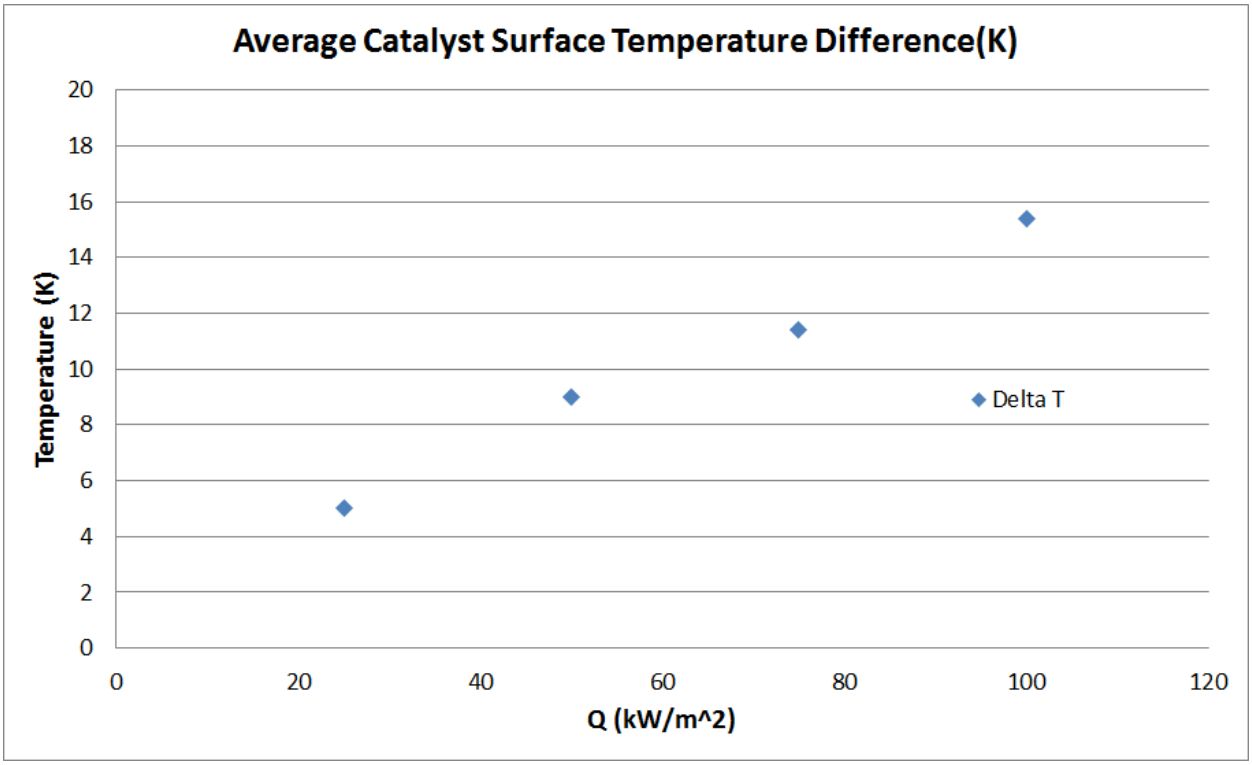

Figure 73. Average catalyst surface temperature difference (PB temp. – MFEC temp.) as a function of catalyst surface heat flux as determined by COMSOL simulations

Chapter 6: Suggested Future Work

6.1 Suggested Future Work

While the single-step dimethyl ether synthesis results are promising, the temperature gradients within each reactor show a need for better reactor design. As the diameter of the reactor increases, the surface area to volume ratio decreases. This in turn means more heat is generated, but with less wall surface area to remove the heat. Instead of a heating tape, a temperature controlled liquid (or steam jacket) would provide a larger heat transfer coefficient on the outside wall. This would allow for the heat generated within the reactor to be more effectively removed from the reactor thanks to the use of MFEC.

Further research concerning the production of fuels is an area that has great promise thanks to the improvement that the MFEC gave on the production of DME. Another possible area of process intensification is to further convert the DME into gasoline within the same reactor. This process is already known in literature, but requires excellent temperature control due to varying temperature ranges of the reaction.

Lastly, the COMSOL research in this dissertation lays the groundwork for future research concerning catalyst surface temperature. In particular, it should be noted that the MFEC bed used in this dissertation does not actually contain metallic fibers that have contact with the wall, nor contact with the catalyst particles, nor other fibers. However, despite this, a significant (>15°C) temperature difference exists between the surface temperature of the catalysts within the MFEC bed and the packed bed. By adding direct contact points between the fibers and other fibers, the wall, and catalyst particles, even further improvements should be seen that better explain heat transfer within the MFEC. Varying fiber diameters can also be included to predict if larger diameter fibers would further improve the MFEC reactor.

References

Aguayo, A. T., Ereña, J., Mier, D., Arandes, J. M., Olazar, M., & Bilbao, J. (2007). Kinetic Modeling of Dimethyl Ether Synthesis in a Single Step on a CuO-ZnO-Al2O3/gamma-Al2O3 Catalyst. *Industrial & Engineering Chemistry Research, 46*, 5522-5530.

Arcoumanis, C., Bae, C., Crookes, R., & Kinoshita, E. (2008). The potential of di-methyl ether (DME) as an alternative fuel for compression-ignition engines: A review. *Fuel, 87*, 1014-1030.

Bae, J.-W., Potdar, H. S., Kang, S.-H., & Jun, K.-W. (2008). Coproduction of Methanol and Dimethyl Ether from Biomass-Derived Syngas on a CuO-Zn-O-Al2O3/gamma-Al2O3 Hybrid Catalyst. *Energy and Fuels, 22*, 223-230.

Baltes, C., Vukojević, S., & Schüth, F. (2008). Correlations between sunthesis, precursor, and catalyst structure and activity of a large set of CuO/ZnO/Al2O3 catalysts for methanol synthesis. *Journal of Catalysis, 258*, 334-344.

Bos, A. N., Borman, P. C., Kuczynski, M., & Westerterp, K. R. (1989). The kinetics of the methanol synthesis on a copper catalyst: an experimental study. *Chemical Engineering Science, 44, No. 11*, 2435-2449.

Brodén, G., Rhondin, T. N., Brucker, C., Benbow, R., & Hurych, Z. (1976). Synchrotron radiation study of chemisorptive bonding of CO on transition metals - Polarization effecty on Ir (100). *Surface Science, 59, Issue 2*, 593-611.

Duggirala, R. K. (2008). *Computational Fluid Dynamics Simulation of Chemically Reacting Gas Flows through Microfibrous Materials (PhD Dissertation).* Auburn University.

Fogler, H. S. (2009). *Elements of Chemical Reaction Engineering - 4th Ed.* Upper Saddle River: Prentice Hall.

Friedel, R. A. (1950). Composistion of synthetic liquid fuels. I. Product distribution and analysis of C5-C8 paraffin isomers from cobalt catalyst. *J. Am. Chem. Soc., 72 (3)*, 1212-1215.

Jager, B. (2003). Fischer-Tropsch Reactors. New Orleans.

Jamshidi, L., Barbosa, C., Nascimento, L., & Rodbari, J. (2013). Catalytic dehydration of methanol to dimethyl ether (DME) using the A(162,2)Cu(25,3)Fe(12,5) quasicrystalline alloy. *Chemical Engineering & Process Technology, 4 (5)*.

Klier, K. (1982). Methanol Synthesis. *Advances in Catalysis, 31*, 243-313.

Koempel, H., Liebner, W., & Wagner, M. (2005). Lurgi's Gas to Chemicals (GTC): Advanced technologies for natural gas monetisation. *Gastech 2005.* Bilbao, Spain.

Kölbel, H., & Ralek, M. (1980). The Fischer-Tropsch Synthesis in the Liquid Phase. *Catal. Rev. Sci. Eng., 21 (2)*, 225-274.

Lei, Z., Zou, Z., Dai, C., Li, Q., & Chen, B. (2011). Synthesis of dimethyl ether (DME) by catalytic distillation. *Chemical Engineering Science, 66*, 3195-3203.

Li, J. L., & Inui, T. (1996). Characterization of precursors of methanol synthesis catalysts, copper/zinc/aluminum oxides, precipitated at different pHs and temperatures. *Applied Catalysis: A, 137*, 105-117.

Matulewicz, E., Keijser, M. d., Mol, J. C., & Kapteijn, F. (1984). Characterization of CuO-ZnO-Al2O3 methanol synthesis catalysts using temperature programmed reduction and thermal stability. *Thermochimica Acta, 72*, 111-116.

Milani, D., Khalilpour, R., Zahedi, G., & Abbas, A. (2015). A model-based analysis of CO2 utilization in methanol synthesis plant. *Journal of CO2 Utilization, 10*, 15-22.

Mittasch, A., & Pier, M. (1924, September 4). *United States Patent No. US1569775.*

Mittasch, A., Muller, C., & Pier, M. (1923, September 15). *United States Patent No. US1791568.*

Montebelli, A., Visconti, C. G., Groppi, G., Tronconi, E., & Kohler, S. (2014). Optimization of compact mutlitubular fixed-bed reactors for the methanol synthesis loaded with highly conductive structure catalysts. *Chemical Engineering Journal, 255*, 257-265.

Ogawa, T., Inoue, N., Shikada, T., & Ohno, Y. (2003). Direct dimethyl ether synthesis. *Journal of Natural Gas Chemistry, 12*, 219-227.

Omata, K., Watanabe, Y., Umegaki, T., Ishiguro, G., & Yamada, M. (2002). Low-pressure DME synthesis with Cu-based hybrid catalysts using temperature-gradient reactor. *Fuel, 81*, 1605-1609.

Pontzen, F., Liebner, W., Gronemann, V., Rothaemel, M., & Ahlers, B. (2011). CO2-based methanol and DME - Efficient technologies for industrial scale production. *Catalysis Today, 171*, 242-250.

Poutsma, M. L., Elek, L. F., Ibarbia, P. A., Risch, A. P., & Rabo, J. A. (1978). Selective formation of methanol from synthesis gas over palladium catalysts. *Journal of Catalysis, 52, Issue 1*, 157-168.

Prasad, P. S., Bae, J. W., Kang, S.-H., Lee, Y.-J., & Jun, K.-W. (2008). Single-step synthesis of DME from syngas on Cu-ZnO-Al2O3/zeolite bifunctional catalysts: The superiority of ferrierite over the other zeolites. *Fuel Processing Technology, 89*, 1281-1286.

Qiang Gu, H. R. (2015). A CFD pressure drop model for microfibrous entrapped catalyst filters using micro-scale imaging. *Engineering Applications of Computational Fluid Mechanics, 9*(1), 567-576.

Semelsberger, T. A., Borup, R. L., & Greene, H. L. (2006). Dimethyl ether (DME) as an alternative fuel. *Journal of Power Sources, 156*, 497-511.

Sheng Et Al. (2013). Micro Scale Heat Transfer Comaprison Between Packed Beds and Microfibrous Entrapped Catalysts. *Engineering Applications of Computational Fluid Mechanics, 7*(4), 471-485.

Sheng, M., Yang, H., Cahela, D. R., & Tatarchuk, B. J. (2011). Novel catalyst structures with enhanced heat transfer characteristics. *Journal of Catalysis, 281, Issue 2*, 254-262.

Sheng, M., Yang, H., Cahela, D. R., Yantz Jr., W. R., Gonzalez, C. F., & Tatarchuk, B. J. (2012). High conductivity catalyst structures for applications in exothermic reactions. *Applied Catalysis A: General, 445-446*, 143-152.

Song, H., Ramkrishn, D., Trinh, S., & Wright, H. (2004). Operating strategies for Fischer-Tropsch reactors: A model-directed study. *Korean J. Chem. Eng., 21 (2)*, 308-317.

Spath, P., & Dayton, D. (2003). *Preliminary screening - Technical and economic assessment of synthesis gas to fuels and chemicals with emphasis on the potential for bio-mass derived syngas.* National Renewable Energy Laboratory, Golden, Colorado.

Spencer, M. (1999). The role of zinc oxide in Cu/ZnO catalysts for methanol synthesis and the water-gas shift reaction. *Topics in Catalysis, 8*, 259-266.

Strunk, J., Kähler, K., Xia, X., Comotti, M., Schüth, F., & Reinecke, T. (2009). Au/ZnO as catalyst for methanol synthesis: The role of oxygen vacancies. *Applied Catalysis A, 359, Issues 1-2*, 121-128.

Sun, K., Lu, W., Qiu, F., Liu, S., & Xu, X. (2003). Direct synthesis of DME over bifunctional catalyst: surface properties and catalytic performance. *Applied Catalysis A: General, 252*, 243-249.

Takeuchi, A., & Katzer, J. R. (1981). Mechanism of Methanol Formation. *Journal of Physical Chemistry, 85*, 937-939.

Wang, G., Zuo, Y., Han, M., & Wang, J. (2011). Cu-Zr-Zn catalysts for methanol synthesis in a fluidized bed reactor. *Applied Catalysis A, 394, Issues 1-2*, 281-286.

Yoo, C.-J., Lee, D.-W., Kim, M.-S., Moon, D. J., & Lee, K.-Y. (2013). The synthesis of methanol from CO/CO2/H2 gas over Cu/Ce1-xZrxO2 catalysts. *Journal of Molecular Catalysis A, 378*, 255-262.

Appendix

i. Code for MethanolEquilibriumConversion.m

```
function [ CO_Conversion ] = MethanolEquilibriumConversion(T_Input,P_Input)
%Program to calculate equilibrium conversions for methanol reduction

%Overall reaction (gas-phase):
%CO + 2H2 <--> CH3OH
%Gibbs energies of formation at 298.15K (gas phase)
delta_G_298K_CO = -137169;      %J/mol
delta_G_298K_CO2 = -394359;     %J/mol
delta_G_298K_CH4 = -50460;      %J/mol
delta_G_298K_CH3OH = -161960;   %J/mol
delta_G_298K_CH3OCH3 = 0;
delta_G_298K_H2 = 0;
delta_G_298K_H2O = -228600;     %J/mol

%Standard enthalpies of formation at 298.15K (gas phase)
delta_H_298K_CO = -110525;      %J/mol
delta_H_298K_CO2 = -393509;     %J/mol
delta_H_298K_CH4 = -74520;      %J/mol
delta_H_298K_CH3OH = -200660;   %J/mol
delta_H_298K_CH3OCH3 = 0;
delta_H_298K_H2 = 0;
delta_H_298K_H2O = -241800;     %J/mol

%Universal gas constant
R = 8.314;      %J/(mol*K)

%Reference temperature
T_ref = 298.15; %K

T = T_Input + 273.15; %Convert to K
P = P_Input;          %bar

Init_CO2 = 0;       %moles
Init_CO = 1;        %moles
Init_H2 = 2;        %moles
Init_CH3OH = 0;     %moles
Init_H2O = 0;       %moles

CO2_Coeff = 0;      %stoich coefficient
CO_Coeff = 1;       %stoich coefficient
H2_Coeff = 2;       %stoich coefficient
CH3OH_Coeff = 1;    %stoich coefficient
H2O_Coeff = 0;      %stoich coefficient

delta_G_rxn = (delta_G_298K_CH3OH*CH3OH_Coeff)-...
    (delta_G_298K_CO*CO_Coeff+delta_G_298K_H2*H2_Coeff);

delta_H_rxn = (delta_H_298K_CH3OH*CH3OH_Coeff)-...
    (delta_H_298K_CO*CO_Coeff+delta_H_298K_H2*H2_Coeff);
```

```
K_eq_ref = exp(-delta_G_rxn/(R*T_ref));

K_eq = K_eq_ref*exp(-delta_H_rxn/R*(1/T-1/T_ref));

Extent = 0;   %Initial guess for extent of reaction

%Mole amounts of compounds
Moles_CO = Init_CO - Extent;
Moles_H2 = Init_H2 - 2*Extent;
Moles_CH3OH = Init_CH3OH + Extent;
Total_Moles = Moles_CO + Moles_H2 + Moles_CH3OH;

%Mole fractions of compounds
y_CO = Moles_CO/Total_Moles;            %Gas fraction of CO2
y_H2 = Moles_H2/Total_Moles;            %Gas fraction of H2
y_CH3OH = Moles_CH3OH/Total_Moles;      %Gas fraction of CH3OH

%Activities of compounds
a_CO = y_CO*P;
a_H2 = y_H2*P;
a_CH3OH = y_CH3OH*P;

a_products = (a_CH3OH)^(CH3OH_Coeff);
a_reactants = (a_CO)^(CO_Coeff)*(a_H2)^(H2_Coeff);

K_eq2 = a_products/a_reactants;

K_zero = abs(K_eq2 - K_eq);

Iterations = 0;

%Loop used to find a suitable extent value
while K_zero > 0.0001

    Extent = Extent + 0.00001;   %Find the best fit

    Moles_CO = Init_CO - Extent;
    Moles_H2 = Init_H2 - 2*Extent;
    Moles_CH3OH = Init_CH3OH + Extent;
    Total_Moles = Moles_CO + Moles_H2 + Moles_CH3OH;

    y_CO = Moles_CO/Total_Moles;            %Gas fraction of CO2
    y_H2 = Moles_H2/Total_Moles;            %Gas fraction of H2
    y_CH3OH = Moles_CH3OH/Total_Moles;      %Gas fraction of CH3OH

    a_CO = y_CO*P;
    a_H2 = y_H2*P;
    a_CH3OH = y_CH3OH*P;

    a_products = (a_CH3OH)^(CH3OH_Coeff);
    a_reactants = (a_CO)^(CO_Coeff)*(a_H2)^(H2_Coeff);

    K_eq2 = a_products/a_reactants;
```

```
    K_zero = abs(K_eq2 - K_eq);

    Iterations = Iterations + 1;

    if Iterations == 10000000

        break

    end

end

CO_Conversion = 1 - Moles_CO/Init_CO;

T = T_Input;
P = P_Input;

end
```

ii. Executable Equilibrium_Conversion_Methanol.m

```
clear;
clc;

T = 230;
TempCount = 1;
TempCountMax = 7;

while TempCount < TempCountMax

    PressureCount = 1;

    while PressureCount < 7

        if PressureCount == 1
            P = 1;
            EquilibriumArray(1, 2) = P;
        end
        if PressureCount == 2
            P = 5;
            EquilibriumArray(1, 3) = P;
        end
        if PressureCount == 3
            P = 10;
            EquilibriumArray(1, 4) = P;
        end
        if PressureCount == 4
            P = 30;
            EquilibriumArray(1, 5) = P;
        end
```

```
        if PressureCount == 5
            P = 50;
            EquilibriumArray(1, 6) = P;
        end
        if PressureCount == 6
            P = 100;
            EquilibriumArray(1, 7) = P;
        end

        EquilibriumArray(TempCount + 1, 1) = T;
        EquilibriumArray(TempCount + 1, PressureCount + 1) = ...
            MethanolEquilibriumConversion(T,P);
        PressureCount = PressureCount + 1;

    end

    TempCount = TempCount + 1;
    T = T + 15;

end

EquilibriumArray
```

iii. Code for DimethylEtherEquilibriumConversion.m

```
function [CH3OH_Conversion] = DimethylEtherEquilibriumConversion(T_Input,
P_Input)
%Program to calculate equilibrium conversions for the conversion of
%methanol into dimethyl ether

%Overall reaction (gas-phase):
%2CH3OH <--> CH3OCH3 + H2O

%Gibbs energies of formation at 298.15K (gas phase)
delta_G_298K_CO = -137169;      %J/mol
delta_G_298K_CO2 = -394359;     %J/mol
delta_G_298K_CH4 = -50460;      %J/mol
delta_G_298K_CH3OH = -161960;   %J/mol
delta_G_298K_CH3OCH3 = -112900; %J/mol
delta_G_298K_H2 = 0;            %J/mol
delta_G_298K_H2O = -228600;     %J/mol

%Standard enthalpies of formation at 298.15K (gas phase)
delta_H_298K_CO = -110525;      %J/mol
delta_H_298K_CO2 = -393509;     %J/mol
delta_H_298K_CH4 = -74520;      %J/mol
delta_H_298K_CH3OH = -200660;   %J/mol
delta_H_298K_CH3OCH3 = -184100; %J/mol
delta_H_298K_H2 = 0;            %J/mol
delta_H_298K_H2O = -241800;     %J/mol

%Universal gas constant
R = 8.314;      %J/(mol*K)
```

```
%Reference temperature
T_ref = 298.15; %K

T = T_Input + 273.15; %Convert to K
P = P_Input;          %bar

Init_CO2 = 0;       %moles
Init_CO = 0;        %moles
Init_H2 = 0;        %moles
Init_CH3OH = 2;     %moles
Init_H2O = 0;       %moles
Init_CH3OCH3 = 0;   %moles

CO2_Coeff = 0;      %stoich coefficient
CO_Coeff = 0;       %stoich coefficient
H2_Coeff = 0;       %stoich coefficient
CH3OH_Coeff = 2;    %stoich coefficient
H2O_Coeff = 1;      %stoich coefficient
CH3OCH3_Coeff = 1;  %stoich coefficient

delta_G_rxn =
(delta_G_298K_CH3OCH3*CH3OCH3_Coeff+delta_G_298K_H2O*H2O_Coeff)-...
    (delta_G_298K_CH3OH*CH3OH_Coeff);

delta_H_rxn =
(delta_H_298K_CH3OCH3*CH3OCH3_Coeff+delta_H_298K_H2O*H2O_Coeff)-...
    (delta_H_298K_CH3OH*CH3OH_Coeff);

K_eq_ref = exp(-delta_G_rxn/(R*T_ref));

K_eq = K_eq_ref*exp(-delta_H_rxn/R*(1/T-1/T_ref));

Extent = 0;   %Initial guess for extent of reaction

%Mole amounts of compounds
Moles_CO = 0;
Moles_H2 = 0;
Moles_CO2 = 0;
Moles_H2O = Init_H2O + Extent;
Moles_CH3OH = Init_CH3OH - 2*Extent;
Moles_CH3OCH3 = Init_CH3OCH3 + Extent;
Total_Moles = Moles_CH3OH + Moles_CH3OCH3 + Moles_H2O;

%Mole fractions of compounds
y_CO = Moles_CO/Total_Moles;            %Gas fraction of CO
y_H2 = Moles_H2/Total_Moles;            %Gas fraction of H2
y_CO2 = Moles_CO2/Total_Moles;          %Gas fraction of CO2
y_H2O = Moles_H2O/Total_Moles;          %Gas fraction of H2O
y_CH3OH = Moles_CH3OH/Total_Moles;      %Gas fraction of CH3OH
y_CH3OCH3 = Moles_CH3OCH3/Total_Moles;  %Gas fraction of CH3OCH3

%Activities of compounds
a_CO = y_CO*P;
```

```
a_H2 = y_H2*P;
a_CO2 = y_CO2*P;
a_H2O = y_H2O*P;
a_CH3OH = y_CH3OH*P;
a_CH3OCH3 = y_CH3OCH3*P;

a_products = (a_CH3OCH3)^(CH3OCH3_Coeff)*(a_H2O)^(H2O_Coeff);
a_reactants = (a_CH3OH)^(CH3OH_Coeff);

K_eq2 = a_products/a_reactants;

K_zero = abs(K_eq2 - K_eq);

Iterations = 0;

%Loop used to find a suitable extent value
while K_zero > 0.1

    Extent = Extent + 0.0001;   %Find the best fit

    %Mole amounts of compounds
    Moles_CO = 0;
    Moles_H2 = 0;
    Moles_CO2 = 0;
    Moles_H2O = Init_H2O + Extent;
    Moles_CH3OH = Init_CH3OH - 2*Extent;
    Moles_CH3OCH3 = Init_CH3OCH3 + Extent;
    Total_Moles = Moles_CH3OH + Moles_CH3OCH3 + Moles_H2O;

    %Mole fractions of compounds
    y_CO = Moles_CO/Total_Moles;            %Gas fraction of CO
    y_H2 = Moles_H2/Total_Moles;            %Gas fraction of H2
    y_CO2 = Moles_CO2/Total_Moles;          %Gas fraction of CO2
    y_H2O = Moles_H2O/Total_Moles;          %Gas fraction of H2O
    y_CH3OH = Moles_CH3OH/Total_Moles;      %Gas fraction of CH3OH
    y_CH3OCH3 = Moles_CH3OCH3/Total_Moles;  %Gas fraction of CH3OCH3

    %Activities of compounds
    a_CO = y_CO*P;
    a_H2 = y_H2*P;
    a_CO2 = y_CO2*P;
    a_H2O = y_H2O*P;
    a_CH3OH = y_CH3OH*P;
    a_CH3OCH3 = y_CH3OCH3*P;

    a_products = (a_CH3OCH3)^(CH3OCH3_Coeff)*(a_H2O)^(H2O_Coeff);
    a_reactants = (a_CH3OH)^(CH3OH_Coeff);

    K_eq2 = a_products/a_reactants;

    K_zero = abs(K_eq2 - K_eq);

    Iterations = Iterations + 1;
```

```
    if Iterations == 10000000

        break

    end

end

CH3OH_Conversion = 1 - Moles_CH3OH/Init_CH3OH;

T = T_Input;
P = P_Input;


end
```

iv. Executable Equilibrium_Conversion_DimethylEther.m

```
clear;
clc;

T = 180;
TempCount = 1;
TempCountMax = 10;

while TempCount < TempCountMax

    PressureCount = 1;

    while PressureCount < 7
        if PressureCount == 1
            P = 1;
            EquilibriumArray(1, 2) = P;
        end
        if PressureCount == 2
            P = 5;
            EquilibriumArray(1, 3) = P;
        end
        if PressureCount == 3
            P = 10;
            EquilibriumArray(1, 4) = P;
        end
        if PressureCount == 4
            P = 25;
            EquilibriumArray(1, 5) = P;
        end
        if PressureCount == 5
            P = 50;
            EquilibriumArray(1, 6) = P;
        end
        if PressureCount == 6
            P = 100;
            EquilibriumArray(1, 7) = P;
```

```
        end

        EquilibriumArray(TempCount + 1, 1) = T;
        EquilibriumArray(TempCount + 1, PressureCount + 1) = ...
            DimethylEtherEquilibriumConversion(T,P);
        PressureCount = PressureCount + 1;

    end

    TempCount = TempCount + 1;
    T = T + 20;

end

EquilibriumArray
```

v. Code for WaterGasShiftEquilibriumConversion.m

```
function [CO_Conversion] = WaterGasShiftEquilibriumConversion(T_Input,
P_Input)
%Program to calculate equilibrium conversions for the water-gas shift
%reaction

%Overall reaction (gas-phase):
%CO + H2O <--> CO2 + H2

%Gibbs energies of formation at 298.15K (gas phase)
delta_G_298K_CO = -137169;      %J/mol
delta_G_298K_CO2 = -394359;     %J/mol
delta_G_298K_CH4 = -50460;      %J/mol
delta_G_298K_CH3OH = -161960;   %J/mol
delta_G_298K_CH3OCH3 = 0;
delta_G_298K_H2 = 0;
delta_G_298K_H2O = -228600;     %J/mol

%Standard enthalpies of formation at 298.15K (gas phase)
delta_H_298K_CO = -110525;      %J/mol
delta_H_298K_CO2 = -393509;     %J/mol
delta_H_298K_CH4 = -74520;      %J/mol
delta_H_298K_CH3OH = -200660;   %J/mol
delta_H_298K_CH3OCH3 = 0;
delta_H_298K_H2 = 0;
delta_H_298K_H2O = -241800;     %J/mol

%Universal gas constant
R = 8.314;      %J/(mol*K)

%Reference temperature
T_ref = 298.15; %K

T = T_Input + 273.15; %Convert to K
P = P_Input;          %bar
```

```
Init_CO2 = 0;        %moles
Init_CO = 1;         %moles
Init_H2 = 0;         %moles
Init_CH3OH = 0;      %moles
Init_H2O = 1;        %moles

CO2_Coeff = 1;       %stoich coefficient
CO_Coeff = 1;        %stoich coefficient
H2_Coeff = 1;        %stoich coefficient
CH3OH_Coeff = 0;     %stoich coefficient
H2O_Coeff = 1;       %stoich coefficient

delta_G_rxn = (delta_G_298K_CO2*CO2_Coeff+delta_G_298K_H2*H2_Coeff)-...
    (delta_G_298K_CO*CO_Coeff+delta_G_298K_H2O*H2O_Coeff);

delta_H_rxn = (delta_H_298K_CO2*CO2_Coeff+delta_H_298K_H2*H2_Coeff)-...
    (delta_H_298K_CO*CO_Coeff+delta_H_298K_H2O*H2O_Coeff);

K_eq_ref = exp(-delta_G_rxn/(R*T_ref));

K_eq = K_eq_ref*exp(-delta_H_rxn/R*(1/T-1/T_ref));

Extent = 0;   %Initial guess for extent of reaction

%Mole amounts of compounds
Moles_CO = Init_CO - Extent;
Moles_H2 = Init_H2 + Extent;
Moles_CO2 = Init_CO2 + Extent;
Moles_H2O = Init_H2O - Extent;
Total_Moles = Moles_CO + Moles_H2 + Moles_CO2 + Moles_H2O;

%Mole fractions of compounds
y_CO = Moles_CO/Total_Moles;            %Gas fraction of CO
y_H2 = Moles_H2/Total_Moles;            %Gas fraction of H2
y_CO2 = Moles_CO2/Total_Moles;      %Gas fraction of CO2
y_H2O = Moles_H2O/Total_Moles;          %Gas fraction of H2O

%Activities of compounds
a_CO = y_CO*P;
a_H2 = y_H2*P;
a_CO2 = y_CO2*P;
a_H2O = y_H2O*P;

a_products = (a_CO2)^(CO2_Coeff)*(a_H2)^(H2_Coeff);
a_reactants = (a_CO)^(CO_Coeff)*(a_H2O)^(H2O_Coeff);

K_eq2 = a_products/a_reactants;

K_zero = abs(K_eq2 - K_eq);

Iterations = 0;

%Loop used to find a suitable extent value
```

```
while K_zero > 1

    Extent = Extent + 0.0001;   %Find the best fit

    %Moles of compounds
    Moles_CO = Init_CO - Extent;
    Moles_H2 = Init_H2 + Extent;
    Moles_CO2 = Init_CO2 + Extent;
    Moles_H2O = Init_H2O - Extent;
    Total_Moles = Moles_CO + Moles_H2 + Moles_CO2 + Moles_H2O;

    %Mole fractions of compounds
    y_CO = Moles_CO/Total_Moles;            %Gas fraction of CO
    y_H2 = Moles_H2/Total_Moles;            %Gas fraction of H2
    y_CO2 = Moles_CO2/Total_Moles;          %Gas fraction of CO2
    y_H2O = Moles_H2O/Total_Moles;          %Gas fraction of H2O

    %Activities of compounds
    a_CO = y_CO*P;
    a_H2 = y_H2*P;
    a_CO2 = y_CO2*P;
    a_H2O = y_H2O*P;

    a_products = (a_CO2)^(CO2_Coeff)*(a_H2)^(H2_Coeff);
    a_reactants = (a_CO)^(CO_Coeff)*(a_H2O)^(H2O_Coeff);

    K_eq2 = a_products/a_reactants;

    K_zero = abs(K_eq2 - K_eq);

    Iterations = Iterations + 1;

    if Iterations == 10000000

        break

    end

end

CO_Conversion = 1 - Moles_CO/Init_CO;

T = T_Input;
P = P_Input;


end
```

vi. Executable Equilibrium_Conversion_WaterGasShift.m

```
clear;
clc;
```

```
T = 180;
TempCount = 1;
TempCountMax = 10;

while TempCount < TempCountMax

    PressureCount = 1;

    while PressureCount < 7

        if PressureCount == 1
            P = 1;
            EquilibriumArray(1, 2) = P;
        end
        if PressureCount == 2
            P = 5;
            EquilibriumArray(1, 3) = P;
        end
        if PressureCount == 3
            P = 10;
            EquilibriumArray(1, 4) = P;
        end
        if PressureCount == 4
            P = 25;
            EquilibriumArray(1, 5) = P;
        end
        if PressureCount == 5
            P = 50;
            EquilibriumArray(1, 6) = P;
        end
        if PressureCount == 6
            P = 100;
            EquilibriumArray(1, 7) = P;
        end

        EquilibriumArray(TempCount + 1, 1) = T;
        EquilibriumArray(TempCount + 1, PressureCount + 1) = ...
            WaterGasShiftEquilibriumConversion(T,P);
        PressureCount = PressureCount + 1;

    end

    TempCount = TempCount + 1;
    T = T + 20;

end

EquilibriumArray
```

vii. Code for SingleDimethylEtherEquilibriumConversion.m

```
function [CO_Conversion] = SingleDimethylEtherEquilibriumConversion(T_Input,
P_Input)
%Program to calculate equilibrium conversions for the conversion of
%syngas to dimethyl ether (as a single reaction)

%Overall reaction (gas-phase):
%3H2 + 3CO <--> CH3OCH3 + CO2

%Gibbs energies of formation at 298.15K (gas phase)
delta_G_298K_CO = -137169;      %J/mol
delta_G_298K_CO2 = -394359;     %J/mol
delta_G_298K_CH4 = -50460;      %J/mol
delta_G_298K_CH3OH = -161960;   %J/mol
delta_G_298K_CH3OCH3 = -112900; %J/mol
delta_G_298K_H2 = 0;            %J/mol
delta_G_298K_H2O = -228600;     %J/mol

%Standard enthalpies of formation at 298.15K (gas phase)
delta_H_298K_CO = -110525;      %J/mol
delta_H_298K_CO2 = -393509;     %J/mol
delta_H_298K_CH4 = -74520;      %J/mol
delta_H_298K_CH3OH = -200660;   %J/mol
delta_H_298K_CH3OCH3 = -184100; %J/mol
delta_H_298K_H2 = 0;            %J/mol
delta_H_298K_H2O = -241800;     %J/mol

%Universal gas constant
R = 8.314;      %J/(mol*K)

%Reference temperature
T_ref = 298.15; %K

T = T_Input + 273.15; %Convert to K
P = P_Input;          %bar

Init_CO2 = 0;       %moles
Init_CO = 3;        %moles
Init_H2 = 9;        %moles
Init_CH3OH = 0;     %moles
Init_H2O = 0;       %moles
Init_CH3OCH3 = 0;   %moles

CO2_Coeff = 1;      %stoich coefficient
CO_Coeff = 3;       %stoich coefficient
H2_Coeff = 3;       %stoich coefficient
CH3OH_Coeff = 0;    %stoich coefficient
H2O_Coeff = 0;      %stoich coefficient
CH3OCH3_Coeff = 1;  %stoich coefficient

delta_G_rxn =
(delta_G_298K_CH3OCH3*CH3OCH3_Coeff+delta_G_298K_CO2*CO2_Coeff)-...
    (delta_G_298K_CO*CO_Coeff+delta_G_298K_H2*H2_Coeff);

delta_H_rxn =
(delta_H_298K_CH3OCH3*CH3OCH3_Coeff+delta_H_298K_CO2*CO2_Coeff)-...
```

```
    (delta_H_298K_CO*CO_Coeff+delta_H_298K_H2*H2_Coeff);

K_eq_ref = exp(-delta_G_rxn/(R*T_ref));

K_eq = K_eq_ref*exp(-delta_H_rxn/R*(1/T-1/T_ref));

Extent = 0;   %Initial guess for extent of reaction

%Mole amounts of compounds
Moles_CO = Init_CO - 3*Extent;
Moles_H2 = Init_H2 - 3*Extent;
Moles_CO2 = Init_CO2 + Extent;
Moles_H2O = 0;
Moles_CH3OH = 0;
Moles_CH3OCH3 = Init_CH3OCH3 + Extent;
Total_Moles = Moles_CO + Moles_H2 + Moles_CH3OCH3 + Moles_CO2;

%Mole fractions of compounds
y_CO = Moles_CO/Total_Moles;             %Gas fraction of CO
y_H2 = Moles_H2/Total_Moles;             %Gas fraction of H2
y_CO2 = Moles_CO2/Total_Moles;           %Gas fraction of CO2
y_H2O = Moles_H2O/Total_Moles;           %Gas fraction of H2O
y_CH3OH = Moles_CH3OH/Total_Moles;       %Gas fraction of CH3OH
y_CH3OCH3 = Moles_CH3OCH3/Total_Moles;   %Gas fraction of CH3OCH3

%Activities of compounds
a_CO = y_CO*P;
a_H2 = y_H2*P;
a_CO2 = y_CO2*P;
a_H2O = y_H2O*P;
a_CH3OH = y_CH3OH*P;
a_CH3OCH3 = y_CH3OCH3*P;

a_products = (a_CH3OCH3)^(CH3OCH3_Coeff)*(a_CO2)^(CO2_Coeff);
a_reactants = (a_CO)^(CO_Coeff)*(a_H2)^(H2_Coeff);

K_eq2 = a_products/a_reactants;

K_zero = abs(K_eq2 - K_eq);

Iterations = 0;

%Loop used to find a suitable extent value
while K_zero > 0.000001

    Extent = Extent + 0.0000001;   %Find the best fit

    %Mole amounts of compounds
    Moles_CO = Init_CO - 3*Extent;
    Moles_H2 = Init_H2 - 3*Extent;
    Moles_CO2 = Init_CO2 + Extent;
    Moles_H2O = 0;
    Moles_CH3OH = 0;
    Moles_CH3OCH3 = Init_CH3OCH3 + Extent;
```

```
    Total_Moles = Moles_CO + Moles_H2 + Moles_CH3OCH3 + Moles_CO2;

    %Mole fractions of compounds
    y_CO = Moles_CO/Total_Moles;             %Gas fraction of CO
    y_H2 = Moles_H2/Total_Moles;             %Gas fraction of H2
    y_CO2 = Moles_CO2/Total_Moles;           %Gas fraction of CO2
    y_H2O = Moles_H2O/Total_Moles;           %Gas fraction of H2O
    y_CH3OH = Moles_CH3OH/Total_Moles;       %Gas fraction of CH3OH
    y_CH3OCH3 = Moles_CH3OCH3/Total_Moles;   %Gas fraction of CH3OCH3

    %Activities of compounds
    a_CO = y_CO*P;
    a_H2 = y_H2*P;
    a_CO2 = y_CO2*P;
    a_H2O = y_H2O*P;
    a_CH3OH = y_CH3OH*P;
    a_CH3OCH3 = y_CH3OCH3*P;

    a_products = (a_CH3OCH3)^(CH3OCH3_Coeff)*(a_CO2)^(CO2_Coeff);
    a_reactants = (a_CO)^(CO_Coeff)*(a_H2)^(H2_Coeff);

    K_eq2 = a_products/a_reactants;

    K_zero = abs(K_eq2 - K_eq);

    Iterations = Iterations + 1;

    if Iterations == 500000000

        break

    end

end

%Will output temperature and moles
% T_Input
% Moles_H2
% Moles_CO
% Moles_CH3OCH3
% Moles_CO2
% Moles_CH3OH

%Will output temperature and mass percents
T_Input
Mass_H2 = Moles_H2*2;
Mass_CO = Moles_CO*28.01;
Mass_DME = Moles_CH3OCH3*46.07;
Mass_CO2 = Moles_CO2*44.01;
Mass_MeOH = Moles_CH3OH*32.04;

Total_Mass = Mass_H2 + Mass_CO + Mass_DME + Mass_CO2 + Mass_MeOH;

MassPercentH2 = Mass_H2/Total_Mass
```

```
MassPercentCO = Mass_CO/Total_Mass
MassPercentDME = Mass_DME/Total_Mass
MassPercentCO2 = Mass_CO2/Total_Mass

CO_Conversion = 1 - Moles_CO/Init_CO;
```

viii. Executable Equilibrium_Conversion_SingleDimethylEther.m

```
clear;
clc;

T = 245;
P = 30;
TempCount = 1;
TempCountMax = 5;

while TempCount < TempCountMax

    PressureCount = 1;

    while PressureCount < 2
        if PressureCount == 1
            P = 30;
            EquilibriumArray(1, 2) = P;
        end
        if PressureCount == 2
            P = 5;
            EquilibriumArray(1, 3) = P;
        end
        if PressureCount == 3
            P = 10;
            EquilibriumArray(1, 4) = P;
        end
        if PressureCount == 4
            P = 25;
            EquilibriumArray(1, 5) = P;
        end
        if PressureCount == 5
            P = 50;
            EquilibriumArray(1, 6) = P;
        end
        if PressureCount == 6
            P = 100;
            EquilibriumArray(1, 7) = P;
        end

        EquilibriumArray(TempCount + 1, 1) = T;
        EquilibriumArray(TempCount + 1, PressureCount + 1) = ...
            SingleDimethylEtherEquilibriumConversion(T,P);
        PressureCount = PressureCount + 1;

    end
```

```
    TempCount = TempCount + 1;
    T = T + 15;

end

EquilibriumArray
```

ix. Code for Single-Step DME Synthesis

```
function dFdV = Simple_Combined_Rxn(W,F)
%Function for the Single Step DME Reaction
%CO + 2H2 <--> CH3OH (Methanol formation) - Reaction #1
%2CH3OH <--> DME + H2O (Methanol dehydration) - Reaction #2
%CO2 + H2 <--> CO + H2O (Water-gas shift) - Reaction #3
%CO + 3H2 <--> CH4 + H2O (Parafin formation, just C1) - Reaction #4

%F is the vector containing the molar flows of the species Fi
%F(1) = Flow of Carbon Monoxide (CO)
%F(2) = Flow of Hydrogen (H2)
%F(3) = Flow of Methanol (MeOH)
%F(4) = Flow of Dimethyl Ether (DME)
%F(5) = Flow of H2O
%F(6) = Flow of CO2
%F(7) = Flow of CH4

F_CO = F(1);    %(mol/h)
F_H2 = F(2);    %(mol/h)
F_MeOH = F(3);  %(mol/h)
F_DME = F(4);   %(mol/h)
F_H2O = F(5);   %(mol/h)
F_CO2 = F(6);   %(mol/h)
F_CH4 = F(7);   %(mol/h)

F_Total = F_CO + F_H2 + F_MeOH + F_DME + F_H2O + F_CO2 + F_CH4;

%Reaction Parameters
T_ref = 300 + 273.15;       %300C
T = 275 + 273.15;           %275C
P = 3;                      %3 MPa
R = 8.314;                  %kJ/(mol*K)
k_star_DME = 2.64*10^(-7);  %mol/(g_cat*h*Pa^2)
k_star_DME2 = k_star_DME... %mol/(g_cat*h*MPa^2)
   *10^(12);
k1_star = 3.37 * 10^(-6);   %1/(mol_H2*g_cat*h*bar^3)
k1_star2 = k1_star*1000;    %1/(mol_H2*g_cat*h*MPa^3)
k2_star = 1.57;             %1/(mol_H2*g_cat*h*bar^2)
```

```
k2_star2 = k2_star*100;     %1/(mol_H2*g_cat*h*MPa^2)
k4_star = 2.81*10^(-7);     %1/(mol_H2*g_cat*h*bar^4)
k4_star2 = k4_star*10000;   %1/(mol_H2*g_cat*h*MPa^4)
Ea_MeOH = 26.95;            %kcal/mol
Ea_MeOH2 = Ea_MeOH * 4.184; %kJ/mol
Ea_DME = 84.14;             %kcal/mol
Ea_DME2 = Ea_DME * 4.184;   %kJ/mol
Ea_CH4 = 54.32;             %kcal/mol
Ea_CH42 = Ea_CH4 * 4.184;   %kJ/mol
%Ea_DME = 263.6;            %kJ/mol

%Concentrations
C_T0 = P/(R*T);
C_CO = C_T0*F_CO/F_Total;
C_H2 = C_T0*F_H2/F_Total;
C_MeOH = C_T0*F_MeOH/F_Total;
C_DME = C_T0*F_DME/F_Total;
C_H2O = C_T0*F_H2O/F_Total;
C_CO2 = C_T0*F_CO2/F_Total;
C_CH4 = C_T0*F_CH4/F_Total;

%Values for constants in Ki expressions
a3 = 21.84; b3 = 9.04*10^(3); c3 = -7.66;
d3 = 54.07*10^(-4); e3 = -57.50*10^(-8); f3 = -6.75*10^3;

a4 = -9.76; b4 = 3.2*10^(3); c4 = 1.07;
d4 = -6.57*10^(-4); e4 = 4.9*10^(-8); f4 = 6.05*10^3;

a5 = 18.01; b5 = -5.87*10^(3); c5 = -1.86;
d5 = 2.7*10^(-4); e5 = 0*10^(-8); f5 = 58.20*10^3;

a6 = 24.90; b6 = 22.78*10^(3); c6 = -7.95;
d6 = 43.54*10^(-4); e6 = -36.07*10^(-8); f6 = -4.85*10^3;

%Definition of equilibrium constants Ki
K_1 = exp(a3+b3/T+c3*log10(T)+d3*T+e3*T^2+f3/(T^2));
K_2 = exp(a4+b4/T+c4*log10(T)+d4*T+e4*T^2+f4/(T^2));
K_3 = exp(a5+b5/T+c5*log10(T)+d5*T+e5*T^2+f5/(T^2));
K_4 = exp(a6+b6/T+c6*log10(T)+d6*T+e6*T^2+f6/(T^2));
K_H2O = 1.02*exp((65.99/0.001987)*((1/T)-(1/548)));

%Partial pressures (Pi = Ci*R*T), pressure in MPa
P_CO = C_CO*R*T;        %MPa
P_H2 = C_H2*R*T;        %MPa
P_MeOH = C_MeOH*R*T;    %MPa
P_DME = C_DME*R*T;      %MPa
```

```
P_H2O = C_H2O*R*T;      %MPa
P_CO2 = C_CO2*R*T;      %MPa
P_CH4 = C_CH4*R*T;      %MPa

%Reparametrization of the kinetic parameters with Arrhenius
k1 = k1_star2*exp(-Ea_MeOH2/R*(1/T-1/T_ref));
k2 = k2_star2*exp(-Ea_DME2/R*(1/T-1/T_ref));
k3 = 1;
k4 = k4_star2*exp(-Ea_CH42/R*(1/T-1/T_ref));

%Simple elementary rate laws
r1 = k1*(P_CO*P_H2^2-(P_MeOH/K_1))*Theta;
r2 = k2*(P_MeOH^2 - (P_DME*P_H2O/K_2));
r3 = k3*(P_CO*P_H2O-(P_CO2*P_H2/K_3));
r4 = k4*(P_CO*P_H2^3-(P_CH4*P_H2O/K_4))*Theta;

%Determintation of new flows
dF_COdW = -r1-r3-r4;
dF_H2dW = -2*r1+r3-3*r4;
dF_MeOHdW = -2*r2+r1;
dF_DMEdW = r2;
dF_H2OdW = r2-r3+r4;
dF_CO2dW = r3;
dF_CH4dW = r4;

dFdV = [dF_COdW; dF_H2dW; dF_MeOHdW; dF_DMEdW; dF_H2OdW; dF_CO2dW;
dF_CH4dW];

end
```

x. Code for PBR Model

```
%Testing the Simple_Combined_Rxn function


clear all;  %Clears variables
clc;        %Clears command window

%Initial flow conditions
CO_0 = 0.37;    %Flows pulled from my experimental numbers
H2_0 = 0.61;    %Flows pulled from my experimental numbers
MeOH_0 = 0;     %Flows pulled from my experimental numbers
DME_0 = 0;      %Flows pulled from my experimental numbers
H2O_0 = 0;      %Flows pulled from my experimental numbers
CO2_0 = 0;      %Flows pulled from my experimental numbers
CH4_0 = 0;      %Flows pulled from my experimental numbers
```

```
WRange = [0 20];            %Grams of catalyst (in PBR) in model
F0 = [CO_0 H2_0 MeOH_0 DME_0 H2O_0 CO2_0 CH4_0];

[W,F] = ode45('Simple_Combined_Rxn',WRange, F0);

n = numel(F)/7; %Determines the number of iterations in the ode solver
            %This allows for the determination of the final flow rate

%Determine the overall conversion, flow rates, and selectivities
CO_Conversion = (1-(F(n,1)/CO_0))*100
H2_Conversion = (1-(F(n,2)/H2_0))*100
Final_MeOH = F(n,3)
Final_DME = F(n,4)
Final_H2O = F(n,5)
Final_CO2 = F(n,6)
Final_CH4 = F(n,7)

%Plot the results
plot(W,F(:,1),'-',W,F(:,2),'-',W,F(:,3),'-',W,F(:,4),'-', ...
   W,F(:,5),'-',W,F(:,6),'-',W,F(:,7),'-');
xlabel('Catalyst Mass (g)');
ylabel('Flow Rate (mol/h)');
legend ('CO','H2','MeOH', 'DME', 'H2O', 'CO2', 'CH4');
```

xi. Code for Layered Model

```
%Testing the Layered Bed Design
%Use Simple_JustMeOH_Rxn for the MeOH catalyst portion
%Use Simple_JustDME_Rxn for the DME catalyst portion

clear all;  %Clears variables
clc;        %Clears command window

%Initial flow conditions
CO_0 = 0.37;    %Flows pulled from my experimental numbers
H2_0 = 0.61;    %Flows pulled from my experimental numbers
MeOH_0 = 0;     %Flows pulled from my experimental numbers
DME_0 = 0;      %Flows pulled from my experimental numbers
H2O_0 = 0;      %Flows pulled from my experimental numbers
CO2_0 = 0;      %Flows pulled from my experimental numbers
CH4_0 = 0;      %Flows pulled from my experimental numbers

TotalLayers = 10;
```

```
TotalCatalyst = 20;         %Grams of catalyst (in PBR) in model

CatalystPerLayer = TotalCatalyst/TotalLayers;
CatalystCount = 0;
DME_Catalyst_Layer_Amount = 0.1;

F = [CO_0 H2_0 MeOH_0 DME_0 H2O_0 CO2_0 CH4_0];

n = numel(F)/7;
%Determines the number of rows in the previous run
%This allows for the determination of the final flow rate

CompleteW = [0];
CompleteCO = [0];
CompleteH2 = [0];
CompleteMeOH = [0];
CompleteDME = [0];
CompleteH2O = [0];
CompleteCO2 = [0];
CompleteCH4 = [0];

for i = 1:TotalLayers

    LayerStart = CatalystCount;
    CatalystCount = CatalystCount + CatalystPerLayer;
    MeOH_Layer_End = CatalystCount - DME_Catalyst_Layer_Amount;
    DME_Layer_End = MeOH_Layer_End + DME_Catalyst_Layer_Amount;

    %MeOH Synthesis Layer
    WRange = [LayerStart MeOH_Layer_End];
    F = [F(n,1) F(n,2) F(n,3) F(n,4) F(n,5) F(n,6) F(n,7)];

    [W,F] = ode45('Simple_JustMeOH_Rxn',WRange, F);

    FCO_1_Layer = F(:,1);
    FH2_1_Layer = F(:,2);
    FMeOH_1_Layer = F(:,3);
    FDME_1_Layer = F(:,4);
    FH2O_1_Layer = F(:,5);
    FCO2_1_Layer = F(:,6);
    FCH4_1_Layer = F(:,7);
    W_1_Layer = W;

    n = numel(F)/7;
    %Determines the number of rows in the previous run
    %This allows for the determination of the final flow rate
```

```
    %DME Synthesis Layer
    WRange = [MeOH_Layer_End DME_Layer_End];
    F0 = [F(n,1) F(n,2) F(n,3) F(n,4) F(n,5) F(n,6) F(n,7)];

    [W,F] = ode45('Simple_JustDME_Rxn',WRange, F0);

    FCO_2_Layer = F(:,1);
    FH2_2_Layer = F(:,2);
    FMeOH_2_Layer = F(:,3);
    FDME_2_Layer = F(:,4);
    FH2O_2_Layer = F(:,5);
    FCO2_2_Layer = F(:,6);
    FCH4_2_Layer = F(:,7);
    W_2_Layer = W;

    n = numel(F)/7;
    %Determines the number of rows in the previous run
    %This allows for the determination of the final flow rate

    NewLayerW = [W_1_Layer; W_2_Layer];
    NewLayerCO = [FCO_1_Layer; FCO_2_Layer];
    NewLayerH2 = [FH2_1_Layer; FH2_2_Layer];
    NewLayerMeOH = [FMeOH_1_Layer; FMeOH_2_Layer];
    NewLayerDME = [FDME_1_Layer; FDME_2_Layer];
    NewLayerH2O = [FH2O_1_Layer; FH2O_2_Layer];
    NewLayerCO2 = [FCO2_1_Layer; FCO2_2_Layer];
    NewLayerCH4 = [FCH4_1_Layer; FCH4_2_Layer];

    CompleteW = [CompleteW; NewLayerW];
    CompleteCO = [CompleteCO; NewLayerCO];
    CompleteH2 = [CompleteH2; NewLayerH2];
    CompleteMeOH = [CompleteMeOH; NewLayerMeOH];
    CompleteDME = [CompleteDME; NewLayerDME];
    CompleteH2O = [CompleteH2O; NewLayerH2O];
    CompleteCO2 = [CompleteCO2; NewLayerCO2];
    CompleteCH4 = [CompleteCH4; NewLayerCH4];

end

%Determine the overall conversion, flow rates, and selectivities
CO_Conversion = (1-(F(n,1)/CO_0))*100
H2_Conversion = (1-(F(n,2)/H2_0))*100
Final_MeOH = F(n,3)
Final_DME = F(n,4)
Final_H2O = F(n,5)
```

```
Final_CO2 = F(n,6)
Final_CH4 = F(n,7)

W = CompleteW;

%Plot the results
plot(W,CompleteCO,'-',W,CompleteH2,'-',W,CompleteMeOH,'-',...
   W,CompleteDME,'-',W,CompleteH2O,'-',W,CompleteCO2,'-',...
   W,CompleteCH4,'-');
xlabel('Catalyst Mass (g)');
ylabel('Flow Rate (mol/h)');
legend ('CO','H2','MeOH', 'DME', 'H2O', 'CO2', 'CH4');
```